Non-equilibrium Dynamics of Active Enzymes

Tunrayo Adeleke-Larodo

St John's College

University of Oxford

A thesis submitted for the degree of

Doctor of Philosophy

Trinity 2020

Non-equilibrium Dynamics of Active Enzymes

Tunrayo Adeleke-Larodo

St John's College, University of Oxford

A thesis submitted for the degree of Doctor of Philosophy

Trinity 2020

Abstract

Observations of behaviour usually associated with micron-scale living systems and self-propelled particles in enzymatic systems have been attributed to their catalytic activity. In light of the conformational changes that accompany the catalytic cycle, the exciting possibility that an enzyme molecule can generate enough mechanical work to overcome the noisy conditions inside a cell is being investigated, due to its implications on biological self-organisation and intracellular transport. To this end, we develop a theoretical framework for studying the effect of catalytic activity on the dynamics of catalysing enzymes.

Using a simple generic model of an asymmetric dumbbell made of two subunits that are coupled through hydrodynamic interactions, we study the effect of conformational fluctuations of modular macromolecules, such as enzymes, on their dynamical properties. We show that thermal fluctuations can lead to an interplay between the internal and external degrees of freedom, with the consequence of a negative fluctuation-induced correction to the overall diffusion coefficient of the asymmetric dumbbell compared to a rigid symmetric object. This result is directly applicable to studying the effect of the catalytic cycle on the diffusion of the model enzyme, by considering the internal fluctuations in the presence of substrate molecules which can bind and unbind to the enzyme.

We investigate the effect of the modular structure and internal fluctuations on the dynamics of the model enzyme in a concentration gradient of its substrate. The model enzyme is shown to have three types of response to the chemical gradient, including a drift velocity that is modified by hydrodynamic interactions between its constituents, and alignment. In addition to the chemically induced alignment, we predict a second alignment mechanism in response to density gradients.

Finally, we study the effect of hydrodynamic coupling of a pair of our model enzymes on their internal dynamics and show that the sign and strength of the coupling depend on their separation and proximity to a symmetry-breaking region

Acknowledgements

I would like to express my gratitude for the guidance I have received throughout my DPhil. I am grateful to my supervisor, Prof. Ramin Golestanian, who has always encouraged and motivated me to be a more confident researcher. I am thankful to my collaborators, Pierre Illien and Jaime Agudo-Canalejo, from whom I have learnt a great deal, for their mentorship. Indeed, it was Pierre's willingness to share his science that sparked my interest in the project. I would like to thank my second supervisor, Prof. Julia Yeomans, for her readiness to help in difficult situations.

I have received the support of not one but two departments, at the Rudolf Peierls Centre in Oxford and the Department of Living Matter Physics in Götthingen. The opportunities I have had and the people I have met at both places have been enormously inspiring. I am particularly indebted to Prof. John Chalker and Michelle Bosher for their unfailing support from my very first day at the Rudolf Peierls Centre.

The past few years would not have been filled with such fond memories without the incredible friends I have made in Oxford, at St John's and the Rudolf Peierls Centre, and in Göttingen. I continue to be grateful for the companionship and support of my friends from London and Edinburgh.

I would like to thank my family: my parents for their prayers and encouragement, my sisters for so much more than I dare to list and my nieces and nephews for never failing to put a smile on my face.

I am grateful for financial support from an EPSRC Studentship.

Finally, I am thankful for the love of God, for giving me the strength to undertake this research and perseverance to complete this thesis.

Statement of originality

The thesis contains material from the following co-authored publications:

- T. Adeleke-Larodo, J. Agudo-Canalejo and R. Golestanian. “Chemical and hydrodynamic alignment of an enzyme". In *J. Chem. Phys.* 150.11 (2019), p. 115102
- T. Adeleke-Larodo, P. Illien and R. Golestanian. “Fluctuation-induced hydrodynamic coupling in an asymmetric, anisotropic dumbbell". In *Eur. Phys. J. E* 42.3 (2019), p. 39
- J. Agudo-Canalejo, T. Adeleke-Larodo, P. Illien and R. Golestanian. “Enhanced Diffusion and Chemotaxis at the Nanoscale". In *Acc. Chem. Res.* 51.10 (2018), pp. 2365–2372
- P. Illien, T. Adeleke-Larodo and R. Golestanian. “Diffusion of an enzyme: The role of fluctuation-induced hydrodynamic coupling". In *EPL* 119.4 (2017), p. 40002

The thesis is the result of my own work except where specifically indicated in the text. The calculation in Section 4.2.3.3 was performed by Jaime Agudo-Canalejo.

Contents

CHAPTER 1

Introduction

The peculiarities of non-equilibrium systems are as beautiful as they are perplexing. In active matter, where time-reversal symmetry is broken by local energy input, such as at the level of individual particles where each active particle converts the available free-energy into motion, rather than at the boundaries of the system [1], there are emergent phenomena that are impossible in equilibrium systems. Intrinsically non-equilibrium behaviour in active systems include pattern formation, order-disorder transitions, atypical mechanical and rheological properties, the formation of structures with collective behaviour that is different from that of the individual constituents and dynamical instabilities [1]. These are the result of complex interactions between individual constituents and with the surrounding medium. An interesting observation is that many of the macroscopic phenomena are universal– even across length scales.

Living systems provide the foremost example of active matter. Arguably, the primary goal of research in active matter is to understand the mechanics and statistical properties of living matter: from the subcellular biofilaments and molecular motors that make up the cytoskeleton of eukaryotic cells to swarms of bacteria and animal flocks. A theoretical description of the general principles governing the behaviour of living systems is so far unavailable due to their complexity. A good understanding of these systems feeds into the second goal of successfully

imitating natural machinery to create synthetic engines (particularly at the smallest scales) that can replicate the behaviour of nature's machines and are controllable as need be. The approach that is being taken is to study the most promising natural systems along these lines.

1.1 Enzymes

Due to their ability to perform specialised and sophisticated tasks with high efficiency in crowded, noisy, and viscous environments such as the interior of cells, enzymes have recently attracted a lot of attention as possible biocompatible nanoengines. Enzymatic systems are ubiquitous in nature and their catalytic cycles are an apparent example of non-equilibrium phenomena that is commonly studied in statistical physics and non-linear dynamics.

Over the last decade, there have been many innovative demonstrations of enzyme-powered micro- and nanomachines, that convert chemical free-energy into motion and are capable of cargo transport and nanoscale assembly. These synthetic systems typically rely on the combined activity of many enzymes to provide the necessary power to achieve their intended purpose. Some notable examples are illustrated in Fig. 1.1, including enzyme-powered DNA motors such as DNA-based rolling motors that hybridise to RNA tracks, whose motion is based on selective hydrolysis by the enzyme RNase H [2]; enzymes entrapped in nanoscale polymer bowl-like structures [3]; Janus hollow microcapsules [4]; microengines powered by catalase covalently bonded to the inside surface of a rolled-up microtube, which self-propel due to the release of bubbles from one end of the tube [5]; enzyme-powered micropumps, where the activity of enzymes immobilised to a surface changes the flow rate of the nearby fluid [6]; and enzyme coated microparticles, which can perform directed motion in substrate concentration gradients [7].

The mechanism (or indeed mechanisms) that is responsible for the enzyme motion that drives these motors is still a topic of much debate. Perhaps the most intriguing and bewildering suggestion for a motor that is depicted in Fig 1.1 is a single enzyme molecule. If truly realisable, it opens the possibility that a

single nanoscale molecule can replicate the behaviour of active systems that are typically orders of magnitude larger.

In order to fully understand the dynamics of the synthetic enzyme-powered systems that have been mentioned and realise the potential applications of enzymes as nanoengines, we must understand the mechanism for the dynamics of the apparent motor-like dynamics of single enzyme molecules. Before describing the

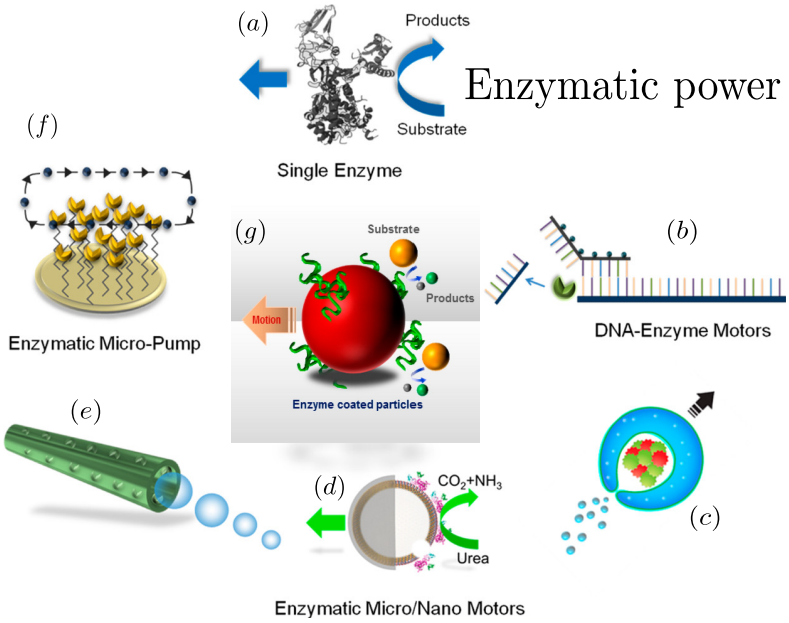

Figure 1.1. Schematic illustrations of micro- and nanomachines powered by enzymes: (a) a single catalytically active enzyme molecule, (b) an enzyme-powered DNA based motor, (c) an enzyme-driven supramolecular nanomotor [3], (d) a Janus hollow microcapsule [4], (e) a microengine powered by catalase covalently bonded to the inside surafce of a rolled-up microtube [5], (f) an enzyme-powered micropump [6] and (g) an enzyme coated microparticle [7]. Adapted with permission from ref. [8]. Copyright 2020 American Chemical Society.

remarkable observations that have led to the inclusion of a single enzyme molecule in Fig 1.1, we mention some properties of enzymes that will be important for our forthcoming discussions.

1.1.1 Function

Enzymes are biomolecules, typically proteins, that catalyse biochemical reactions– including almost all of the chemical reactions that occur inside living cells. The complex environment inside a cell is maintained by many enzymes working in concert.

The chemical activity of the enzymes maintains the non-equilibrium stationary state of the cell. For instance, through signal transduction, cargo transportation as part of the cell's cytoskeleton and ion pumping in the cell membrane. The molecular motors required for intracellular motility, namely myosins and kinesins and dyenins, generate energy to move from the hydrolysis of ATP by enzymes such as ATPase [9, 10]. Enzymes are also responsible for assembling other structures inside a cell: DNA is synthesised by the enzyme DNA Polymerase [11]. Incredibly, they are even capable of detecting and correcting errors during biosynthesis [11]. Additionally, enzymes also have the crucial role of breaking down large molecules in the digestive system.

Possibly their most important and interesting role is in metabolism, where they are essential for ensuring that the series of chemical reactions that make up metabolic pathways are sustainable in the cell environment [12]. A metabolic pathway typically consists of many different enzymes working collectively and interacting through the exchange of substrate (the reactants in enzymatic reactions) and product molecules in a way that the product of one enzyme is a substrate for another enzyme in the pathway. The combinations of enzymes and enzyme activity in metabolic pathways can lead to very complex collective behaviour.

1.1.2 Structure

Enzymes are generally globe-like structures consisting of many individual components. In their equilibrium state, their sizes are in the range of several nm–generally much larger than their substrates. The functional part of an enzyme is known as the active site and includes the catalytic site, where catalysis of substrate into product takes place and one or more binding sites which orient substrate molecules for catalysis. The rest of the enzyme works to maintain the functionality of the binding site [13]. An enzyme may also contain *allosteric sites* that bind small molecules (and are not the same as the binding site), inducing conformational changes or changes in the enzyme's dynamics that regulate catalytic activity through a dynamical feedback loop [14].

1.1.3 Mechanism

Substrate must bind to the enzyme's binding site before catalysis can take place. Once in place, enzymes increase the rate of reactions involving their substrates by lowering the free-energy barrier required for the reactions to occur. This can be understood in terms of a Kramers escape process in the reaction space: The substrate correspond to higher energy states and chemical reactions are transitions to the lower energy product states, which must overcome an energy barrier that is much larger than $k_{\mathrm{B}}T$ (see Fig. 1.2) [15] . Enzymes can lower the energy barrier to speed up reactions in a number of ways: by destabilising substrate states or stabilising the product states to make transitions more thermodynamically favourable or by providing alternative pathways for reactions with lower energy barriers than in the uncatalysed reaction [16–19].

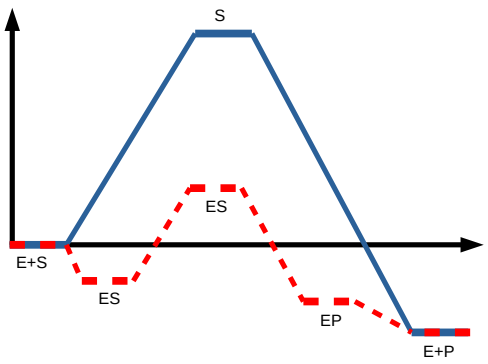

Figure 1.2. The free-energy profile of the alternative routes for a biochemical reaction: the uncatalysed reaction (solid blue line) has a higher free-energy barrier between the initial reactant state and the final product state than the catalysed reaction (dashed red line). Also note that the reactant state has a higher energy than the products. Figure adapted from ref. [20].

An interesting feature of the thermodynamics of enzyme catalysis is that reactions that are thermodynamically unfavourable can be driven through coupling to thermodynamically favourable reactions, if overall the product state has lower energy than the substrates [21].

1.1.4 Kinetics

Enzyme kinetics describes the process of substrate binding and conversion into products. Although a typical enzyme cycle may involve several steps and reaction intermediates, it can be reduced to a minimal description of just three steps, known as *Michaelis-Menten* kinetics. We will assume Michaelis-Menten kinetics throughout the thesis. In the simplified description, a free enzyme (E) binds reversibly to its substrate (S), forming an enzyme-substrate complex (ES) that is subsequently converted into an enzyme-product complex (EP) in the catalytic step (which typically has an associated heat transfer ΔQ). In the final step the product (P) is released from the enzyme-product complex. Each step occurs at a specific rate seen in

$$\mathrm{E} + \mathrm{S} \underset{k_{\mathrm{off}}}{\overset{k_{\mathrm{on}}}{\rightleftharpoons}} \mathrm{ES} \xrightarrow{k_{\mathrm{cat}}} \mathrm{EP} \rightleftharpoons \mathrm{E} + \mathrm{P}, \tag{1.1}$$

where k_{on} and k_{off} are the rates of substrate binding and unbinding respectively, and k_{cat}, the catalytic rate constant, is the number of substrate molecules that are turned-over in one active site each second. The catalytic rate constant is determined by the Michaelis-Menten equation:

$$\frac{\mathrm{dP}}{\mathrm{d}t} = k_{\mathrm{cat}} \mathrm{E}_0 \frac{\mathrm{S}}{\mathrm{K_M} + \mathrm{S}}, \tag{1.2}$$

where E_0 is the initial enzyme concentration and $\mathrm{K_M}$ is the Michaelis constant, the substrate concentration when the reaction rate is at half-maximum. In (1.1), dissociation of the product is also assumed to be reversible, with rates that are generally different to those associated to substrate binding. It should also be mentioned that enzymes are not consumed by catalysis so that their total number is conserved, although some may be bound in a complex. Finally, the steps in the catalytic cycle are typically accompanied by conformational changes in the enzyme. This is a feature that we exploit and will therefore be discussed in detail.

1.1.5 Single enzyme dynamics

To be able to harness their functionality for applications outside of their usual environment, it is important to go beyond questions related to the structure and

kinetics of enzymes, which have been well studied, to probe their mechanical response to the biochemical environment and its effect on their functionality. The goal at the forefront of this line of research is to be able to control and manipulate the dynamics of enzymatic systems externally. The question that is being asked is whether enzyme molecules undergoing catalytic turnover can exhibit similar behaviour to synthetic self-propelled particles. In addition to the importance of understanding mechanical and dynamical response for applications outside the cell, there could also be important implications for cellular processes such as self-organisation in metabolic pathways [22–25]. Furthermore, other major components of the cell such as the cytoskeleton, have been well studied.

Positive results along this line include experimental reports that the diffusion coefficient of catalytically active enzymes is enhanced in the presence of their substrate. The increase in diffusion coefficient has a Michaelis-Menten dependence on substrate concentration: increasing linearly for low substrate concentration and reaching a maximum– typically of the same order of magnitude as the diffusion coefficient in the absence of substrate– at which it plateaus at substrate saturation [26–31]. More recent experiments have reported directed motion, or "chemotaxis", of catalytically active enzymes when the substrate concentration is non-uniform so that there is a concentration gradient. The effect has been observed for a number of enzymes, and has typically been seen to cause movement in the direction of increasing concentration (reported for the enzymes catalase and urease [29, 32], RNA polymerase [27], DNA polymerase [30], and hexokinase and aldolase [22]). The opposite has also been reported, where enzymes (so far urease and acetylcholinesterase) have been seen to move in the direction of decreasing substrate concentration [33].

Despite the many proposals that have been made for the underlying mechanisms responsible for enhanced enzyme diffusion and chemotaxis, the two effects are still far from being fully understood [34]. Initial theories to explain enhanced diffusion relied on the non-equilibrium aspects of enzyme activity [31, 35–38]. Specifically, the effect was typically linked to the heat released in the catalytic

cycle (as is the case for enzymes that catalyse exothermic reactions) or the rate of catalysis, favouring "fast" enzymes that catalyse fast reactions and have a high turn-over rate. These initial theories will be discussed in detail in Chapter 3 but have been shown to be individually incapable of reproducing the level of enhancement reported from experiments [37]. The effect of enzyme chemotaxis has proven to be more of a curiosity.

The observation of enhanced diffusion for the slow enzyme aldolase, which has a low turn-over rate and catalyses endothermic reactions that take in heat rather than releasing it, in the presence of its substrate but also in the presence of an inhibitor (which is not a reactant but binds to an enzyme's binding site), further justified the need for a new paradigm that is independent of catalytic activity. Indeed, we should also question the role of non-equilibrium activity in enzyme chemotaxis. A better understanding of these two phenomena could justify the inclusion of single enzyme molecules in Fig. 1.1. The intrigue, but also complication is increased by the variety of enzyme molecules, meaning that there are many possible applications, but that their physical properties do not obviously fit into one universality class.

1.2 Overview

In Chapter 2 we provide a theoretical background to the thesis. We briefly discuss hydrodynamic theories in active matter as a method for deriving the long-time statistical properties of active systems. We motivate our use of the *moment expansion* for deriving the hydrodynamic equations for an active enzyme suspension. The moment expansion is introduced with the simple example of active Brownian particles, which highlights the key principles of the method. In Chapter 3 the method is extended to study the effect of catalytic activity on the long-time diffusion of a model enzyme. With our minimal model, we study the role of thermal fluctuations on the diffusion of an enzyme in suspension. The result is placed in the context of substrate-driven enhanced enzyme diffusion by considering the effect of catalytic activity in the model. Following the results of Chapter 3 for the long-time dynamics of an enzyme in a uniform substrate concentration, in Chapter 4

we investigate the effect of a substrate concentration gradient on the dynamics of our model enzyme. In Chapter 5 we begin to explore collective behaviour in enzymatic systems by studying the hydrodynamic coupling of a pair of our model enzymes. The thesis concludes with a summary of our findings and some open questions that we would like to explore.

CHAPTER 2

Moment expansion

2.1 Hydrodynamic theories in active matter

To understand the collective behaviour and transport properties of active systems such as diffusion, it is necessary to study their dynamics on length scales that are larger than the size of individual agents and at times greater than the time it takes for their microscopic dynamics to equilibrate. In this continuum limit, also referred to as the "hydrodynamic" limit, dynamics is controlled by the interplay between local energy consumption, interactions, and thermal fluctuations. The aim of a generalised hydrodynamic theory is to identify the relevant fields and mean field equations for a description of a system in the large wavelength and large timescale limit. These are the fields for which perturbations away from an equilibrium value are long lasting. More precisely, their relaxation time grows infinitely large at large wavelength [39]. These are the "slow" modes of a system, and all other modes with fast relaxing perturbations, that are seen as damped in the equations of motion are "fast" modes, with variations that do not extend to the macroscopic scale. Hence, the slow variables are the conserved quantities in the macroscopic limit and broken symmetry variables whose fluctuations relax infinitely slowly at large wavelength.

The symmetry we will be interested in is rotational symmetry, due to the importance of orientation in active and driven systems: active particles have a

direction of self-propulsion due to non-equilibrium driving or are elongated so that they have an intrinsic orientation. On the macroscopic scale we can ask questions about emergent rotational order and identify a rotational order parameter– indeed active matter systems have been classified by the behaviour of their rotational order parameter. There are interesting examples of long-range rotational order emerging spontaneously from local interactions [40–43]– even in two dimensional systems where, in equilibrium, the spontaneous breaking of a continuous symmetry is prohibited due to long wavelength modes [44]. A situation in which spontaneous breakdown of discrete symmetry induces collective motion has been described [45].

Several methods have been used to derive the continuum limit for active systems. From the purely phenomenological approach, where the equations for the hydrodynamic fields are constructed from symmetry considerations and conservation laws. Since the system is out of equilibrium, the forces in the equation of motion are not necessarily derived from a free-energy so all the terms allowed by symmetry and conservation laws– which may not be present in an equilibrium system– must be included in the theory [41, 43, 46]. For example, a nematic system should be invariant under rotation by angle π so all the possible terms in the equation of motion with this symmetry should be included. This method has the advantage that the theory is universal and independent of microscopic details. Hence, it is straightforward to identify phenomena that are derived purely from non-equilibrium activity as opposed to a unique property of the microscopic system. However, the parameters of the continuum equations derived in this way are typically undetermined and are difficult to obtain experimentally [1].

A more systematic approach relies on an expansion of the active system close to equilibrium, where linear response is assumed. The hydrodynamic equations are then derived using the Onsager reciprocal relations for thermodynamic systems, that relate fluxes in thermodynamic variables to conjugate forces [47]. The method requires first writing conservation laws for the thermodynamic variables of the problem. From the First law of thermodynamics, the rate of entropy production in the system is given by generalised fluxes in the thermodynamic variables and the

conjugate forces that produce the fluxes. The sign of each contribution is determined by the behaviour of the forces and fluxes under time-reversal. To construct the dynamical equations, phenomenological equations are written for the generalised fluxes in terms of the conjugate forces at the level of linear response, which include all the terms that are allowed by symmetry. Again, the method is generic and has been widely used to describe complex fluids such as "active gels" and active liquid crystals [48–50]. However, it comes with the shortcoming that the biological systems we would like to describe are generally far from equilibrium and thus not faithfully represented by a near equilibrium approximation.

Finally, it is possible to derive the hydrodynamic equations for an active system systematically from a microscopic description of the system. This can at least be done for simple models where the dynamics of individuals can be described by simple equations and in the limit of low-density, where the hydrodynamic equations should not be strongly dependent on details of local interactions. For "dry" systems[1] with aligning interactions [40], the hydrodynamic equations have been derived from microscopic models. Notably by coarse-graining the Smoluchowksi description for the stochastic dynamics [51, 52] and the Boltzmann equation [53–55], and these two methods have been compared [56]. The result is that the parameters of the derived macroscopic dynamics are found in terms of the parameters of the microscopic model which are experimentally accessible, as opposed to the undetermined parameters of the phenomenological methods. This means that phenomena arising in the macroscopic limit can be understood from the level of the underlying microscopic mechanisms. Furthermore, knowledge of the parameter space is necessary to study the stability of the emergent macroscopic states. Ultimately, the hydrodynamic equations that are derived from different microscopic models with the same symmetries have the same structure and are distinguished only by parameter values. This is the case for the coarse-grained dynamics of active filament mixtures [57, 58] and self-propelled particles [59, 60]. The topic of this chapter is one of the methods in this class.

[1] Systems that are modelled as non-momentum conserving.

2.2 From fluctuating microscopic dynamics to macroscopic dynamics

2.2.1 Overview

In what follows we describe in detail, a generic analytical method for deriving the hydrodynamic equations for fluctuating systems– active or not– where translational and rotational dynamics are coupled. It is easily extendable to studying collective dynamics [61] in the active systems previously mentioned [53, 58–60, 62–64]. We limit our discussion in this chapter to dilute systems, neglecting interactions to provide the most basic illustration of the theory. However, the method has been applied to systems with long- and short-range interactions [65, 66]. The inclusion of long-range interactions will be a principal feature in subsequent chapters.

2.2.2 The multipole expansion

Another reason one may turn to a hydrodynamic description of fluctuating systems is due to the difficulty of solving the stochastic microscopic equations for all length- and timescale regimes. In the probabilistic description of stochastic dynamics, it is in general difficult to find the full probability distribution function everywhere for all times. In fact, there are few cases for which it can be found exactly (the exceptions being highly symmetric systems). Otherwise, approximations can be made to extract only the information required whilst preserving the symmetries of the system. The approximation we will use will be to consider the probability distribution at large scales and, Maxwell's multipole expansion provides a mathematical framework to study rotational symmetry. After the large-time approximation has been taken, we can identify the hydrodynamic variables and eliminate the remaining fast variables with large decay rates.

Like the multipole expansion for the potential outside a charge distribution in electrostatics [67] and the velocity field of a particle in ambient flow [68], the probability of finding a particle in a particular configuration can be written as a multipole expansion, where the expansion coefficients are the "multipole moments"

and, the complete set of moments uniquely specifies the function. Indeed the moments of the probability distribution are comparable to the same quantities for the charge distribution: the zeroth moment (the monopole in electrostatics and drag force in hydrodynamics) is a density field; the first moment (the dipole and Stokes dipole) gives the average orientation and changes sign upon rotation by an angle π; the second moment (the quadrupole and Stokes quadrupole) gives information about the spread of orientations and is an order parameter for rotational symmetry, and so on. In standard notation, the expansion is written in terms of the spherical harmonics in three dimensions and a Fourier series in two dimensions. We will use the *irreducible tensor* formalism which is equivalent and has become standard in active matter. In this tensorial description, a suitable order parameter is easily identified.

Briefly, the moment expansion can be summarised as the following procedure: starting from the probabilistic description of the microscopic dynamics (Fokker-Planck or Smoluchowksi equations), we expand the equations about the isotropic state of the system, which yields an infinite hierarchy of equations in the fields that parameterise perturbations from this state *i.e.,* the multipole moments. The infinite hierarchy can either be solved numerically for a large (but finite) number of the moments or, for an analytic solution, we need a closure strategy to extract the hydrodynamic modes. Firstly, a separation of timescales gives an equation for the linear dependence of the hierarchy so that not all the fields are independent. Using the large wavelength approximation, we can neglect high order derivatives to find closed expressions for the remaining fields, and finally express the higher order moments in terms of the lowest order moments which are the hydrodynamic fields. We consider diffusive motion, where time and space are not on equal footing so that the hydrodynamic limit is equivalent to taking an expansion in ϵ with $\nabla \sim \epsilon$, $\partial_t \sim \epsilon^2$ for $\epsilon \ll 1$[2]. We can then write the dynamical coefficients of the system explicitly in terms of their field dependence.

For the remainder of this chapter we will formulate the multipole moment expansion in irreducible tensors. The method will be illustrated for the simple

[2]This is only true if there is no ballistic regime.

example of an active Brownian particle (ABP), a commonly studied toy model of self-propelled particles. But first, in the next section, we briefly discuss an explicit example of adiabatic elimination of a fast variable as a method for solving the Fokker-Planck equation. The procedure is intimately related to the moment expansion, but the generality reveals some important and useful properties that are also found in the hydrodynamic equations we will encounter.

2.3 Adiabatic elimination by eigenfunction expansion

2.3.1 Overview

A common method for solving the Fokker-Planck equation is to expand the probability distribution in the eigenfunctions of an auxiliary problem, assuming that the set of eigenfunctions is complete and forms an orthonormal basis. The classic book by Risken, on methods for solving Fokker-Planck equations [69], shows how such an expansion can be used to eliminate rapidly decaying variables in a multivariate system, to obtain a reduced equation for the evolution of the probability distribution of the remaining slow variables, which are the relevant variables in the hydrodynamic limit. The method is illustrated below with the example of a bivariate system [69].

2.3.2 Adiabatic elimination for a two-variable system

The system to be reduced is a two-dimensional stochastic process in the variables x and y with a probability distribution $P(x, y; t)$ that obeys the Fokker-Planck equation

$$\frac{\partial P}{\partial t} = [\mathcal{L}_x(x, y) + \gamma \mathcal{L}_y(x, y)]P \tag{2.1}$$

and has no boundaries except at infinity. The operators $\mathcal{L}_x$ and $\mathcal{L}_y$ are given by

$$\mathcal{L}_x(x, y) = -\frac{\partial}{\partial x} D_x^{(1)}(x, y) + \frac{\partial^2}{\partial x^2} D_x^{(2)}(x, y), \tag{2.2}$$

$$\mathcal{L}_y(x, y) = -\frac{\partial}{\partial y} D_y^{(1)}(x, y) + \frac{\partial^2}{\partial y^2} D_y^{(2)}(x, y). \tag{2.3}$$

The coefficients $D_x^{(1)}(x,y)$ and $D_x^{(2)}(x,y)$ are the drift and diffusion coefficients in x and $D_y^{(1)}(x,y)$ and $D_y^{(2)}(x,y)$ are the equivalent coefficients for y, and derivatives act on everything to their right. It is assumed that the y variable decays much faster than x. This is indicated by the decay rate γ which characterises the difference in timescales between the two terms on the right-hand side of (2.1) and separates the dynamics of the two variables. At times large compared to the decay time (γ^{-1}) of the variable y, the process described by (2.1) will be determined by the dynamics of the slow variable x, as y will have relaxed to an equilibrium value. The equation of motion for the distribution of the slow variable is derived with this assumption. The derivation relies on the expansion of the joint distribution for x, y and t into a complete set with respect to y.

The auxiliary problem that provides a suitable basis for expansion is the eigenvalue problem for the operator $\mathcal{L}_y$:

$$\mathcal{L}_y(x,y)\phi_n(y,x) = -\lambda_n(x)\phi_n(y,x), \tag{2.4}$$

with eigenvalues $\lambda_n(x)$ and eigenfunctions $\phi_n(y,x)$ that may depend on x. If the eigenfunctions are assumed to be normalised, they are orthonormal:

$$\int \phi_n^\dagger(x,y)\phi_m(x,y)\mathrm{d}y = \delta_{nm}, \tag{2.5}$$

where $\phi_n^\dagger(x,y)$ are the eigenfunctions of the adjoint operator $\mathcal{L}_y^\dagger$. The set of eigenfunctions is assumed to be complete so that

$$\sum_{n=0}^{\infty} \phi_n^\dagger(x,y)\phi_n(x,y') = \delta(y-y'). \tag{2.6}$$

It is also assumed that a stationary distribution exists for every x. Then $\lambda_0 = 0$ and the $n = 0$ eigenfunction gives the stationary solution

$$\phi_0(x,y) = P_{st}(x,y); \quad \phi_0^\dagger(x,y) = 1. \tag{2.7}$$

In order to eliminate y from the Fokker-Planck equation (2.1), the probability distribution is expanded in a series of the eigenfunctions of the operator $\mathcal{L}_y$ as

$$P(x,y;t) = \sum_{n=0}^{\infty} c_n(x,t)\phi_n(x,y). \tag{2.8}$$

This amounts to an expansion about the stationary state at $n = 0$. Substituting this expansion into (2.1), then multiplying the result by $\phi_n^\dagger$ and integrating over y, yields an infinite system of coupled differential equations for the expansion coefficients

$$\left[\frac{\partial}{\partial t} + \gamma\lambda_n(x)\right] c_n = \sum_{m=0}^{\infty} \mathcal{L}_{n,m} c_m(x,t), \tag{2.9}$$

where

$$\mathcal{L}_{n,m} = \int \phi_n^\dagger(x,y)\mathcal{L}_x(x,y)\phi_m(x,y)\mathrm{d}y \tag{2.10}$$

are operators with respect to x. Note that the set of equations (2.9) is exact. For $n = 0$,

$$\dot{c}_0 = \sum_{m=0}^{\infty} \mathcal{L}_{0,m} c_m. \tag{2.11}$$

Already from the exact equations (2.9) and (2.11), it can be seen that $c_0(x,t)$ is a conserved quantity, as the right-hand-side of (2.11) only contains spatial derivatives. In (2.9) we see that for $n \geq 1$, since $\lambda_n(x) > 0$, there is necessarily damping for these coefficients.

From (2.5), (2.7) and (2.8), one sees that c_0 is the distribution function for the slow variable

$$c_0(x,t) = \int P(x,y,t)\mathrm{d}y \equiv \rho(x,t). \tag{2.12}$$

For $n \geq 1$, the time derivative in (2.9) is neglected by considering timescales that are large compared to the relaxation time $(\gamma\lambda)^{-1}$. This gives

$$c_n = [\gamma\lambda_n]^{-1} \sum_{m=0}^{\infty} \mathcal{L}_{n,m} c_m. \tag{2.13}$$

Clearly, not all the expansion coefficients are independent. Finally, using (2.13) in (2.11), keeping only the leading order contribution to (2.13), which comes from the $m = 0$ term, as all other terms contribute an additional factor of γ^{-1} and setting $c_0 \to \rho$, the equation of motion for the distribution function for the remaining slow variable is then

$$\dot{\rho} = \left[\mathcal{L}_{0,0} + \gamma^{-1} \sum_{n=1}^{\infty} \mathcal{L}_{0,n} \left[\lambda_n(x)\right]^{-1} \mathcal{L}_{n,0} + \mathcal{O}(\gamma^{-2})\right] \rho. \tag{2.14}$$

It is straightforward to determine the operator $\mathcal{L}_{0,0}$ from (2.10), given that $\phi_0(x,y) = P_{st}(x,y)$ and $\phi_0^\dagger(x,y) = 1$. The second term on the right-hand-side requires knowledge of the remaining eigenvalues and eigenfunctions of $\mathcal{L}_y(x,y)$ and analytic calculation of the matrix elements. Nonetheless, this simple example demonstrates how the infinite hierarchy of equations for the expansion coefficients can be truncated in the large time limit.

It is possible that due to the structure of the system of coupled equations that only a finite number of nearest-neighbour coefficients are coupled. This is generally the case if the drift and diffusion coefficients are rational functions of x. In the example that follows, we will find that the coupling is *tridiagonal* so that each coefficient is only coupled to the neighbouring one above and below.

2.4 Expansion in irreducible tensors

2.4.1 Overview

In this section we will discuss the series expansion of the joint probability distribution for a stochastic system with coupled position $\boldsymbol{r}$ and orientation $\hat{\boldsymbol{n}}$ vectors. The expansion will be in the basis of eigenfunctions of the rotational Laplacian (to be compared to $\mathcal{L}_y$). This is a harmonic expansion: in $3d$, the eigenfunctions are the spherical harmonics and in $2d$ the eigenfunctions are the Fourier sine and cosine series. However, we will use their Cartesian tensorial equivalents, which have useful tensorial properties that will simplify our calculations.

2.4.2 The basis of irreducible tensors

Any function of orientation parameterised by angles (θ,ϕ) can be written as a power series in the orientation unit vector $\hat{\boldsymbol{n}}$ as

$$\begin{aligned} F(\hat{\boldsymbol{n}}) &= Q^{(0)} + Q_i^{(1)}\hat{n}_i + Q_{i_1 i_2}^{(2)}\hat{n}_{i_1}\hat{n}_{i_2} + \cdots + Q_{i_1 i_2 \cdots i_l}^{(l)}\hat{n}_{i_1}\hat{n}_{i_2}\cdots\hat{n}_{i_l} \\ &= \sum_{l=0}^{\infty} Q_{i_1 i_2 \cdots i_l}^{(l)}\hat{n}_{i_1}\hat{n}_{i_2}\cdots\hat{n}_{i_l} \end{aligned} \tag{2.15}$$

[70]. In 2 and 3d, $\hat{\boldsymbol{n}}$ is given by

$$\hat{\boldsymbol{n}} = \sin\theta \boldsymbol{e}_1 + \cos\theta \boldsymbol{e}_2; \quad \hat{\boldsymbol{n}} = \sin\theta\cos\phi \boldsymbol{e}_1 + \sin\theta\sin\phi \boldsymbol{e}_2 + \cos\theta \boldsymbol{e}_3. \tag{2.16}$$

The summation convention is used so that repeated indices are summed from 1 to the dimensionality d of the underlying Cartesian basis, and $Q^{(l)}_{i_1 i_2 \cdots i_l}$ are the components of a rank l irreducible tensor. The zeroth order irreducible tensor $Q^{(0)}$ is a scalar, the first order tensor $Q^{(1)}_i$ is a vector and the second order tensor $Q^{(2)}_{i_1 i_2}$ is a matrix. The construction of (2.15) in terms of irreducible tensors is allowed because any generic tensor of rank l can be decomposed into a linear combination of irreducible tensors of rank no higher than l [71]. The tensors are symmetric in all indices so that

$$Q^{(l)}_{i_1 i_2 \cdots i_l} = Q^{(l)}_{j_1 j_2 \cdots j_l},$$

where $\{j_1 j_2 \cdots j_l\}$ is any permutation of $\{i_1 i_2 \cdots i_l\}$. They are traceless in the sense that if any two indices are set equal and summed, the result is equal to zero:

$$Q^{(l)}_{i_1 i_2 \cdots i_{l-2} j j} = 0.$$

Hence, the tensors are *irreducible*, as a tensor of lower order cannot be formed by contraction of their indices.

As in the example in the previous section, each term in (2.15) is an eigenfunction of the rotational Laplacian $\boldsymbol{\mathcal{R}}^2$ with eigenvalue $-l(l+1)$ in $3d$ and $-l^2$ in $2d$, where the rotational gradient is defined as $\boldsymbol{\mathcal{R}} \equiv \hat{\boldsymbol{n}} \times \frac{\partial}{\partial \hat{\boldsymbol{n}}}$ [72] and satisfies $\mathcal{R}_i \hat{n}_j = -\epsilon_{ijk} n_k$ in $3d$. To show that

$$\boldsymbol{\mathcal{R}}^2 \left[Q^{(l)}_{i_1 i_2 \cdots i_l} \hat{n}_{i_1} \hat{n}_{i_2} \cdots \hat{n}_{i_l} \right] = -l(l+1) Q^{(l)}_{i_1 i_2 \cdots i_l} \hat{n}_{i_1} \hat{n}_{i_2} \cdots \hat{n}_{i_l} \tag{2.17}$$

in $3d$, we calculate the action of the rotational Laplacian on the third term in (2.15) and deduce the action on all other terms. The rotational gradient of $\hat{n}_j \hat{n}_k$ is

$$\mathcal{R}_i \hat{n}_j \hat{n}_k = -\epsilon_{ijl} \hat{n}_l \hat{n}_k - \epsilon_{ikl} \hat{n}_j \hat{n}_l, \tag{2.18}$$

leading to the Laplacian

$$\boldsymbol{\mathcal{R}}^2 \hat{n}_j \hat{n}_k = -6 \left(\hat{n}_j \hat{n}_k - \frac{1}{3} \delta_{jk} \right). \tag{2.19}$$

Hence

$$\boldsymbol{\mathcal{R}}^2 \left[Q^{(2)}_{jk} \hat{n}_j \hat{n}_k \right] = -6 Q^{(2)}_{jk} \hat{n}_j \hat{n}_k, \tag{2.20}$$

since $Q^{(2)}_{jk} \delta_{jk} = 0$. Given that any symmetric tensor can be written as the sum of a diagonal tensor and an irreducible tensor as in the following example for the matrix A_{ij}:

$$\frac{1}{2}(A_{ij} + A_{ji}) = [A_{ij}]^{TS} + \frac{1}{d} A_{kk} \delta_{ij} \tag{2.21}$$

where the first time on the right-hand-side is the irreducible part, and that the product $\hat{n}_j \hat{n}_k$ is a component of a symmetric matrix, we have that the right-hand-side of (2.19) is proportional to an irreducible matrix. Similarly, the product $\hat{n}_{i_1} \hat{n}_{i_2} \dots \hat{n}_{i_l}$ is a component of a rank l symmetric tensor, and thus, it can be decomposed into an irreducible part and a diagonal part. As in (2.20), the product of the coefficients $Q^{(l)}_{i_1 i_2 \cdots i_l}$ with the diagonal contributions vanishes, since the coefficients are irreducible tensors. Thus, we have the result that the rotational Laplacian must be proportional to $Q^{(l)}_{i_1 i_2 \cdots i_l} \hat{n}_{i_1} \hat{n}_{i_2} \dots \hat{n}_{i_l}$ for all l. The numerical prefactor is determined from a counting argument: from the example it is clear that in $3d$, the rotational gradient of $\hat{n}_{i_1} \hat{n}_{i_2} \dots \hat{n}_{i_l}$ will produce l terms similar to (2.18) as the gradient acts on l independent components. For the Laplacian, the second $\mathcal{R}_i$ acts on the $(l+1)$ independent components to the right of it for each of the l terms, including the $\hat{\boldsymbol{n}}$ from the first rotational gradient, giving a prefactor of $-l(l+1)$. A similar consideration gives the prefactor of $-l^2$ in $2d$. Putting everything together gives the result (2.17).

The spherical harmonics and Fourier sine and cosine series are eigenfunctions of $\boldsymbol{\mathcal{R}}^2$ with the same eigenvalues as the terms in the expansion (2.15). Furthermore, a counting argument shows that there are $2l+1$ irreducible tensors of rank l in $3d$, which is the same as the number of spherical harmonics. It follows that the standard harmonic expansion is equivalent to (2.15) where a choice of basis for the $2l+1$ independent irreducible tensors leads to the spherical harmonics [70].

When there is azimuthal symmetry, the irreducible tensors are proportional to the Legendre polynomials.

We now construct some irreducible tensors. Generalising (2.21), a rank l irreducible tensor can be constructed from the symmetric tensors $\hat{n}_{i_1}\hat{n}_{i_2}\ldots\hat{n}_{i_l}$ by subtracting the diagonal part. Following this protocol, the first six irreducible tensors in $d = 2$ or 3 are:

$$D^{(0)} = 1; \tag{2.22}$$

$$D^{(1)}_i = \hat{n}_i; \tag{2.23}$$

$$D^{(2)}_{ij} = \hat{n}_i\hat{n}_j - \frac{1}{d}\delta_{ij}; \tag{2.24}$$

$$D^{(3)}_{ijk} = \hat{n}_i\hat{n}_j\hat{n}_k - \frac{1}{d+2}\left(\hat{n}_i\delta_{jk} + \hat{n}_j\delta_{ik} + \hat{n}_k\delta_{ij}\right); \tag{2.25}$$

$$\begin{aligned} D^{(4)}_{ijkl} &= \hat{n}_i\hat{n}_j\hat{n}_k\hat{n}_l + \frac{1}{(d+2)(d+4)}\Delta_{ijkl} \\ &- \frac{1}{d+4}\left(\hat{n}_i\hat{n}_j\delta_{kl} + \hat{n}_i\hat{n}_k\delta_{jl} + \hat{n}_i\hat{n}_l\delta_{jk} + \hat{n}_j\hat{n}_k\delta_{il} + \hat{n}_j\hat{n}_l\delta_{ik} + \hat{n}_k\hat{n}_l\delta_{ij}\right); \end{aligned} \tag{2.26}$$

$$\begin{aligned} D^{(5)}_{ijklm} &= \hat{n}_i\hat{n}_j\hat{n}_k\hat{n}_l\hat{n}_m \\ &- \frac{1}{d+6}\left(\hat{n}_i\hat{n}_j\hat{n}_k\delta_{lm} + \hat{n}_i\hat{n}_j\hat{n}_l\delta_{km} + \hat{n}_i\hat{n}_j\hat{n}_m\delta_{lk} + \hat{n}_j\hat{n}_k\hat{n}_l\delta_{im}\right. \\ &\left.+\hat{n}_j\hat{n}_l\hat{n}_m\delta_{ik} + \hat{n}_k\hat{n}_l\hat{n}_m\delta_{ij} + \hat{n}_k\hat{n}_l\hat{n}_i\delta_{jm} + \hat{n}_k\hat{n}_m\hat{n}_i\delta_{jl} + \hat{n}_k\hat{n}_m\hat{n}_j\delta_{il} + \hat{n}_l\hat{n}_m\hat{n}_i\delta_{jk}\right) \\ &+ \frac{1}{(d+4)(d+6)}\left(\hat{n}_i\Delta_{jklm} + \hat{n}_j\Delta_{iklm} + \hat{n}_k\Delta_{ijlm} + \hat{n}_l\Delta_{ijkm}\right. \\ &\left.+\hat{n}_m\Delta_{ijkl}\right), \end{aligned} \tag{2.27}$$

where $D^{(l)}$ is an irreducible tensor of rank l and

$$\Delta_{ijkl} = (\delta_{ij}\delta_{kl} + \delta_{ik}\delta_{jl} + \delta_{il}\delta_{jk}) \tag{2.28}$$

satisfies $\Delta_{iijk} = (d+2)\delta_{jk}$ and $\Delta_{iijj} = d(d+2)$.

2.4.3 The general moment expansion

Using (2.15), the joint distribution for position, orientation and time has an exact expansion in the basis of irreducible tensors, given by

$$P(\boldsymbol{r}, \hat{\boldsymbol{n}}; t) = \sum_{l=0}^{\infty} Q^{(l)}_{i_1 i_2 \cdots i_l}(\boldsymbol{r}, t)\hat{n}_{i_1}\hat{n}_{i_2}\cdots\hat{n}_{i_l}. \tag{2.29}$$

In (2.29), the irreducible tensors are now tensor-valued functions of position and time. An important property of irreducible tensors is the following:

$$AB^{TS} = A^{TS}B = A^{TS}B^{TS}, \tag{2.30}$$

where A and B are tensors of the same dimensionality and A^{TS}, B^{TS} are their irreducible parts. Using this, we are free to choose the product $\hat{n}_{i_1}\hat{n}_{i_2}\dots\hat{n}_{i_l}$ in (2.29) to be the irreducible part.

Finally, from the orthogonality and completeness of the irreducible tensors, the expansion coefficients of (2.29) are given by

$$Q^{(l)}_{j_1 j_2 \cdots j_l}(\boldsymbol{r},t)\int \mathrm{d}\hat{\boldsymbol{n}}\, D^{(l)}_{j_1 j_2 \cdots j_l}(\hat{\boldsymbol{n}}) D^{(l)}_{i_1 i_2 \cdots i_l}(\hat{\boldsymbol{n}}) = \int \mathrm{d}\hat{\boldsymbol{n}}\, D^{(l)}_{i_1 i_2 \cdots i_l} P(\boldsymbol{r},\hat{\boldsymbol{n}};t) = \left(D^{(m)}_{i_1 i_2 \cdots i_m}, P\right) \tag{2.31}$$

[58]. The scalar product of orientation-dependent functions is defined as

$$(A,B) = \int \mathrm{d}\hat{\boldsymbol{n}} A(\hat{\boldsymbol{n}}) B(\hat{\boldsymbol{n}}), \tag{2.32}$$

where the integral is over a sphere of unit radius [73]. In this notation, we have the following relations

$$\begin{aligned}
(\hat{n}_i, \hat{n}_j) &= \frac{\Omega}{d}\delta_{ij} \\
(\hat{n}_i\hat{n}_j, \hat{n}_k\hat{n}_l) &= \frac{\Omega}{d(d+2)}\Delta_{ijkl}, \\
\left(D^{(2)}_{ij}, D^{(2)}_{kl}\right) &= \frac{\Omega}{d(d+2)}\left(\delta_{ik}\delta_{jl} + \delta_{il}\delta_{jk} - \frac{2}{d}\delta_{ij}\delta_{kl}\right),
\end{aligned} \tag{2.33}$$

where Ω is the solid angle of the unit d-dimensional sphere [60]. Thus, the first three moments of the probability distribution are given by

$$\begin{aligned}
(1, P(\boldsymbol{r},\hat{\boldsymbol{n}};t)) &= \Omega\rho(\boldsymbol{r},t), \\
(\hat{n}_i, P(\boldsymbol{r},\hat{\boldsymbol{n}};t)) &= \frac{\Omega}{d}p_i(\boldsymbol{r},t), \\
\left(D^{(2)}_{ij}, P(\boldsymbol{r},\hat{\boldsymbol{n}};t)\right) &= \frac{\Omega}{d}\frac{2}{d+2}Q_{ij}(\boldsymbol{r},t).
\end{aligned} \tag{2.34}$$

The coefficients ρ, $\boldsymbol{p}$ and $\mathbf{Q}$ are the renamed scalar, vector and matrix multipole moments $Q^{(0)}$, $Q^{(1)}_i$ and $Q^{(2)}_{ij}$.

2.5 Example: Active Brownian Particles

As a first complete example, we now describe the moment expansion for the simple case of ABPs using the results of Sections 2.3 and 2.4. In the idealised spherical ABP model, each particle is driven by a constant external force along its swimming direction and undergoes continuous reorientation due to rotational diffusion. In the absence of any aligning interactions, it is clear that the particles exert no torque and, if there are no other particles or the particle density is low, the propulsion force is equal and opposite to the drag force on a moving particle so that they also experience no net force. In the basic model, as in this example, the drag force acts on a single particle– interactions between particles and the hydrodynamics of a solvent are not considered.

The translations and rotations of a single ABP with constant propulsion speed v are given by the following Langevin equations

$$\frac{\mathrm{d}}{\mathrm{d}t}\boldsymbol{r}(t) = v\hat{\boldsymbol{n}}(t) + \boldsymbol{\xi}(t); \quad \frac{\mathrm{d}}{\mathrm{d}t}\hat{\boldsymbol{n}}(t) = \boldsymbol{\chi}(t) \tag{2.35}$$

where $\boldsymbol{r}(t)$ and the unit vector $\hat{\boldsymbol{n}}(t)$ are the position and orientation of the particle. The first equation is both deterministic and random, while the second equation describes purely random motion on the surface of a d-dimensional unit sphere. The stochastic dynamics due to thermal fluctuations is characterised by zero-mean Gaussian white noises $\boldsymbol{\xi}(t)$ and $\boldsymbol{\chi}(t)$, whose correlations are given by

$$\langle \xi_i(t)\xi_j(t')\rangle = 2D_t\delta_{ij}\delta(t-t'); \quad \langle \chi_i(t)\chi_j(t')\rangle = 2D_r\delta_{ij}\delta(t-t') \text{ and } \langle \chi_i(t)\xi_j(t')\rangle = 0, \tag{2.36}$$

where D_t and D_r are respectively the translational and rotational diffusivities of the particle and the average is over the stochastic trajectories. For spherical particles of radius a, the diffusivities are given by the Einstein relation: $D_t = k_\mathrm{B}T/6\pi\eta a$ and $D_r = k_\mathrm{B}T/8\pi\eta a^3$, where T is the temperature of the suspending medium and η its viscosity.

We define the probability of finding the particle at position $\boldsymbol{r}$ moving in direction $\hat{\boldsymbol{n}}$ at time t by the distribution

$$P(\boldsymbol{r}, \hat{\boldsymbol{n}}; t) = \langle \delta(\boldsymbol{r} - \boldsymbol{r}(t)) \delta(\hat{\boldsymbol{n}} - \hat{\boldsymbol{n}}(t)) \rangle \,, \tag{2.37}$$

where the average is again over the stochastic trajectories and the distribution is normalised by $\int \mathrm{d}\boldsymbol{r}\, \mathrm{d}\hat{\boldsymbol{n}} P(\boldsymbol{r}, \hat{\boldsymbol{n}}; t) = 1$. Then eq. (2.35) corresponds to the following Smoluchowski equation

$$\frac{\partial}{\partial t} P(\boldsymbol{r}, \hat{\boldsymbol{n}}; t) = -\nabla \cdot [v \hat{\boldsymbol{n}} P] + \nabla \cdot [D_t \nabla P] + \boldsymbol{\mathcal{R}} \cdot [D_r \boldsymbol{\mathcal{R}} P], \tag{2.38}$$

describing the evolution of the probability distribution. In (2.38), ∇ is the gradient with respect to position $\boldsymbol{r}$. The first term on the right-hand-side is the divergence of the advective current due to self-propulsion and the last two terms are due to translational and rotational diffusion.

2.5.1 Moment expansion

The following derivation of the hydrodynamic equations for ABPs using the moment expansion of the probability distribution follows [59, 60, 73]. For an unconfined particle, the relevant length- and timescales beyond which this is a valid continuum description is at distances larger than the particle size and for times greater than the angular reorientation time $1/D_r$.

In the basis of irreducible tensors, the probability distribution has the following expansion

$$P(\boldsymbol{r}, \hat{\boldsymbol{n}}; t) \simeq \rho(\boldsymbol{r}, t) + p_i(\boldsymbol{r}, t) \hat{n}_i + Q_{ij}(\boldsymbol{r}, t)(\hat{n}_i \hat{n}_j - \delta_{ij}/d), \tag{2.39}$$

with only the first three terms of (2.29) being shown. The evolution equations for the three moments are obtained by the same procedure as was used to derive (2.9): substituting eq. (2.39) for P in the Fokker-Planck equation (2.38) and taking the scalar product with the first three irreducible tensors.

From the definitions of the moments in eq. (2.34) and using orthogonality of the irreducible tensors, the equation for the zeroth moment is

$$\dot{\rho}(\boldsymbol{r}, t) = -\frac{1}{d} \nabla \cdot [v \boldsymbol{p}] + \nabla \cdot [D_t \nabla \rho]. \tag{2.40}$$

This is an expression of the local conservation of probability density.

The scalar product of (2.38) with $\hat{\boldsymbol{n}}$ gives

$$\frac{\Omega}{d}\dot{\boldsymbol{p}}(\boldsymbol{r},t) = -\left(\hat{\boldsymbol{n}}, \nabla\cdot[v\hat{\boldsymbol{n}}P]\right) + D_r\left(\hat{\boldsymbol{n}}, \boldsymbol{\mathcal{R}}^2 P\right) + \nabla\cdot[D_t\nabla\left(\hat{\boldsymbol{n}}, P\right)]. \tag{2.41}$$

Since the diffusion coefficients are independent of the local orientation. We evaluate the scalar products individually. For the first term on the right-hand-side

$$\begin{aligned}\left(\hat{n}_i, \partial_j[v\hat{n}_j P]\right) &= \partial_j v\left(\hat{n}_i, \hat{n}_j P\right)\\ &= \partial_j v\left(D_{ij}, P\right) + \frac{1}{d}\partial_j v\delta_{ij}\left(1, P\right)\\ &= \frac{\Omega}{d}\frac{2}{d+2}\partial_j v Q_{ij} + \frac{\Omega}{d}\partial_i v\rho,\end{aligned} \tag{2.42}$$

using the definition of D_{ij} to obtain the second line. ∂_i is the ith component of the gradient with respect to $\boldsymbol{r}$. For the second term, we use the fact that irreducible tensors are eigenvectors of $\boldsymbol{\mathcal{R}}^2$ and orthogonality of the basis. In $d = 2$ or 3 this gives

$$D_r\left(\hat{\boldsymbol{n}}, \boldsymbol{\mathcal{R}}^2 P\right) = -D_r(d-1)\frac{\Omega}{d}\boldsymbol{p}, \tag{2.43}$$

since $l(l+1) = d-1$. Finally,

$$\nabla\cdot[D_t\nabla\left(\hat{\boldsymbol{n}}, P\right)] = \frac{\Omega}{d}\nabla\cdot[D_t\nabla\boldsymbol{p}]. \tag{2.44}$$

Altogether, we find that

$$\dot{p}_i = -\partial_i(v\rho) - D_r(d-1)p_i + \partial_j[D_t\partial_j p_i] - \frac{2}{d+2}\partial_j(vQ_{ij}). \tag{2.45}$$

The first term on the right-hand-side can be interpreted as a pressure gradient and, it is this term that is responsible for density instabilities in the collective dynamics of self-propelled systems, that are caused by the growth of fluctuations in the density field $\delta\rho(\boldsymbol{r},t)$ [62, 63]. The case of a density dependent self-propulsion speed– specifically where the speed is a decreasing function of the local density– has been studied and shown to lead to pattern formation and phase separation [62, 74]. From the second term we see that the first moment is not conserved. Note the hierarchical structure of the moment equations: It is clear from the independence

of the drift and diffusion coefficients on orientation that the first moment should only be coupled to the zeroth and second order moments.

Similarly, the scalar product of (2.38) with D_{ij} is

$$\frac{\Omega}{d}\frac{2}{d+2}\dot{Q}_{ij} = -\left(D_{ij}^{(2)}, \nabla\cdot[v\hat{\boldsymbol{n}}P]\right) + D_r\left(D_{ij}^{(2)}, \boldsymbol{\mathcal{R}}^2 P\right) + \nabla\cdot\left[D_t\nabla\left(D_{ij}^{(2)}, P\right)\right]. \tag{2.46}$$

The first term on the right-hand-side evaluates to

$$\begin{aligned}\left(D_{ij}^{(2)}, \nabla\cdot[v\hat{\boldsymbol{n}}P]\right) &= \partial_k v\left(D_{ij}^{(2)}, n_k P\right)\\ &= \frac{\Omega}{d}\frac{1}{d+2}\partial_k v\left(p_i\delta_{jk} + p_j\delta_{ik} - \frac{2}{d}p_k\delta_{ij}\right) + \frac{\Omega}{d}\partial_k v\left(D_{ijk}^{(3)}, P\right),\end{aligned} \tag{2.47}$$

where the second line follows from the definition of the rank 3 irreducible tensor $D_{ijk}^{(3)}$. For the second term

$$D_r\left(D_{ij}^{(2)}, \boldsymbol{\mathcal{R}}^2 P\right) = -2dD_r\frac{\Omega}{d}\frac{2}{d+2}Q_{ij}, \tag{2.48}$$

since D_{ij} is an eigenvector of $\boldsymbol{\mathcal{R}}^2$ with eigenvalue $-2d$ in $d = 2$ and 3. The final term to be evaluated is

$$\nabla\cdot\left[D_t\nabla\left(D_{ij}^{(2)}, P\right)\right] = \frac{\Omega}{d}\frac{2}{d+2}\nabla\cdot[D_t\nabla Q_{ij}]. \tag{2.49}$$

Finally, combining the results for the scalar products gives

$$\begin{aligned}\dot{Q}_{ij} = &-\frac{1}{2}\partial_k v\left(p_i\delta_{jk} + p_j\delta_{ik} - \frac{2}{d}p_k\delta_{ij}\right) - \frac{d+2}{2}\partial_k\left[v\left(D_{ijk}^{(3)}, P\right)\right] - 2dD_rQ_{ij}\\ &+ \nabla\cdot[D_t\nabla Q_{ij}],\end{aligned} \tag{2.50}$$

where the scalar product $\left(D_{ijk}^{(3)}, P\right)$ is proportional to the third harmonic, Q_{ijk}.

So far, eqs. (2.40), (2.45) and (2.50) are the exact evolution equations for the first three moments of the probability distribution. To describe the dynamics of an ABP in the continuum limit, we perform a coarse graining of the moment equations. From eq. (2.40) we see that ρ is a hydrodynamic variable as density fluctuations are not damped by the dynamics. $\boldsymbol{p}$ and $\mathbf{Q}$ however, are damped and their relaxation times are of the order of the reorientation time, $1/D_r$. Hence, at times much larger than $1/D_r$, we assume that the first and second moments

have equilibrated so that $\dot{\boldsymbol{p}} = \dot{\mathbf{Q}} = 0$, as are the time derivatives for all higher order moments (as in (2.13)). The large length-scale assumption allows us to neglect higher order derivatives in eqs. (2.45) and (2.50). In this limit, we have the following closed expressions for $\boldsymbol{p}$ and $\mathbf{Q}$

$$Q_{ij} = -\frac{1}{4dD_r}\partial_k v \left(p_i\delta_{jk} + p_j\delta_{ik} - \frac{2}{d}p_k\delta_{ij} \right), \tag{2.51}$$

$$p_i = -\frac{\partial_i(v\rho)}{D_r(d-1)}. \tag{2.52}$$

The derivation of Q_{ij} has been included for completeness, in the absence of aligning forces that can provide a mechanism for nematic ordering, we can set $Q_{ij} = 0$.

Finally, inserting (2.52) into the continuity equation (2.40) gives the following diffusion equation for the large length- and timescale dynamics

$$\dot{\rho} = -\nabla \cdot \left[-D_{\text{eff}}\nabla\rho + \mathbf{v}_{\text{eff}}\rho \right], \tag{2.53}$$

with effective diffusion coefficient and velocity

$$D_{\text{eff}} = D_t + \frac{v^2}{D_r d(d-1)}; \quad \mathbf{v}_{\text{eff}} = -\frac{v\nabla v}{D_r d(d-1)}. \tag{2.54}$$

In the hydrodynamic limit, the translational diffusion of the ABP is enhanced by an amount that is proportional to the square of the constant self-propulsion velocity. To resolve the dynamics below the large length-scale approximation used to close the hierarchy in the moment equations, higher order gradients must be included in the expressions for the moments. While the moment equations can be solved numerically, it should be highlighted that the analytic approach has some advantages. Firstly, the analytic equations provide a route to studying the stability of stationary states against perturbations. Furthermore, the hydrodynamic equations could be numerically integrated to study larger systems than are accessible with direct simulations of particles.

In the next chapter we will consider the more general case of dynamics that is not isotropic. With our model enzyme we provide an example of a system where the transport coefficients depend on the local orientation $\hat{\boldsymbol{n}}$. This dependence arises not

because of an external force but rather because of the geometric complexity of the enzyme and fluid-mediated hydrodynamic interactions, which also couple its position and orientation variables. In addition to the position $\boldsymbol{r}$ and orientation $\hat{\boldsymbol{n}}$, the model includes other microscopic degrees of freedom which represent the internal dynamics of a real enzyme. We must therefore extend the moment expansion to multiple domains.

CHAPTER 3

Enhanced diffusion and fluctuation-induced hydrodynamic coupling

3.1 Introduction

3.1.1 Experimental Observations

In vitro experiments on suspensions of the enzyme urease, using fluorescence correlation spectroscopy (FCS)[1], revealed that its diffusion coefficient is enhanced when placed in a uniform concentration of its substrate. Furthermore, that the enhancement increases with increasing substrate concentration– following a Michaelis-Menten-like dependence on the concentration [28]. Similar experiments followed for several other enzymes such as catalase [29], DNA polymerase [30] and alkaline phosphatase [31], with the same outcome of the diffusion coefficient of the enzymes being up to 80% higher in a solution containing their substrate. Enhanced diffusion in the presence of substrate has also been observed in nano particles that are decorated with the enzymes urease, catalase and glucose oxidase [76]. A study of the dynamics of enzymes in the Krebs cycle, an essential series of chemical reactions for metabolism, opens up the possibility of a role for the phenomenon in biological self-organisation such as the formation of metabolic structures [23].

[1] A method that is used to measure the diffusion coefficient of molecules in typically dilute conditions using fluorescent labelling [75].

All the enzymes mentioned so far have the common features that they catalyse exothermic reactions and have a high catalytic rate.

Following a suggestion by Riedel et al. that the enhancement in diffusivity could be linked to the enthalpy of the reaction catalysed by the enzyme [31], FCS experiments on the enzyme aldolase, which catalyses endothermic reactions and has a low catalytic rate, reported enhanced diffusion for it also in the presence of its substrate [26]. Even more remarkable, was the observation that the diffusivity of aldolase also increased in the presence of an inhibitor which binds reversibly to the active site without being converted into product. The measurements on aldolase put into question the necessity of the catalytic step for observing enhanced diffusion and the role of thermodynamics and kinetics in enhanced enzyme diffusion. Table 3.1 shows the range in the thermodynamic and kinetic properties of some of the enzymes that have been reported to display substrate-driven enhanced diffusion.

Enzyme	$k_{\text{cat}}\,(s^{-1})$	ΔQ (kJ mol^{-1})	$D_0\,(\mu m^2/s)$	$\Delta D/D_0$	Ref.
Urease	2×10^4	-59.6	31.8	0.28	[28, 31]
Catalase	5.8×10^4	-100	61	0.3	[31]
Alkaline phosphatase	1.4×10^4	-43.5	NM	0.8	[31]
Acetylcholinesterase	NM	NM	22	0.23	[77]
Hexokinase	200	NM	72.4	0.46	[22, 78]
Aldolase	5	30-60	42.6	0.31	[26]

Table 3.1. Experimental data on enzymes that have been reported to show significant enhanced diffusion. Adapted from ref. [31, 79]. NM: not mentioned.

3.1.2 Models of Enhanced Diffusion

A number of suggestions have been put forward as possible mechanisms to explain the substrate-driven enhanced diffusion of enzymes, broadly falling into the two categories of active and passive mechanisms. Initial proposals favoured active mechanisms which rely on the non-equilibrium step of the catalytic cycle. These have been reviewed by Golestanian [37]. For the first mechanism which depends on the heat released in exothermic reactions, Riedel et al. suggested that the heat from the catalytic cycle is converted into a boost in kinetic energy through the generation

of asymmetric compressions of the enzyme [31]. However, this disproportionate partitioning of the energy from the reaction into only some of the degrees of freedom of the enzyme is not justified, and an estimate of the relative change in diffusion coefficient is four orders of magnitude below the reported values [37]. The possibility that the intrinsic asymmetry of an enzyme creates gradients in temperature (due to the heat released during the catalytic cycle) and substrate concentration across the enzyme that can induce self-phoresis has also been studied. However, the contribution from such a phoretic mechanism was again shown to produce an enhancement of many orders of magnitude below the reported values due to the large rotational diffusion coefficient of nm-size enzymes [37]. Also relying on the heat released in catalytic reactions is the suggestion that enhanced diffusion is due to collective heating of the suspension causing increased fluctuations and a decrease in the viscosity of the suspending fluid [37]. Although the mechanism leads to enhancement values that are comparable to experimental figures, no evidence of collective heating was found in experiments with urease [7].

In a proposal where the enhancement in diffusivity is not related to the exothermicity of enzymatic reactions, an enzyme is modelled as a stochastic swimmer [37]. In the model, conformational changes in the enzyme due to the catalytic cycle, leads to stochastic swimming, with an increase in the diffusion coefficient of the enzyme that is proportional to the amplitude of the conformational changes and to the catalytic rate [36, 37].

It has also been suggested that the enhanced diffusion of enzymes in the presence of substrate can be explained by their directed self-propulsion due to a stochastic force at each catalytic step, with an enhancement in diffusivity that is proportional to the catalytic rate [77]. This suggestion is comparable to that of Riedel et al. [31], with the improvement that the predicted boost is sustained over a longer period so that the predicted increase in diffusivity is more substantial. The same study also reported the observation of enhanced diffusion in the presence of inhibitors but without the ballistic behaviour of the enzymes that was observed for the substrate-driven case. A conclusion that can be drawn from the experimental reports is

that while the effect appears to follow the Michaelis-Menten kinetics for substrate dependence, it has not been shown to be dependent on the catalytic rate [79].

In a different direction, a theory based on collective effects was put forward by Mikhailov and Kapral. In their description, catalytically active enzymes are modelled as fluctuating force dipoles that are coupled through fluid-mediated hydrodynamic interactions. It is suggested that the resulting fluctuating hydrodynamic flows lead to enhanced diffusion of all objects in the suspension [35]. However, the low volume fraction of enzymes required for FCS experiments would not yield a sufficient flow in this way for enhancement that is comparable to the reported values.

In this chapter, we discuss a theoretical model for a catalytically active enzyme that has been used to demonstrate the possibility of increasing the translational diffusion coefficient without appealing to any non-equilibrium aspect of the catalytic cycle. By considering the fluid-mediated hydrodynamic interactions between the different parts of a single enzyme, we show how the internal degrees of freedom affect its overall diffusivity. We show that the diffusion coefficient of the model enzyme, after a sufficiently long time, has the generic form

$$D_{\text{eff}} = D_{\text{ave}} - \delta D_{\text{fluc}}, \tag{3.1}$$

where the first term is the equilibrium average of the contributions due to its translational modes and the second term represents fluctuation-induced corrections due to internal elongations and rotations. In the context of a mechanism for substrate-driven enhanced enzyme diffusion, we describe a proposal based on the mechanical aspect of the catalytic cycle which is an application of this model [26, 80].

3.1.3 Protein dynamics

It is generally accepted that proteins are not rigid objects but exist in a number of conformational states which are determined by environmental factors such as temperature, pH, ion concentration, or the binding of a ligand. The conformational states of a given protein can be described by a complex energy landscape [81] and has been credited to their modular structure [82]. Many highly flexible enzymes

transition to more constrained states upon binding to a substrate or inhibitor [83]. The observation of different fluorescence emission spectra for the enzyme aldolase in the presence of different substrates (see Fig.3.1), at different concentrations, signals a substrate-driven response in the observed conformational changes [84]. Transitions of the enzyme urease between open and closed states, through the motion of a "flap" in a substrate dependent manner has also been observed [85]. Conformational change can cause a change in size of up to the order of the original size of the protein [82], with the transition taking place over timescales in the range of ns to s so that statistical properties such as the diffusion coefficient, that are measured in experiments are averages over different conformations.

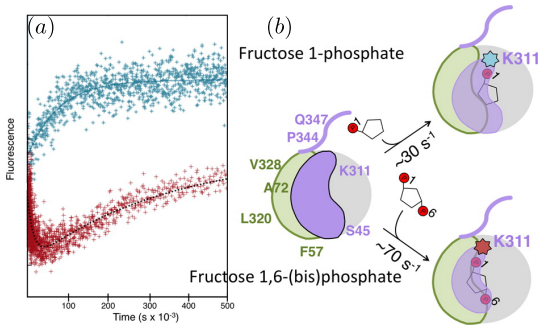

Figure 3.1. (a) Fluorescence emission spectra of the enzyme aldolase in the presence of the substrates Fructose 1,6-(bis)phosphate (red) and Fructose 1-phosphate (teal) at substrate saturation. (b) A schematic of the conformational change in the enzyme after binding to the two substrates. Reprinted with permission from ref. [84]. Copyright 2020 American Chemical Society.

There is much experimental evidence to suggest that protein dynamics has an important role in regulating the activity of enzymes [86]. It is known that some regions in proteins are more constrained than others, and the more dynamic regions have been linked to functionally and regulation [82, 87]: Flexible linkers that connect domains allow the domains to rotate in order to aid binding, and their binding induced fluctuations can propagate information of a binding event across domains [82, 88]. In addition to the effect of linkers, transitions between states can become correlated for different domains by direct interactions between the domains [89].

Given that the global fluctuations and conformational changes that accompany ligand binding at the allosteric site of an enzyme can transmit information of

the binding event to other sites, models of *allosteric effects*, which describes this propagation of information, typically appeal to the coordinated dynamics of enzyme subunits. In one of these models, it is assumed that subunits can exist in two conformations in which they are tensed or relaxed, and that conformational changes in the subunits away from an equilibrium state (which can be shifted by the binding of a ligand to the allosteric site) are necessarily symmetric. The affinity for substrate is presumed to be different for the different states, with binding typically favouring the conformation in which the subunits are relaxed and able to move freely [90]. In other models, while the conformations of subunits are correlated, they are not necessarily symmetric [91]. Hawkins and McLeish have proposed a theoretical model in which coupling of local and global modes leads to amplification of entropic allostery [92]. They show that when coupled to the global dynamics, the local modes can contribute to entropic allostery.

3.1.4 Modelling protein dynamics

To describe the diffusion properties of catalytically active enzymes in suspension, our model must include at least some of the properties of the dynamics of proteins that were mentioned in the previous section. We would like to describe a flexible object with distinct domains that is suspended in a fluid environment. Due to the large number of domains and linkers, an enzyme has many degrees of freedom. Since enzymatic environments are subject to thermal fluctuations, these degrees of freedom should be considered as random variables. Hence, statistical mechanics is required to describe the time evolution of the distribution function of the different conformational states. In the presence of a fluid, there are hydrodynamic interactions between the constituents of the enzyme. The complex and highly asymmetric geometry will result in the coupling of translational and rotational motion and the global and local modes of the enzyme are also expected to be coupled [93]. We note that these properties are generic to other macromolecules and polymer suspensions and so comparisons can be made with previous models in the polymer literature.

In the standard microscopic descriptions of the dynamics of flexible polymers, including macromolecules, each polymer is modelled as a system of spherical Brownian beads of equal size that are connected along a chain. The first model of this type was proposed by Rouse [94]. In the Rouse model, interactions between beads are localised and the Langevin equation is linear in the position of the beads. The model does not include excluded volume interactions nor the long-range hydrodynamic interactions that are important for dynamics in solution. This leads to an inconsistency between the dynamical coefficients (specifically, the translational and rotational diffusion coefficients) that are calculated in the Rouse model and the experimental values [72]. Nonetheless, it is the basis from which subsequent models of polymer dynamics have been built because of its simplicity.

The Zimm model is the extension of the Rouse model to include fluid-mediated hydrodynamic interactions between the beads that make up the polymer. They are introduced into the dynamical equations through the generalised mobility tensor, which relates the forces exerted by the beads on the fluid to the instantaneous velocity of the beads. The mobility tensor is an intrinsic property of the beads which depends only on their size and the instantaneous configuration of the polymer. Since hydrodynamic interactions are non-linear, the mobility tensor is a non-linear function of the position of the beads.

To simplify the analysis, the mobility tensor is approximated by its equilibrium configurational average in the "preaveraging" approximation [95]. This method, initially proposed by Kirkwood and Riseman [96], was used by Zimm to approximate the average statistics of a flexible chain by considering the average of many instantaneous rigid conformations. It is assumed that the distribution of the orientation vector separating two beads and the distribution of the size of the relative spacing are independent so that the mobility tensor can be linearized, and its orientation-dependence averaged. This leads to dynamics that is linear but non-local.

In the original model the mobility tensor is approximated by the equilibrium-averaged *Oseen tensor*, the Green's function for fluid motion due to a point force [72]. This provides the simplest description of the hydrodynamic interactions, as the

geometric dependence on particles is omitted. However, it may not be a very good description if the particles are too close, as the tensor may become negative, which cannot be the case as it is essentially a generalised diffusion coefficient [97]. The breakdown of the Oseen tensor at small separations is remedied by the Rotne-Prager-Yamakawa tensor (RPY) which accounts for the finite size of the particles [98].

The Zimm model has been extended to include such effects as the coupling between the motion of an entire polymer chain and its internal configuration and the effect of a constant external force on the configurations of a polymer [99]. Fluctuations in the hydrodynamic interactions of a model polymer were introduced by assuming a Gaussian form for the configurational distribution of the polymer [100, 101]. The distribution of configurations has been studied numerically to examine, in addition to diffusion properties, the rheology of model polymers, such as their behaviour under shear [72], and cyclization kinetics [102, 103].

The preaveraging approximation has been reviewed and compared to some other common methods for calculating the hydrodynamic properties of macromolecules in solution [104]; including the diagonal approximation, introduced by Garcia de la Torre and Bloomfield [105], which neglects the off-diagonal terms of the mobility tensor that couple forces and velocities along different axes[2]; and double-sum formulas, where hydrodynamic properties are calculated by taking a double sum of the friction matrix [106]. The preaveraging approximation is found to lead to typically higher errors for the diffusion coefficient and the intrinsic viscosity of rigid macromolecules.

We now propose a model to investigate effects that were previously overlooked but are expected to play a role in the dynamics of suspensions of enzyme molecules. We study the effect of fluctuation-induced hydrodynamic coupling between the domains of a model enzyme and show that it leads to a change in the diffusion coefficient in the presence of asymmetry, which is a feature of real enzyme molecules. We also study the effect of fluctuations of the orientations of the domains of the enzyme and finally, the effect of the catalytic cycle, which is expected to induce

[2]Since those terms have a higher order dependence on the inverse distance between interacting particles than the diagonal terms.

significant changes in the conformational landscape of the enzyme. To this end, we develop a theoretical framework that produces simple analytical results and is easily extendable to more elaborate models.

3.2 Model

In order to study the role of fluid-mediated hydrodynamic interactions between domains on the dynamics of an enzyme, we consider a simple model that encompasses some of the key features that were described in Section 3.1.3. The large number of internal degrees of freedom of a modular enzyme is reduced to the set of coordinates that describe the local modes of fluctuation. These are compressions due to elasticity and rotations of the domains. We construct a model that exhibits these fluctuations with a minimal number of degrees of freedom. In line with the protein models discussed in Section 3.1.4, we model an enzyme as a generalised dumbbell, which reduces the complex geometry of a real enzyme to a minimal object with two geometrically distinct subunits, which are not necessarily spherical but are assumed to be rigid. The dumbbell is suspended in an incompressible fluid that is unbounded (or we can assume that the boundaries are very far away) and the system is assumed to be at low Reynolds number, owing to the nm size of enzymes and the viscous conditions in which they function. In addition to fluid-mediated hydrodynamic coupling, the subunits are coupled through a potential U that represents steric constraints in real enzymes and sets a preferred separation between them. The instantaneous configuration of a dumbbell is specified by the positions $\boldsymbol{R}_1$ and $\boldsymbol{R}_2$ of its two subunits relative to a fixed origin, and their orientations $\hat{\boldsymbol{u}}^1$ and $\hat{\boldsymbol{u}}^2$, which undergo thermal fluctuations and are thus random variables. The model is depicted in Fig. 3.2.

3.2.1 Hydrodynamic interactions

Motion at low Reynolds number in an incompressible fluid can be described by Stokes flow. In active suspensions, coupling to the fluid has typically been treated in one of two ways. One method is to couple the equation for the fluid velocity

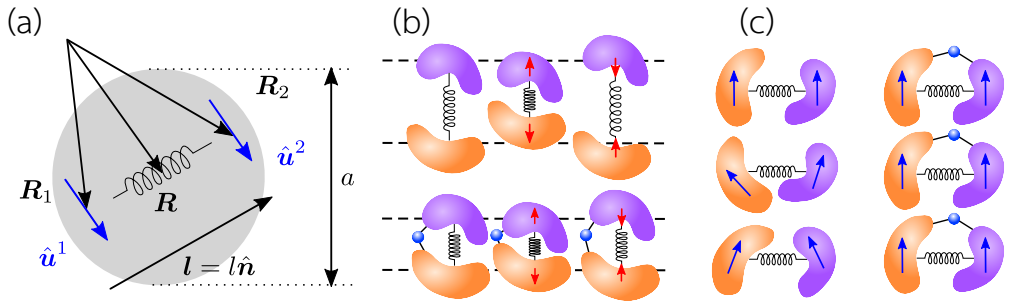

Figure 3.2. (a) A generalised dumbbell, with a typical size a in its relaxed state. It is composed of two fluctuating nonidentical subunits with positions $\boldsymbol{R}_\alpha$ and orientations $\hat{\boldsymbol{u}}^\alpha$. A constraint $U(\boldsymbol{R}_1, \boldsymbol{R}_2, \hat{\boldsymbol{u}}^1, \hat{\boldsymbol{u}}^2)$ between the subunits is represented by a spring. $\boldsymbol{R}$ and $\boldsymbol{l}$ are the centre-of-mass and relative coordinates of the dumbbell. (b) A representation of the compressional modes of the dumbbell about its equilibrium elongation. (c) A representation of orientation fluctuations about the equilibrium configuration [80, 107].

field, the Stokes equation, to the equations of motion or Smoluchowksi equation for the rest of the system. In the second method, the fluid velocity field is not included explicitly, but is considered to mediate effective two-body hydrodynamic interactions. In this thesis we use the second approach.

Fluid-mediated hydrodynamic interactions are governed by linear relations between the forces $\boldsymbol{F}_\alpha$ and torques $\boldsymbol{T}_\alpha$ exerted by the interacting particles on the fluid and their instantaneous linear and angular velocities. For our dumbbell, the response of a subunit to the disturbance of the fluid due to the force or torque exerted by the other subunit is what we refer to as the hydrodynamic interaction between them. The interaction is long-ranged, falling off with the inverse-distance between the subunits. The mobility tensor, which determines the nature of the response, is a function of the geometry and configuration of the subunits (and the non-slip boundary condition at their surface), and is determined by the relation between the generalised forces and velocities. In tensorial notation

$$\begin{pmatrix} \dot{\boldsymbol{R}}_1 \\ \dot{\boldsymbol{R}}_2 \\ \boldsymbol{\omega}_1 \\ \boldsymbol{\omega}_2 \end{pmatrix} = \begin{pmatrix} \mathbf{M}^{11}_{\mathrm{TT}} & \mathbf{M}^{12}_{\mathrm{TT}} & \mathbf{M}^{11}_{\mathrm{TR}} & \mathbf{M}^{12}_{\mathrm{TR}} \\ \mathbf{M}^{21}_{\mathrm{TT}} & \mathbf{M}^{22}_{\mathrm{TT}} & \mathbf{M}^{21}_{\mathrm{TR}} & \mathbf{M}^{22}_{\mathrm{TR}} \\ \mathbf{M}^{11}_{\mathrm{RT}} & \mathbf{M}^{12}_{\mathrm{RT}} & \mathbf{M}^{11}_{\mathrm{RR}} & \mathbf{M}^{12}_{\mathrm{RR}} \\ \mathbf{M}^{21}_{\mathrm{RT}} & \mathbf{M}^{22}_{\mathrm{RT}} & \mathbf{M}^{21}_{\mathrm{RR}} & \mathbf{M}^{22}_{\mathrm{RR}} \end{pmatrix} \begin{pmatrix} \boldsymbol{F}_1 \\ \boldsymbol{F}_2 \\ \boldsymbol{T}_1 \\ \boldsymbol{T}_2 \end{pmatrix}, \tag{3.2}$$

where $\dot{\boldsymbol{R}}_\alpha$ is the instantaneous velocity at position $\boldsymbol{R}_\alpha$ and $\boldsymbol{\omega}_\alpha$ is the angular velocity at the same position.

The diagonal blocks of the mobility tensor, denoted by $\mathbf{M}_{\mathrm{TT}}^{\alpha\beta}$ and $\mathbf{M}_{\mathrm{RR}}^{\alpha\beta}$, are the translational and rotational tensors which, respectively, describe the translational response of the subunits to the forces exerted on the fluid and their rotational response to the torques on the fluid. The off-diagonal blocks, denoted by $\mathbf{M}_{\mathrm{RT}}^{\alpha\beta}$ and $\mathbf{M}_{\mathrm{TR}}^{\alpha\beta}$, which are non-vanishing because of the asymmetry of the subunits, represent a coupling of translational and rotational modes. Each of the terms in $\mathbf{M}_{\mathrm{AB}}^{\alpha\beta}$ (with A,B = T,R) represents a 3×3-matrix. Elements with repeated superscripts $\mathbf{M}_{\mathrm{AB}}^{\alpha\alpha}$ correspond to the self-mobilities of subunit α in the presence of the other subunit, reducing to the classic Stokes law equations in the absence of hydrodynamic interaction. The off-diagonal terms, $\mathbf{M}_{\mathrm{AB}}^{\alpha\beta}$, with mixed superscripts, describe the two-body hydrodynamic interaction. The hydrodynamic interaction is a manifestation of multiplicative noise as the response to fluctuations depends on the dynamical variables of the system.

Determining the generalised mobility tensor is a problem of fundamental importance for establishing the motion of particles in viscous fluids. In theory it can be determined from hydrodynamic calculations, but in practice the mobility tensor is not easily found, as hydrodynamic interactions have a complex non-linear dependence on the relative positions, relative motion, and the geometries of the interacting particles. Progress in hydrodynamic calculations, particularly analytic, relies on symmetries of the mobility tensor.

For any geometry of the subunits, it is symmetric and positive definite in its exact form so that

$$\mathbf{M}_{\mathrm{AB}}^{\alpha\beta} = \left(\mathbf{M}_{\mathrm{BA}}^{\beta\alpha}\right)^{\mathrm{T}} \tag{3.3}$$

$$\sum_{\alpha,\beta=1}^{2} \boldsymbol{F}_\alpha \mathbf{M}_{\mathrm{AB}}^{\alpha\beta} \boldsymbol{F}_\beta \geq 0 \quad \text{and} \quad \sum_{\alpha,\beta=1}^{2} \boldsymbol{T}_\alpha \mathbf{M}_{\mathrm{AB}}^{\alpha\beta} \boldsymbol{T}_\beta \geq 0 \quad \text{for all} \quad \boldsymbol{F}_\alpha \text{ and } \boldsymbol{T}_\alpha \tag{3.4}$$

[72]. It is straightforward to show (3.3) using the Lorentz reciprocal theorem for two solutions of the Stokes equation and the definitions of the generalised forces exerted by the fluid on the subunits as they translate and rotate in the fluid [108]. The number of independent components of the mobility tensor in (3.2) is reduced even further for axisymmetric geometries. In [109], the translational diffusion

tensor, which is related to the translational mobility tensor, is calculated for two unequal freely rotating spheres as a series expansion in the inverse-distance between the spheres. Numerical methods for computing the hydrodynamic properties of configurations of non-identical spheres are presented in [105, 110, 111].

Hydrodynamic interactions can also be simplified by assuming that the interacting particles are well-separated *i.e.,* that the distance between the closest points on their surfaces is greater than the particle sizes. In this limit, the mobility tensor is given by the Oseen tensor. For translational motion, the Oseen tensor is

$$\mathbf{M}_{\mathrm{TT}}^{\alpha\alpha} = \frac{1}{6\pi\eta a_\alpha}\mathbf{1}; \quad \mathbf{M}_{\mathrm{TT}}^{\alpha\beta} = \frac{1}{8\pi\eta l}\left(\mathbf{1} + \hat{\boldsymbol{n}}\hat{\boldsymbol{n}}\right) \quad \text{for } \alpha \neq \beta. \tag{3.5}$$

In (3.5), $\mathbf{1}$ is the 3×3 identity matrix, η is the viscosity of the fluid, a_α is the radius of the subunits (so that the combination $6\pi\eta a_\alpha$ is the friction coefficient of subunit α) and their relative coordinate is $\boldsymbol{l} = \boldsymbol{R}_2 - \boldsymbol{R}_1 = l\hat{\boldsymbol{n}}$, where $\hat{\boldsymbol{n}}$ is a unit vector along the axis of the dumbbell and l is the elongation of the dumbbell. The finite size of the subunits is included in the hydrodynamic interaction tensor in the Rotne-Prager-Yamakawa tensor. For translational motion, the RPY tensor is

$$\mathbf{M}_{\mathrm{TT}}^{\alpha\beta} = \frac{1}{8\pi\eta l}\left[\left(1 + \frac{a_\alpha^2 + a_\beta^2}{3l^2}\right)\mathbf{1} + \left(1 - \frac{a_\alpha^2 + a_\beta^2}{l^2}\right)\hat{\boldsymbol{n}}\hat{\boldsymbol{n}}\right] \tag{3.6}$$

[105]. Corrections to (3.6) and the mobility tensors for rotational motion and motion due to translation-rotation coupling can be calculated using the the multipole expansion described in [110].

3.2.2 Smoluchowski equation

To describe the evolution of the dumbbell in phase space a description of the stochastic dynamics is required. There are two possibilities which are essentially equivalent: we can construct the Langevin equation, which describes the evolution of the dynamical variables or the Smoluchowski equation, which describes the evolution of the configurational distribution function. For the asymmetric dumbbell we define the distribution function as $P(\boldsymbol{R}_1, \boldsymbol{R}_2, \hat{\boldsymbol{u}}^1, \hat{\boldsymbol{u}}^2; t)$, which is the probability of finding the subunits at positions $\boldsymbol{R}_1$ and $\boldsymbol{R}_2$ with orientations $\hat{\boldsymbol{u}}^1$ and $\hat{\boldsymbol{u}}^2$ at time

t. For our calculation, we start from the probabilistic description for the following reasons; the phenomenological Smoluchowski equation for polymer solutions in equilibrium is well established [72] and can be applied directly to our model; it provides a direct route to calculating the configuration-averaged properties of the dumbbell; the stochastic equations of motion in the Langevin description necessarily lead to ambiguity in the solution due to the multiplicative nature of the noise, which requires careful consideration of the stochastic calculus and may result in the introduction of "spurious drift" terms [15].

The Smoluchowski equation is derived from the continuity equation

$$\frac{\partial P}{\partial t} = -\sum_{\alpha=1,2} \left[\nabla_\alpha \cdot (\mathbf{J}_{\mathrm{T}}^{\alpha} + \mathcal{J}_{\mathrm{C}}^{\alpha}) + \boldsymbol{\mathcal{R}}^{\alpha} \cdot (\mathcal{J}_{\mathrm{R}}^{\alpha} + \mathbf{J}_{\mathrm{C}}^{\alpha})\right], \tag{3.7}$$

where ∇_α and $\boldsymbol{\mathcal{R}}^{\alpha} \equiv \hat{\boldsymbol{u}}^{\alpha} \times \frac{\partial}{\partial \hat{\boldsymbol{u}}^{\alpha}}$ are the gradient operator and rotational gradient operator with respect to the position and orientation variables of subunit α. We have defined the following four probability currents: $\mathbf{J}_{\mathrm{T}}^{\alpha}$ is a translational current due to translational motion; similarly, $\mathcal{J}_{\mathrm{R}}^{\alpha}$ is a rotational current due to rotational motion; $\mathcal{J}_{\mathrm{C}}^{\alpha}$ is a translational current from rotational motion and finally; $\mathbf{J}_{\mathrm{C}}^{\alpha}$ is a rotational current due to translational motion. The two coupling currents $\mathcal{J}_{\mathrm{C}}^{\alpha}$ and $\mathbf{J}_{\mathrm{C}}^{\alpha}$ are non-vanishing because of the asymmetry of the dumbbell. Since the positions and orientations of the subunits undergo Brownian motion, all four currents have diffusive contributions as well as contributions due to the potential U. We note that the currents that enter (3.7) include the effect of hydrodynamic interactions, which are incorporated through the mobility tensor.

Combining (3.2) and (3.7), the Smoluchowski equation for a dilute suspension of our model enzymes, including the hydrodynamic interactions between the subunits is

$$\partial_t P = \mathcal{L}_{\mathrm{T}} P + \mathcal{L}_{\mathrm{R}} P, \tag{3.8}$$

where we have split the equation into translational and rotational parts that are given by

$$\mathcal{L}_{\mathrm{T}} P(\boldsymbol{R}_1, \boldsymbol{R}_2, \hat{\boldsymbol{u}}^1, \hat{\boldsymbol{u}}^2; t) = \sum_{\alpha,\beta=1,2} \nabla_\alpha \cdot \mathbf{M}_{\mathrm{TT}}^{\alpha\beta} \cdot [(\nabla_\beta U) P + k_{\mathrm{B}} T \nabla_\beta P] \tag{3.9}$$

and

$$\mathcal{L}_{\mathrm{R}}P(\boldsymbol{R}_1,\boldsymbol{R}_2,\hat{\boldsymbol{u}}^1,\hat{\boldsymbol{u}}^2;t) = \sum_{\alpha,\beta=1,2}\Big\{\nabla_\alpha\cdot\mathbf{M}^{\alpha\beta}_{\mathrm{TR}}\cdot\Big[(\boldsymbol{\mathcal{R}}^\beta U)P + k_{\mathrm{B}}T\boldsymbol{\mathcal{R}}^\beta P\Big] + \boldsymbol{\mathcal{R}}^\alpha\cdot\mathbf{M}^{\alpha\beta}_{\mathrm{RR}}\cdot\Big[(\boldsymbol{\mathcal{R}}^\beta U)P + k_{\mathrm{B}}T\boldsymbol{\mathcal{R}}^\beta P\Big] + \boldsymbol{\mathcal{R}}^\alpha\cdot\mathbf{M}^{\alpha\beta}_{\mathrm{RT}}\cdot[(\nabla_\beta U)P + k_{\mathrm{B}}T\nabla_\beta P]\Big\}. \tag{3.10}$$

It is convenient to rewrite (3.9) and (3.10) in the centre-of-mass (com) and relative coordinates $\boldsymbol{R} = (\boldsymbol{R}_1+\boldsymbol{R}_2)/2$ and $\boldsymbol{l}$. We find

$$\mathcal{L}_{\mathrm{T}}P(\boldsymbol{R},\boldsymbol{l},\hat{\boldsymbol{u}}^1,\hat{\boldsymbol{u}}^2;t) = \frac{k_{\mathrm{B}}T}{4}\nabla_{\boldsymbol{R}}\cdot\mathbf{M}\cdot\nabla_{\boldsymbol{R}}P + \frac{k_{\mathrm{B}}T}{2}\nabla_{\boldsymbol{l}}\cdot\boldsymbol{\Gamma}\cdot\nabla_{\boldsymbol{R}}P + \frac{1}{2}\nabla_{\boldsymbol{R}}\cdot\boldsymbol{\Gamma}\cdot[k_{\mathrm{B}}T\nabla_{\boldsymbol{l}}P + (\nabla_{\boldsymbol{l}}U)P] + \nabla_{\boldsymbol{l}}\cdot\mathbf{W}\cdot[k_{\mathrm{B}}T\nabla_{\boldsymbol{l}}P + (\nabla_{\boldsymbol{l}}U)P] \tag{3.11}$$

and

$$\mathcal{L}_{\mathrm{R}}P(\boldsymbol{R},\boldsymbol{l},\hat{\boldsymbol{u}}^1,\hat{\boldsymbol{u}}^2;t) = \sum_{\alpha,\beta=1,2}\Big\{\frac{k_{\mathrm{B}}T}{2}\boldsymbol{\mathcal{R}}^\alpha\cdot\boldsymbol{\Phi}^{(\alpha)}\cdot\nabla_{\boldsymbol{R}}P + \frac{1}{2}\nabla_{\boldsymbol{R}}\cdot\boldsymbol{\Phi}^{(\alpha)}\cdot[k_{\mathrm{B}}T\boldsymbol{\mathcal{R}}^\alpha P + (\boldsymbol{\mathcal{R}}^\alpha U)P] + (-1)^\alpha\nabla_{\boldsymbol{l}}\cdot\boldsymbol{\Lambda}^{(\alpha)}\cdot[k_{\mathrm{B}}T\boldsymbol{\mathcal{R}}^\alpha P + (\boldsymbol{\mathcal{R}}^\alpha U)P] + (-1)^\alpha\boldsymbol{\mathcal{R}}^\alpha\cdot\boldsymbol{\Lambda}^{(\alpha)}\cdot[k_{\mathrm{B}}T\nabla_{\boldsymbol{l}}P + (\nabla_{\boldsymbol{l}}U)P] + \boldsymbol{\mathcal{R}}^\alpha\cdot\mathbf{M}^{\alpha\beta}_{\mathrm{RR}}\cdot\Big[k_{\mathrm{B}}T\boldsymbol{\mathcal{R}}^\beta P + (\boldsymbol{\mathcal{R}}^\beta U)P\Big]\Big\}, \tag{3.12}$$

where the gradient operators act on everything to their right, and we have defined new mobility matrices from linear combinations of the old ones using the symmetry of the mobility tensor. The new tensors are defined as follows:

$$\begin{aligned}
&\mathbf{M} = \mathbf{M}^{11}_{\mathrm{TT}} + \mathbf{M}^{22}_{\mathrm{TT}} + 2\mathbf{M}^{12}_{\mathrm{TT}}; \quad \mathbf{W} = \mathbf{M}^{11}_{\mathrm{TT}} + \mathbf{M}^{22}_{\mathrm{TT}} - 2\mathbf{M}^{12}_{\mathrm{TT}}; \quad \boldsymbol{\Gamma} = \mathbf{M}^{22}_{\mathrm{TT}} - \mathbf{M}^{11}_{\mathrm{TT}};\\
&\boldsymbol{\Lambda}^{(1)} = \mathbf{M}^{11}_{\mathrm{TR}} - \mathbf{M}^{21}_{\mathrm{TR}}; \quad \boldsymbol{\Lambda}^{(2)} = \mathbf{M}^{22}_{\mathrm{TR}} - \mathbf{M}^{12}_{\mathrm{TR}}; \quad \boldsymbol{\Psi}^{(1)} = \mathbf{M}^{11}_{\mathrm{RR}}; \quad \boldsymbol{\Psi}^{(2)} = \mathbf{M}^{22}_{\mathrm{RR}};\\
&\boldsymbol{\Phi}^{(1)} = \mathbf{M}^{11}_{\mathrm{TR}} + \mathbf{M}^{21}_{\mathrm{TR}}; \quad \boldsymbol{\Phi}^{(2)} = \mathbf{M}^{22}_{\mathrm{TR}} + \mathbf{M}^{12}_{\mathrm{TR}}; \quad \boldsymbol{\Psi}^{(12)} = \mathbf{M}^{12}_{\mathrm{RR}}.
\end{aligned} \tag{3.13}$$

The physical significance of the new mobility tensors can be read from the Smoluchowski equation. From (3.11), $\mathbf{M}$ is the average mobility of the translational modes, $\mathbf{W}$ is coupled to rotations of the dumbbell and $\boldsymbol{\Gamma}$ is a measure of the asymmetry of the dumbbell as it couples its rotational and translational motion.

From (3.12), the remaining tensors in (3.13) couple translational and rotational modes of the subunits.

Using eq. (3.6) in the definitions above, it is clear that $\mathbf{\Gamma}$ vanishes for a symmetric dumbbell. For freely rotating spherical subunits, $\mathbf{\Phi}^{(\alpha)}$ and $\mathbf{M}_{\mathrm{RR}}^{\alpha\beta}$ also vanish. Since the com coordinate $\boldsymbol{R}$ is the coordinate for the global dynamics of the dumbbell and the relative coordinate $\boldsymbol{l}$ characterises the local internal dynamics, from (3.11) we see that $\mathbf{M}$ is the mobility for the global dynamics. Similarly, $\mathbf{W}$ is the mobility for the local dynamics and the mobility matrix $\mathbf{\Gamma}$ couples local and global motion. From (3.12), $\mathbf{\Phi}^{(\alpha)}$ couple global translations to the rotational modes of the subunits and $\mathbf{\Lambda}^{(\alpha)}$ couple local compressions to the rotational modes of the subunits. We note that the terms that couple global and local modes vanish for a symmetric dumbbell with spherical subunits.

To write the Smoluchowski equation more explicitly, we must specify a form for the interaction potential between the subunits. In the absence of external fields, the potential U can only depend on the internal degrees of freedom of the dumbbell. Assuming that fluctuations are sufficiently small, it can be expanded in the fluctuating degrees of freedom as follows

$$U(q_1, q_2, q_3, \dots) \simeq U_{\min} + \frac{1}{2}\sum_{i=1}^{N}\sum_{j=1}^{N}\left(\frac{\partial^2 U}{\partial q_i \partial q_j}\right) q_i q_j, \tag{3.14}$$

where the q_i are generalised coordinates and $U_{\min}$ is the potential in the equilibrium state so that fluctuations in different coordinates are correlated and the energies of the different configurations only slightly vary from the energy in the equilibrium state. The stiffness of the potential is defined as $k_{ij} \equiv \frac{\partial^2 U}{\partial q_i \partial q_j}$, and anharmonic terms have been neglected for simplicity.

For small fluctuations, the potential of the generalised dumbbell is expanded in the fluctuating angles between the orientation vectors of the subunits $\hat{\boldsymbol{u}}^1$ and $\hat{\boldsymbol{u}}^2$ and the orientation vector of the axis of the dumbbell $\hat{\boldsymbol{n}}$, given by the relative coordinate $\boldsymbol{l} = \boldsymbol{R}_2 - \boldsymbol{R}_1 = l\hat{\boldsymbol{n}}$, as

$$U \simeq V_0(l) + V_1(l)\,\hat{\boldsymbol{n}}\cdot\hat{\boldsymbol{u}}^1 + V_2(l)\,\hat{\boldsymbol{n}}\cdot\hat{\boldsymbol{u}}^2 + V_{12}(l)\,\hat{\boldsymbol{u}}^1\cdot\hat{\boldsymbol{u}}^2. \tag{3.15}$$

We assume that in the lowest energy state only the compressional modes of fluctuation are constrained, and the subunits can rotate freely, hence, the minimum of the potential is just $V_0(l)$. The functions $V_\alpha(l)$ and $V_{12}(l)$ quantify the strength of the constraints on rotational fluctuations. The exact functional form of the potential will depend on the enzyme being modelled, and in the presence of substrate molecules, on the effect of substrate on fluctuations.

3.2.3 Averaging procedure

We will now calculate the effective translational diffusion coefficient of the com of the dumbbell, which is defined as the mean-square displacement of the com coordinate due to Brownian forces

$$D_{\text{eff}} = \lim_{t\to\infty} \frac{1}{6}\frac{\mathrm{d}}{\mathrm{d}t} \int_{\boldsymbol{R}} \int_{\boldsymbol{l}} \int_{\hat{\boldsymbol{u}}^1} \int_{\hat{\boldsymbol{u}}^2} \boldsymbol{R}^2 P(\boldsymbol{R}, \boldsymbol{l}, \hat{\boldsymbol{u}}^1, \hat{\boldsymbol{u}}^2; t), \tag{3.16}$$

where integrals over the dynamical variables are denoted with a subscript. We emphasise that the effective diffusion coefficient corresponds to the motion of the entire dumbbell in real space, whereas the diffusive motion described by eqs. (3.11) and (3.12) is the evolution of the configurational distribution function in the phase space of the dumbbell.

Even for a simpler model where the subunits are axisymmetric and allowed to rotate freely so that $P = P(\boldsymbol{R}, \boldsymbol{l}; t)$, an attempt to find the mean-square displacement directly by naive integration using eqs. (3.11) and (3.12) leads to a hierarchy of correlation functions of the dynamical variables. We will instead deduce the effective diffusion coefficient from the diffusion equation in the hydrodynamic limit as discussed in Chapter 2. This way, the hierarchy of correlation functions can be truncated by an averaging procedure which involves the careful ordering of the integrals in (3.16) to reflect the hierarchy of the characteristic timescales of the dynamical variables.

There are three characteristic timescales associated with the dumbbell: the slowest is associated to the com motion, followed by the reorientation time of the rotational degrees of freedom and finally the relaxation time for internal compressions.

Assuming that the l dependence of (3.15) has a Taylor expansion around the minimum of the potential, as in (3.14), the quadratic term gives a spring constant k from which we define the characteristic relaxation time, $\tau_l = \xi/k$, for fluctuations in l, where ξ is an estimate of the friction coefficient of the dumbbell. The reorientation time of the dumbbell τ_r is the time is takes to loose memory of its orientation, which is given by the correlation $\langle \hat{\boldsymbol{n}}(t) \cdot \hat{\boldsymbol{n}}(0) \rangle \sim \exp(-|t|/\tau_r)$, and is of the order $\xi a^2/k_\mathrm{B}T$. The ratio τ_l/τ_r goes as $\varepsilon^2 = k_\mathrm{B}T/ka^2 \sim (\delta l/a)^2$, where δl is the amplitude of a typical deformation due to fluctuations in l and ε is the relative amplitude of thermal fluctuations about the equilibrium elongation of the dumbbell. Since δl is expected to be much smaller than the equilibrium separation of the subunits, we expect $\tau_l/\tau_r \ll 1$ so that reorientation of the dumbbell is much slower than the relaxation of its elongation fluctuations. The reorientation time of each subunit (the times associated with the diffusion of $\hat{\boldsymbol{u}}^1$ and $\hat{\boldsymbol{u}}^2$) will be of the order of τ_r if the size of the subunits is of the order of the size of the dumbbell.

Following the ordering of the dynamical timescales in (3.16), a closed-form expression for the effective diffusion coefficient is achieved by first performing the average over the separation of the subunits assuming fixed $\hat{\boldsymbol{n}}$, $\hat{\boldsymbol{u}}^1$ and $\hat{\boldsymbol{u}}^2$. The elongation-averaged configurational distribution function is defined as

$$\mathcal{P}(\boldsymbol{R}, \hat{\boldsymbol{n}}, \hat{\boldsymbol{u}}^1, \hat{\boldsymbol{u}}^2; t) = \int_{a_1+a_2}^{\infty} \mathrm{d}l\, l^2 P, \tag{3.17}$$

so that the average of an l-dependent function is given by

$$\langle \cdot \rangle = \frac{1}{\mathcal{P}} \int_{a_1+a_2}^{\infty} \mathrm{d}l\, l^2 \cdot P. \tag{3.18}$$

To calculate the elongation averaged Smoluchowski equation we need the divergence of the hydrodynamic tensors and the gradients of the distribution function and of the interaction potential with respect to the radial coordinate $\boldsymbol{l}$. Hence, we need gradients and divergences of the form $\nabla_{\boldsymbol{l}} A$ and $\nabla_{\boldsymbol{l}} \cdot \mathbf{A}$, where A is a scalar function and $\mathbf{A}$ a tensor function of $\boldsymbol{l}$. By applying the gradient with respect to $\boldsymbol{l}$ in spherical coordinates $\nabla_{\boldsymbol{l}} = \hat{\boldsymbol{n}}\partial_l - \frac{1}{l}\hat{\boldsymbol{n}} \times \boldsymbol{\mathcal{R}}$, we find

$$\nabla_{\boldsymbol{l}} A = \frac{\partial A}{\partial l}\hat{\boldsymbol{n}} - \frac{1}{l}\hat{\boldsymbol{n}} \times \boldsymbol{\mathcal{R}} A \tag{3.19}$$

and

$$\nabla_l \cdot \mathbf{A} = \frac{1}{l^2}\frac{\partial(l^2 \mathbf{A}\cdot\hat{\boldsymbol{n}})}{\partial l^2} + \frac{1}{l}\boldsymbol{\mathcal{R}}\cdot(\hat{\boldsymbol{n}}\times\mathbf{A}) \tag{3.20}$$

in terms of the rotational gradient operator and the derivative with respect to l. Specifically, for the gradients of the interaction potential $\nabla_l U$ and $\boldsymbol{\mathcal{R}}^\alpha U$, we have

$$\nabla_l U = \hat{\boldsymbol{n}}U' + (\mathbf{1}-\hat{\boldsymbol{n}}\hat{\boldsymbol{n}})\cdot\left(\frac{V_1(l)}{l}\hat{\boldsymbol{u}}^1 + \frac{V_2(l)}{l}\hat{\boldsymbol{u}}^2\right), \tag{3.21}$$

using expansion (3.15), where the prime denotes a derivative with respect to l. Applying $\boldsymbol{\mathcal{R}}^\alpha$ to (3.15) gives

$$\boldsymbol{\mathcal{R}}^\alpha U = V_\alpha(l)\hat{\boldsymbol{u}}^\alpha\times\hat{\boldsymbol{n}} + V_{12}(l)\hat{\boldsymbol{u}}^\alpha\times\hat{\boldsymbol{u}}^\beta. \tag{3.22}$$

Inserting expressions (3.21) and (3.22) along with the divergences of the hydrodynamic tensors and the gradient of the distribution function given by (3.20) and (3.19) into the Smoluchowski equation, the average of eq. (3.11) over the radial coordinate, with the orientations fixed is

$$\begin{aligned}
\mathcal{L}_{\mathrm{T}}\mathcal{P} =& \frac{k_{\mathrm{B}}T}{4}\nabla_{\boldsymbol{R}}\cdot\langle\mathbf{M}\rangle\cdot\nabla_{\boldsymbol{R}}\mathcal{P} - \frac{k_{\mathrm{B}}T}{2}\hat{\boldsymbol{n}}\times\boldsymbol{\mathcal{R}}\cdot(\mathbf{1}-\hat{\boldsymbol{n}}\hat{\boldsymbol{n}})\cdot\left\langle\frac{\boldsymbol{\Gamma}}{l}\right\rangle\cdot\nabla_{\boldsymbol{R}}\mathcal{P} \\
&- \frac{k_{\mathrm{B}}T}{2}\nabla_{\boldsymbol{R}}\cdot\left[\hat{\boldsymbol{n}}\times\boldsymbol{\mathcal{R}}\cdot\left\langle\frac{\boldsymbol{\Gamma}}{l}\right\rangle\mathcal{P}\right] + \frac{k_{\mathrm{B}}T}{2}\nabla_{\boldsymbol{R}}\cdot\left[\left\langle\hat{\boldsymbol{n}}\times\boldsymbol{\mathcal{R}}\cdot\frac{\boldsymbol{\Gamma}}{l}\right\rangle\mathcal{P}\right] \\
&+ \frac{1}{2}\nabla_{\boldsymbol{R}}\cdot\left\langle\frac{\boldsymbol{\Gamma}V_1}{l}\right\rangle\cdot(\mathbf{1}-\hat{\boldsymbol{n}}\hat{\boldsymbol{n}})\cdot\hat{\boldsymbol{u}}^1\mathcal{P} + \frac{1}{2}\nabla_{\boldsymbol{R}}\cdot\left\langle\frac{\boldsymbol{\Gamma}V_2}{l}\right\rangle\cdot(\mathbf{1}-\hat{\boldsymbol{n}}\hat{\boldsymbol{n}})\cdot\hat{\boldsymbol{u}}^2\mathcal{P} \\
&+ k_{\mathrm{B}}T\hat{\boldsymbol{n}}\times\boldsymbol{\mathcal{R}}\cdot(\mathbf{1}-\hat{\boldsymbol{n}}\hat{\boldsymbol{n}})\cdot\left[\hat{\boldsymbol{n}}\times\boldsymbol{\mathcal{R}}\cdot\left\langle\frac{\mathbf{W}}{l^2}\right\rangle\mathcal{P}\right] \\
&- k_{\mathrm{B}}T\hat{\boldsymbol{n}}\times\boldsymbol{\mathcal{R}}\cdot(\mathbf{1}-\hat{\boldsymbol{n}}\hat{\boldsymbol{n}})\cdot\left[\left\langle\hat{\boldsymbol{n}}\times\boldsymbol{\mathcal{R}}\cdot\frac{\mathbf{W}}{l^2}\right\rangle\mathcal{P}\right] \\
&+ \hat{\boldsymbol{n}}\times\boldsymbol{\mathcal{R}}\cdot(\mathbf{1}-\hat{\boldsymbol{n}}\hat{\boldsymbol{n}})\cdot\left\langle\frac{\mathbf{W}V_1}{l^2}\right\rangle\cdot\hat{\boldsymbol{u}}^1\mathcal{P} + \hat{\boldsymbol{n}}\times\boldsymbol{\mathcal{R}}\cdot(\mathbf{1}-\hat{\boldsymbol{n}}\hat{\boldsymbol{n}})\cdot\left\langle\frac{\mathbf{W}V_2}{l^2}\right\rangle\cdot\hat{\boldsymbol{u}}^2\mathcal{P}
\end{aligned} \tag{3.23}$$

and for (3.12)

$$\begin{aligned}
\mathcal{L}_{\mathrm{R}}\mathcal{P} =& \sum_{\alpha,\beta=1,2}\left\{\frac{k_{\mathrm{B}}T}{2}\boldsymbol{\mathcal{R}}^\alpha\cdot\left\langle\boldsymbol{\Phi}^{(\alpha)}\right\rangle\cdot\nabla_{\boldsymbol{R}}\mathcal{P}\right. \\
&+ \frac{k_{\mathrm{B}}T}{2}\nabla_{\boldsymbol{R}}\cdot\left[\boldsymbol{\mathcal{R}}^\alpha\cdot\left\langle\boldsymbol{\Phi}^{(\alpha)}\right\rangle\mathcal{P}\right] - \frac{k_{\mathrm{B}}T}{2}\nabla_{\boldsymbol{R}}\cdot\left[\left\langle\boldsymbol{\mathcal{R}}^\alpha\cdot\boldsymbol{\Phi}^{(\alpha)}\right\rangle\mathcal{P}\right] \\
&+ \frac{1}{2}\nabla_{\boldsymbol{R}}\cdot\left\langle\boldsymbol{\Phi}^{(\alpha)}V_\alpha\right\rangle\cdot\hat{\boldsymbol{u}}^\alpha\times\hat{\boldsymbol{n}}\mathcal{P} + \frac{1}{2}\nabla_{\boldsymbol{R}}\cdot\left\langle\boldsymbol{\Phi}^{(\alpha)}V_{12}\right\rangle\cdot\hat{\boldsymbol{u}}^\alpha\times\hat{\boldsymbol{u}}^\beta\mathcal{P} \\
&\left.-(-1)^\alpha k_{\mathrm{B}}T\hat{\boldsymbol{n}}\times\boldsymbol{\mathcal{R}}\cdot(\mathbf{1}-\hat{\boldsymbol{n}}\hat{\boldsymbol{n}})\cdot\left[\boldsymbol{\mathcal{R}}^\alpha\cdot\left\langle\frac{\boldsymbol{\Lambda}^{(\alpha)}}{l}\right\rangle\mathcal{P}\right]\right.
\end{aligned}$$

$$
\begin{aligned}
&+(-1)^{\alpha} k_{\mathrm{B}}T \hat{\boldsymbol{n}} \times \boldsymbol{\mathcal{R}} \cdot (\mathbf{1} - \hat{\boldsymbol{n}}\hat{\boldsymbol{n}}) \cdot \left[\left\langle \boldsymbol{\mathcal{R}}^{\alpha} \cdot \frac{\boldsymbol{\Lambda}^{(\alpha)}}{l} \right\rangle \mathcal{P} \right] \\
&-(-1)^{\alpha} \hat{\boldsymbol{n}} \times \boldsymbol{\mathcal{R}} \cdot (\mathbf{1} - \hat{\boldsymbol{n}}\hat{\boldsymbol{n}}) \cdot \left[\left\langle \frac{\boldsymbol{\Lambda}^{(\alpha)} V_{\alpha}}{l} \right\rangle \cdot \hat{\boldsymbol{u}}^{\alpha} \times \hat{\boldsymbol{n}} \mathcal{P} \right] \\
&-(-1)^{\alpha} \hat{\boldsymbol{n}} \times \boldsymbol{\mathcal{R}} \cdot (\mathbf{1} - \hat{\boldsymbol{n}}\hat{\boldsymbol{n}}) \cdot \left[\left\langle \frac{\boldsymbol{\Lambda}^{(\alpha)} V_{12}}{l} \right\rangle \cdot \hat{\boldsymbol{u}}^{\alpha} \times \hat{\boldsymbol{u}}^{\beta} \mathcal{P} \right] \\
&+(-1)^{\alpha} k_{\mathrm{B}}T \boldsymbol{\mathcal{R}}^{\alpha} \cdot \left[\hat{\boldsymbol{n}} \times \boldsymbol{\mathcal{R}} \cdot \left\langle \frac{\boldsymbol{\Lambda}^{(\alpha)}}{l} \right\rangle \mathcal{P} \right] - (-1)^{\alpha} k_{\mathrm{B}}T \boldsymbol{\mathcal{R}}^{\alpha} \cdot \left[\left\langle \hat{\boldsymbol{n}} \times \boldsymbol{\mathcal{R}} \cdot \frac{\boldsymbol{\Lambda}^{(\alpha)}}{l} \right\rangle \mathcal{P} \right] \\
&+(-1)^{\alpha} \boldsymbol{\mathcal{R}}^{\alpha} \cdot \left\langle \frac{\boldsymbol{\Lambda}^{(\alpha)} V_1}{l} \right\rangle \cdot (\mathbf{1} - \hat{\boldsymbol{n}}\hat{\boldsymbol{n}}) \cdot \hat{\boldsymbol{u}}^{1} \mathcal{P} + (-1)^{\alpha} \boldsymbol{\mathcal{R}}^{\alpha} \cdot \left\langle \frac{\boldsymbol{\Lambda}^{(\alpha)} V_2}{l} \right\rangle \cdot (\mathbf{1} - \hat{\boldsymbol{n}}\hat{\boldsymbol{n}}) \cdot \hat{\boldsymbol{u}}^{2} \mathcal{P} \\
&+k_{\mathrm{B}}T \boldsymbol{\mathcal{R}}^{\alpha} \cdot \left[\boldsymbol{\mathcal{R}}^{\beta} \cdot \left\langle \mathbf{M}_{\mathrm{RR}}^{\alpha\beta} \right\rangle \mathcal{P} \right] - k_{\mathrm{B}}T \boldsymbol{\mathcal{R}}^{\alpha} \cdot \left[\left\langle \boldsymbol{\mathcal{R}}^{\beta} \cdot \mathbf{M}_{\mathrm{RR}}^{\alpha\beta} \right\rangle \mathcal{P} \right] \Big\} ,
\end{aligned}
\tag{3.24}
$$

with all gradients acting on everything to their right. The following relation has been used to simplify terms involving the derivative of U with respect to l

$$
\langle U' \phi(l) \rangle = k_{\mathrm{B}}T \left\langle \phi'(l) + 2 \frac{\phi(l)}{l} \right\rangle , \tag{3.25}
$$

which is valid for any function $\phi(l)$ of the radial coordinate, assuming that the distribution has a Boltzmann-like l-dependence so that $P \propto \mathrm{e}^{-U/k_{\mathrm{B}}T}$.

3.2.4 Moment expansion

For the orientation dependence of eqs. (3.23) and (3.24), we perform the moment expansion as described in Chapter 2, with respect to the three orientation unit vectors $\hat{\boldsymbol{n}}$, $\hat{\boldsymbol{u}}^1$ and $\hat{\boldsymbol{u}}^2$. Similarly to the irreducible tensors defined in Chapter 2, a rank l irreducible tensor can be constructed from symmetric tensors which are mixed products of components of $\hat{\boldsymbol{u}}^1$ and $\hat{\boldsymbol{u}}^2$. For a tensor with respect to only one of the $\hat{\boldsymbol{u}}^{\alpha}$, the irreducible tensors are defined exactly as in Chapter 2. For tensors which are constructed from a combination of the three orientations, we define the following, up to the order that will be encountered in the current moment expansion

$$
D_i^{\alpha} = \hat{u}_i^{\alpha}; \tag{3.26}
$$

$$
D_{ij}^{\alpha\beta} = \hat{u}_i^{\alpha} \hat{u}_j^{\beta} - \frac{1}{3} \delta_{ij} \delta^{\alpha\beta}; \tag{3.27}
$$

$$
D_{(ij)k}^{\alpha\beta\gamma} = D_{ij}^{\alpha\beta} \hat{u}_k^{\gamma}; \tag{3.28}
$$

$$
D_{(ij)(kl)}^{\alpha\beta\gamma\delta} = D_{ij}^{\alpha\beta} D_{kl}^{\gamma\delta}; \tag{3.29}
$$

$$D^{\alpha\beta\gamma\delta\epsilon}_{(ijkl)m} = D^{\alpha\beta\gamma\delta}_{ijkl}\hat{u}^{\epsilon}_{m}; \quad D^{\alpha\beta\gamma\delta\epsilon}_{(ijk)(lm)} = D^{\alpha\beta\gamma}_{ijk}D^{\alpha\beta}_{kl}; \quad D^{\alpha\beta\gamma\delta\epsilon}_{(ij)(kl)m} = D^{\alpha\beta}_{ij}D^{\gamma\delta}_{kl}\hat{u}^{\epsilon}_{m}, \tag{3.30}$$

which are symmetric in the indices in parenthesis and traceless upon contraction of the same indices. $D^{\alpha\beta\gamma}_{ijk}$ and $D^{\alpha\beta\gamma\delta}_{ijkl}$ are defined as in Chapter 2. Defining the scalar product of two orientation-dependent functions as

$$(A,B) = \int \frac{\mathrm{d}\hat{\boldsymbol{n}}}{\Omega_{\hat{\boldsymbol{n}}}} \int \frac{\mathrm{d}\hat{\boldsymbol{u}}^1}{\Omega_{\hat{\boldsymbol{u}}^1}} \int \frac{\mathrm{d}\hat{\boldsymbol{u}}^2}{\Omega_{\hat{\boldsymbol{u}}^2}} A(\hat{\boldsymbol{n}},\hat{\boldsymbol{u}}^1,\hat{\boldsymbol{u}}^2)B(\hat{\boldsymbol{n}},\hat{\boldsymbol{u}}^1,\hat{\boldsymbol{u}}^2) \tag{3.31}$$

gives the following scalar products of the unit vectors

$$(\hat{n}_i,\hat{n}_j) = \frac{1}{3}\delta_{ij}; \quad \left(\hat{u}^{\alpha}_i,\hat{u}^{\beta}_j\right) = \frac{1}{3}\delta_{ij}\delta^{\alpha\beta}; \tag{3.32}$$

$$(\hat{n}_i\hat{n}_j,\hat{n}_k\hat{n}_l) = \frac{1}{15}\Delta_{ijkl}; \quad \left(\hat{u}^{\alpha}_i\hat{u}^{\beta}_j,\hat{u}^{\gamma}_k\hat{u}^{\delta}_l\right) = \frac{1}{9}\delta_{ij}\delta_{kl}\delta^{\alpha\beta}\delta^{\gamma\delta}; \tag{3.33}$$

$$\left(\hat{u}^{\alpha}_i\hat{u}^{\beta}_j,\hat{u}^{\gamma}_k\hat{u}^{\delta}_l\right) = \frac{1}{15}\Delta_{ijkl}\delta^{\alpha\beta\gamma\delta}.$$

The elongation-averaged distribution function $\mathcal{P}(\boldsymbol{R},\hat{\boldsymbol{n}},\hat{\boldsymbol{u}}^1,\hat{\boldsymbol{u}}^2;t)$ can be expanded as follows

$$\begin{aligned}\mathcal{P}(\boldsymbol{R},\hat{\boldsymbol{n}},\hat{\boldsymbol{u}}^1,\hat{\boldsymbol{u}}^2;t) \simeq & \frac{1}{\Omega}\rho(\boldsymbol{R},t) + \frac{3}{\Omega}p_i(\boldsymbol{R},t)\hat{n}_i + \frac{3}{\Omega}p^1_i(\boldsymbol{R},t)\hat{u}^1_i + \frac{3}{\Omega}p^2_i(\boldsymbol{R},t)\hat{u}^2_i \\ & + \frac{3(3+2)}{2\Omega}Q_{ij}(\boldsymbol{R},t)D_{ij} + \frac{3(3+2)}{2\Omega}Q^{\alpha\beta}_{ij}(\boldsymbol{R},t)D^{\alpha\beta}_{ij} + \ldots,\end{aligned} \tag{3.34}$$

up to third order in the moment expansion, where we have defined $\Omega = \Omega_{\hat{\boldsymbol{n}}}\Omega_{\hat{\boldsymbol{u}}^1}\Omega_{\hat{\boldsymbol{u}}^2}$. Using the relations in (3.32) and (3.33) and expansion (3.34), the zeroth, first and second order moments of the elongation-averaged distribution function are, respectively

$$\left(1,\mathcal{P}(\boldsymbol{R},\hat{\boldsymbol{n}},\hat{\boldsymbol{u}}^1,\hat{\boldsymbol{u}}^2;t)\right) = \rho(\boldsymbol{R},t); \tag{3.35}$$

$$\left(\hat{\boldsymbol{n}},\mathcal{P}(\boldsymbol{R},\hat{\boldsymbol{n}},\hat{\boldsymbol{u}}^1,\hat{\boldsymbol{u}}^2;t)\right) = \boldsymbol{p}(\boldsymbol{R},t); \tag{3.36}$$

$$\left(\hat{\boldsymbol{u}}^{\alpha},\mathcal{P}(\boldsymbol{R},\hat{\boldsymbol{n}},\hat{\boldsymbol{u}}^1,\hat{\boldsymbol{u}}^2;t)\right) = \boldsymbol{p}^{\alpha}(\boldsymbol{R},t); \tag{3.37}$$

$$\left(D_{ij},\mathcal{P}(\boldsymbol{R},\hat{\boldsymbol{n}},\hat{\boldsymbol{u}}^1,\hat{\boldsymbol{u}}^2;t)\right) = Q_{ij}(\boldsymbol{R},t); \tag{3.38}$$

$$\left(D^{\alpha\beta}_{ij},\mathcal{P}(\boldsymbol{R},\hat{\boldsymbol{n}},\hat{\boldsymbol{u}}^1,\hat{\boldsymbol{u}}^2;t)\right) = Q^{\alpha\beta}_{ij}(\boldsymbol{R},t). \tag{3.39}$$

In order to find the evolution equations for the moments (3.35)-(3.39) of the elongation-averaged distribution function, we need an approximation for the

orientation dependence of the mobility tensors. We expand the mobility tensors in powers of the orientation unit vectors as follows:

$$\mathbf{M} \simeq [m_0(l) + m_1(l)\hat{\boldsymbol{u}}^1 \cdot \hat{\boldsymbol{n}} + m_2(l)\hat{\boldsymbol{u}}^2 \cdot \hat{\boldsymbol{n}} + m_{12}(l)\hat{\boldsymbol{u}}^1 \cdot \hat{\boldsymbol{u}}^2]\mathbf{1}; \tag{3.40}$$

$$\mathbf{W} \simeq [w_0(l) + w_1(l)\hat{\boldsymbol{u}}^1 \cdot \hat{\boldsymbol{n}} + w_2(l)\hat{\boldsymbol{u}}^2 \cdot \hat{\boldsymbol{n}} + w_{12}(l)\hat{\boldsymbol{u}}^1 \cdot \hat{\boldsymbol{u}}^2]\mathbf{1}; \tag{3.41}$$

$$\boldsymbol{\Gamma} \simeq [\gamma_0(l) + \gamma_1(l)\hat{\boldsymbol{u}}^1 \cdot \hat{\boldsymbol{n}} + \gamma_2(l)\hat{\boldsymbol{u}}^2 \cdot \hat{\boldsymbol{n}} + \gamma_{12}(l)\hat{\boldsymbol{u}}^1 \cdot \hat{\boldsymbol{u}}^2]\mathbf{1}; \tag{3.42}$$

$$\boldsymbol{\Lambda}^{(1)} \simeq [\lambda_0^{(1)}(l) + \lambda_1^{(1)}(l)\hat{\boldsymbol{u}}^1 \cdot \hat{\boldsymbol{n}} + \lambda_2^{(1)}(l)\hat{\boldsymbol{u}}^2 \cdot \hat{\boldsymbol{n}} + \lambda_{12}^{(1)}(l)\hat{\boldsymbol{u}}^1 \cdot \hat{\boldsymbol{u}}^2]\mathbf{1}; \tag{3.43}$$

$$\boldsymbol{\Lambda}^{(2)} \simeq [\lambda_0^{(2)}(l) + \lambda_1^{(2)}(l)\hat{\boldsymbol{u}}^1 \cdot \hat{\boldsymbol{n}} + \lambda_2^{(2)}(l)\hat{\boldsymbol{u}}^2 \cdot \hat{\boldsymbol{n}} + \lambda_{12}^{(2)}(l)\hat{\boldsymbol{u}}^1 \cdot \hat{\boldsymbol{u}}^2]\mathbf{1}; \tag{3.44}$$

$$\boldsymbol{\Phi}^{(1)} \simeq [\phi_0^{(1)}(l) + \phi_1^{(1)}(l)\hat{\boldsymbol{u}}^1 \cdot \hat{\boldsymbol{n}} + \phi_2^{(1)}(l)\hat{\boldsymbol{u}}^2 \cdot \hat{\boldsymbol{n}} + \phi_{12}^{(1)}(l)\hat{\boldsymbol{u}}^1 \cdot \hat{\boldsymbol{u}}^2]\mathbf{1}; \tag{3.45}$$

$$\boldsymbol{\Phi}^{(2)} \simeq [\phi_0^{(2)}(l) + \phi_1^{(2)}(l)\hat{\boldsymbol{u}}^1 \cdot \hat{\boldsymbol{n}} + \phi_2^{(2)}(l)\hat{\boldsymbol{u}}^2 \cdot \hat{\boldsymbol{n}} + \phi_{12}^{(2)}(l)\hat{\boldsymbol{u}}^1 \cdot \hat{\boldsymbol{u}}^2]\mathbf{1}; \tag{3.46}$$

$$\boldsymbol{\Psi}^{(1)} \simeq [\psi_0^{(1)}(l) + \psi_1^{(1)}(l)\hat{\boldsymbol{u}}^1 \cdot \hat{\boldsymbol{n}} + \psi_2^{(1)}(l)\hat{\boldsymbol{u}}^2 \cdot \hat{\boldsymbol{n}} + \psi_{12}^{(1)}(l)\hat{\boldsymbol{u}}^1 \cdot \hat{\boldsymbol{u}}^2]\mathbf{1}; \tag{3.47}$$

$$\boldsymbol{\Psi}^{(2)} \simeq [\psi_0^{(2)}(l) + \psi_1^{(2)}(l)\hat{\boldsymbol{u}}^1 \cdot \hat{\boldsymbol{n}} + \psi_2^{(2)}(l)\hat{\boldsymbol{u}}^2 \cdot \hat{\boldsymbol{n}} + \psi_{12}^{(2)}(l)\hat{\boldsymbol{u}}^1 \cdot \hat{\boldsymbol{u}}^2]\mathbf{1}; \tag{3.48}$$

$$\boldsymbol{\Psi}^{(12)} \simeq [\psi_0^{(12)}(l) + \psi_1^{(12)}(l)\hat{\boldsymbol{u}}^1 \cdot \hat{\boldsymbol{n}} + \psi_2^{(12)}(l)\hat{\boldsymbol{u}}^2 \cdot \hat{\boldsymbol{n}} + \psi_{12}^{(12)}(l)\hat{\boldsymbol{u}}^1 \cdot \hat{\boldsymbol{u}}^2]\mathbf{1}. \tag{3.49}$$

The coefficients in these expressions are non-linear functions of the radial coordinate, their exact form depending on the geometry of the subunits and boundary conditions. As previously mentioned, for spherical subunits they can be calculated numerically using methods such as the one described by Jeffrey and Onishi [110]. For asymmetric subunits, they are not easily determined. It is possible to calculate the functions numerically for non-axisymmetric geometries made of spherical beads as in the Kirkwood construction [105, 111]. However, this would require further approximations to describe the interactions between the beads, so we do not pursue the explicit calculation of the hydrodynamic functions. The expansions (3.40)-(3.49) have been truncated at second order as beyond this, additional terms only contribute quantitatively to the final result. As a further simplification, we have also used the diagonal approximation $\mathbf{A} \simeq \frac{1}{3}\mathrm{tr}(A)\mathbf{1}$ [104]. For an axisymmetric dumbbell whose hydrodynamic tensors can be written as the sum of isotropic and directional parts as $\mathbf{A} = A_I(l)\mathbf{1} + A_D(l)\hat{\boldsymbol{n}}\hat{\boldsymbol{n}}$, contributions from the directional parts vanish after averaging over the radial coordinate in the equation for the translational motion for

all the hydrodynamic tensors except $\mathbf{M}$. It can be seen from eqs. (3.23) and (3.24) that the directional part of the tensors $\mathbf{W}$, $\mathbf{\Gamma}$, and $\mathbf{\Lambda}$ do not contribute.

The dynamical equations for ρ, $\boldsymbol{p}$ and $\boldsymbol{p}_\alpha$ are determined similarly to the moment expansion for the ABP example in Chapter 2, leading to the closed set of equations:

$$\begin{aligned}
\partial_t\rho =& \frac{k_\mathrm{B}T}{4}\langle m_0\rangle \nabla^2_{\boldsymbol{R}}\rho + k_\mathrm{B}T\left\langle\frac{\gamma_0}{l}\right\rangle\nabla_{\boldsymbol{R}}\cdot\boldsymbol{p} \\
&+\frac{1}{3}\sum_{\alpha\neq\beta=1}^{2}\left[\left\langle\frac{\gamma_0 V_\alpha}{l}\right\rangle\nabla_{\boldsymbol{R}}\cdot\boldsymbol{p}^\alpha+\frac{1}{3}\left\langle\frac{\gamma_{12}V_\alpha}{l}\right\rangle\nabla_{\boldsymbol{R}}\cdot\boldsymbol{p}^\beta\right]; \qquad (3.50)\\
\partial_t\boldsymbol{p} =& -\frac{k_\mathrm{B}T}{3}\left\langle\frac{\gamma_0}{l}\right\rangle\nabla_{\boldsymbol{R}}\rho - 2k_\mathrm{B}T\left\langle\frac{w_0}{l^2}\right\rangle\boldsymbol{p} \\
&-\frac{2}{3}\sum_{\alpha\neq\beta=1}^{2}\left[\left\langle\frac{w_0 V_\alpha}{l^2}\right\rangle\boldsymbol{p}^\alpha+\frac{1}{3}\left\langle\frac{w_{12}V_\alpha}{l^2}\right\rangle\boldsymbol{p}^\beta\right]; \qquad (3.51)\\
\partial_t\boldsymbol{p}^\alpha =& \frac{1}{9}\left[\left\langle\frac{\gamma_0 V_\alpha}{l}\right\rangle+\frac{1}{3}\left\langle\frac{\gamma_{12}V_\beta}{l}\right\rangle\right]\nabla_{\boldsymbol{R}}\rho \\
&-\frac{2}{3}\left[\left\langle\psi_0^{(\alpha)}V_\alpha\right\rangle+\frac{1}{3}\left\langle(\psi_\beta^{(\alpha)}-\psi_\beta^{(12)})V_{12}\right\rangle+\frac{1}{3}\left\langle\psi_{12}^{(12)}V_\beta\right\rangle\right]\boldsymbol{p} \quad \text{for } \alpha\neq\beta \\
&-\frac{2}{3}\left[\left\langle(\psi_0^{(\alpha)}-\psi_0^{(12)})V_{12}\right\rangle-\frac{1}{3}\left\langle\psi_\alpha^{(12)}V_\beta\right\rangle+k_\mathrm{B}T\left\langle\psi_{12}^{(12)}\right\rangle\right]\boldsymbol{p}^\beta \\
&-2k_\mathrm{B}T\left\langle\psi_0^{(\alpha)}\right\rangle\boldsymbol{p}^\alpha. \qquad (3.52)
\end{aligned}$$

From eq. (3.50), ρ is locally conserved and is thus a hydrodynamic mode. However, $\boldsymbol{p}$ and $\boldsymbol{p}_\alpha$ are fast modes with finite relaxation times. In the absence of constraints on the rotational motion of the subunits the relaxation time of $\boldsymbol{p}$ is $1/\left(2k_\mathrm{B}T\left\langle w_0/l^2\right\rangle\right)$. By comparison to the ABP example, this corresponds to an average rotational diffusion coefficient of $k_\mathrm{B}T\left\langle w_0/l^2\right\rangle$ for the dumbbell in the absence of rotational constraints on the subunits. If the subunits are unconstrained and not hydrodynamically coupled, each rotates freely with rate $1/\left(2k_\mathrm{B}T\left\langle\psi_0^{(\alpha)}\right\rangle\right)$. The reorientation times for $\boldsymbol{p}$ and $\boldsymbol{p}^\alpha$ will not be much slower for weakly constrained subunits.

In deriving the hydrodynamic equations (3.50)-(3.52), we have already performed a gradient expansion and neglected terms that are higher order derivatives than $\nabla^2_{\boldsymbol{R}}\rho$, $\nabla_{\boldsymbol{R}}\cdot\boldsymbol{p}$ and $\nabla_{\boldsymbol{R}}\cdot\boldsymbol{p}^\alpha$. Furthermore, the inevitable hierarchy in which ρ, $\boldsymbol{p}$ and $\boldsymbol{p}^\alpha$ are coupled to higher order moments has been truncated by re-expressing the higher order moments in terms of ρ, $\boldsymbol{p}$ and $\boldsymbol{p}^\alpha$ using (3.26)-(3.30)'(3.32) and (3.33). This approximation is checked in Appendix A. We also find that these terms would anyway

not survive the gradient expansion. We note that the coupling between the moments of the configurational distribution function of the dumbbell is not tridiagonal as in the ABP example, precisely because the diffusion of the dumbbell is anisotropic.

The coupling between ρ and the first order moments is due to a non-vanishing $\mathbf{\Gamma}$; for a flexible symmetric dumbbell, eq. (3.50) would be a closed equation for the effective diffusion. The coupling between ρ and the first moments of the distribution with respect to the individual subunits $\boldsymbol{p}^\alpha$ would also vanish if the subunits are freely rotating. The absence of the tensors $\mathbf{\Phi}^{(\alpha)}$ and $\mathbf{\Lambda}^{(\alpha)}$ in the hydrodynamic equations signifies that the effect of chirality of the individual subunits is no longer present at this coarse-grained level.

Finally, at times greater than the reorientation times of $\boldsymbol{p}$ and $\boldsymbol{p}^\alpha$ we can take the stationary limit of eqs. (3.51) and (3.52) to find expressions for these fields in terms of the gradient of ρ. From $\partial_t \boldsymbol{p} = 0$ and $\partial_t \boldsymbol{p}^\alpha = 0$ we find the following expressions for the first moments:

$$\begin{aligned}\boldsymbol{p}^\alpha =& \frac{1}{6}\frac{\langle \gamma_0/l\rangle}{\langle w_0/l^2\rangle}\left\{ g_\alpha + \frac{1}{3}g_{12,\beta} - \frac{1}{3}g_\beta \frac{\left\langle \psi_{12}^{(12)}\right\rangle}{\left\langle \psi_0^{(\alpha)}\right\rangle} + \frac{1}{9k_\mathrm{B}T}\frac{\left\langle (\psi_\beta^{(\alpha)} - \psi_\beta^{(12)})V_{12}\right\rangle}{\left\langle \psi_0^{(\alpha)}\right\rangle}\right.\\ &\left. -\frac{1}{3k_\mathrm{B}T}g_\beta \frac{\left\langle \left(\psi_0^{(\alpha)} - \psi_0^{(12)}\right)V_{12}\right\rangle}{\left\langle \psi_0^{(\alpha)}\right\rangle} + \frac{1}{(3k_\mathrm{B}T)^2}\frac{\left\langle \psi_0^{(\alpha)}V_\alpha\right\rangle}{\left\langle \psi_0^{(\alpha)}\right\rangle}\sum_{\gamma=1,2}\frac{\langle w_0 V_\gamma/l^2\rangle}{\langle w_0/l^2\rangle}g_\gamma\right\}\nabla_{\boldsymbol{R}}\rho,\end{aligned} \tag{3.53}$$

for $\alpha \neq \beta$ and

$$\begin{aligned}\boldsymbol{p} =& -\frac{1}{6}\frac{\langle \gamma_0/l\rangle}{\langle w_0/l^2\rangle}\sum_{\alpha\neq\beta=1,2}\left\{1 + \frac{1}{3k_\mathrm{B}T}g_\alpha\frac{\langle w_0 V_\alpha/l^2\rangle}{\langle w_0/l^2\rangle} + \frac{1}{9k_\mathrm{B}T}\frac{\langle w_0 V_\alpha/l^2\rangle}{\langle w_0/l^2\rangle}g_{12,\beta}\right.\\ &+\frac{1}{9k_\mathrm{B}T}g_\beta\frac{\langle w_{12}V_\alpha/l^2\rangle}{\langle w_0/l^2\rangle} + \frac{1}{3(3k_\mathrm{B}T)^2}\frac{\langle w_0 V_\alpha/l^2\rangle}{\langle w_0/l^2\rangle}\frac{\left\langle (\psi_\beta^{(\alpha)} - \psi_\beta^{(12)})V_{12}\right\rangle}{\left\langle \psi_0^{(\alpha)}\right\rangle}\\ &\left.+\frac{1}{(3k_\mathrm{B}T)^2}\frac{\langle w_0 V_\alpha/l^2\rangle}{\langle w_0/l^2\rangle}\frac{\left\langle \left(\psi_0^{(\alpha)} - \psi_0^{(12)}\right)V_{12}\right\rangle + k_\mathrm{B}T\left\langle \psi_{12}^{(12)}\right\rangle}{\left\langle \psi_0^{(\alpha)}\right\rangle}g_\beta\right\}\nabla_{\boldsymbol{R}}\rho\end{aligned} \tag{3.54}$$

which has been written to increasing order in the expansions of the potential (3.15) and hydrodynamic tensors (3.40)-(3.49). We have defined the dimensionless coefficients

$$g_\alpha = \frac{1}{3k_\mathrm{B}T}\left[\frac{\langle \gamma_0 V_\alpha/l\rangle}{\langle \gamma_0/l\rangle}\frac{\langle w_0/l^2\rangle}{\left\langle \psi_0^{(\alpha)}\right\rangle} + \frac{\left\langle \psi_0^{(\alpha)}V_\alpha\right\rangle}{\left\langle \psi_0^{(\alpha)}\right\rangle}\right] \tag{3.55}$$

$$g_{12,\beta} = \frac{1}{3k_{\mathrm{B}}T}\left[\frac{\langle\gamma_{12}V_\beta/l\rangle}{\langle\gamma_0/l\rangle}\frac{\langle w_0/l^2\rangle}{\left\langle\psi_0^{(\alpha)}\right\rangle} + \frac{\left\langle\psi_{12}^{(12)}V_\beta\right\rangle}{\left\langle\psi_0^{(\alpha)}\right\rangle}\right]. \tag{3.56}$$

3.3 Results

3.3.1 The diffusion equation

From the moment expansion we find the diffusion equation, $\partial_t\rho(\boldsymbol{R},t) = D_{\mathrm{eff}}\nabla^2_{\boldsymbol{R}}\rho$, with effective diffusion coefficient

$$\begin{aligned} D_{\mathrm{eff}} =& \frac{k_{\mathrm{B}}T}{4}\langle m_0\rangle - \frac{k_{\mathrm{B}}T}{6}\frac{\langle\gamma_0/l\rangle^2}{\langle w_0/l^2\rangle}\left\{1 - \sum_{\alpha\neq\beta=1,2}\left[\left(\frac{\tilde{v}_\alpha}{k_{\mathrm{B}}T}\right)^2\mathcal{K}_\alpha + \left(\frac{\tilde{v}_\alpha}{k_{\mathrm{B}}T}\right)\left(\frac{\tilde{v}_\beta}{k_{\mathrm{B}}T}\right)\mathcal{L}_{\alpha\beta}\right.\right. \\ &\left.\left. + \left(\frac{\tilde{v}_\alpha}{k_{\mathrm{B}}T}\right)\left(\frac{\tilde{v}_{12}}{k_{\mathrm{B}}T}\right)\mathcal{M}_{\alpha\beta} + \left(\frac{\tilde{v}_\alpha}{k_{\mathrm{B}}T}\right)\left(\frac{\tilde{v}_\beta}{k_{\mathrm{B}}T}\right)\left(\frac{\tilde{v}_{12}}{k_{\mathrm{B}}T}\right)\mathcal{N}_{\alpha\beta}\right]\right\}. \end{aligned} \tag{3.57}$$

The first term in the effective diffusion coefficient is the equilibrium average of contributions from the translational modes of the dumbbell. The remaining terms are corrections due to the fluctuations of the flexible dumbbell and are coupled to its asymmetry through the function γ_0. In (3.57), we have chosen the orientation constraints to be $V_\alpha = ka^2v_\alpha\varphi(l)$ and $V_{12} = ka^2v_{12}\varphi(l)$, where k is the stiffness of the interaction potential and v_α and v_{12} are the constant magnitudes of the constraints on orientations (which have been redefined as $\tilde{v}_\alpha = ka^2v_\alpha$ and $\tilde{v}_{12} = ka^2v_{12}$) and $\varphi(l) = \frac{1}{2}\left(\frac{l}{a}-1\right)^2$. The geometric coefficients $\mathcal{K}_\alpha$, $\mathcal{L}_{\alpha\beta}$, $\mathcal{M}_{\alpha\beta}$ and $\mathcal{N}_{\alpha\beta}$ are dimensionless and of order 1, and are estimated to be positive for a harmonic-like potential. Hence, a dumbbell with freely rotating subunits (with $v_\alpha = v_{12} = 0$) has the largest negative contribution to its effective diffusion coefficient.

Equation (3.57) can be understood by considering the force dipole that the dumbbell exerts on the fluid. The force $\mathbf{F}_2 = -\nabla_2 U$ on a subunit 2 (similarly for subunit 1) after a time when the separation coordinate has equilibrated but the orientation of the dumbbell is constant is $\langle\mathbf{F}_2\rangle = -\langle U'\rangle\,\hat{\boldsymbol{n}}$. Hence, the dumbbell will have a nonzero average dipole if $\langle U'\rangle \neq 0$. With the assumption that the distribution-function has a Boltzmann-like dependence on the radial coordinate,

$$\langle U'\rangle = -\frac{k_{\mathrm{B}}T}{\mathcal{P}}\int_a \mathrm{d}l\, l^{d-1}\frac{\mathrm{d}}{\mathrm{d}l}\left(\mathrm{e}^{-U/k_{\mathrm{B}}T}\right) \tag{3.58}$$

where d is the dimensionality of space. This does not vanish in any dimension other than one (even though $U'|_{l=a} = 0$) due to the entropic contributions in dimensions greater than one. Due to asymmetry, this fluctuating dipole results in a net drift velocity. This does not hold at times before the radial coordinate has relaxed when $\langle U' \rangle$ may vanish. The negative sign of the correction is a generic feature of fluctuation-induced interactions [112] and its proportionality to $-\langle U' \rangle^2$ highlights a similarity to dispersion forces [113].

We note that the relatively simple form of (3.57) is furnished by approximations (3.15) for the interaction between the subunits and (3.40)-(3.49) for the hydrodynamic tensors. The contribution of higher order terms in these expansions is to modify the numerical coefficients of the existing terms.

With the quasi-stationary approximation that was used to close the moment expansion to allow us to write the diffusion equation for $\rho(\boldsymbol{R}, t)$, eq. (3.57) is the diffusion coefficient of the com after a sufficiently long time. The time evolution of the dumbbell can be obtained by treating the stochastic dynamics in the path integral formulation [80, 114]. For freely rotating subunits with hydrodynamic tensors approximated by $\mathbf{A} \simeq \left\langle A_{\mathrm{I}} + \frac{1}{3} A_{\mathrm{D}} \right\rangle \equiv \langle A \rangle \, \mathbf{1}$, using the diagonal approximation as well as orientation preaveraging, the path integral treatment following the Martin-Siggia-Rose method [115], leads to two regimes for the effective diffusion coefficient: At early times, the diffusion coefficient is just the average of the translational modes but at times larger than the rotational diffusion time, it has the same form as (3.57) [80].

3.3.2 Example: An axisymmetric dumbbell

For a more quantitative analysis of the role of thermal fluctuations on the diffusive dynamics of the generalised dumbbell, we consider the simpler case of an axisymmetric dumbbell with spherical subunits of radii a_1 and a_2 (and $a_2 > a_1$). The harmonic interaction potential is

$$U = \frac{1}{2} k (l - a)^2 \left[1 + v_1 \, \hat{\boldsymbol{n}} \cdot \hat{\boldsymbol{u}}^1 + v_2 \, \hat{\boldsymbol{n}} \cdot \hat{\boldsymbol{u}}^2 + v_{12} \, \hat{\boldsymbol{u}}^1 \cdot \hat{\boldsymbol{u}}^2 \right] \tag{3.59}$$

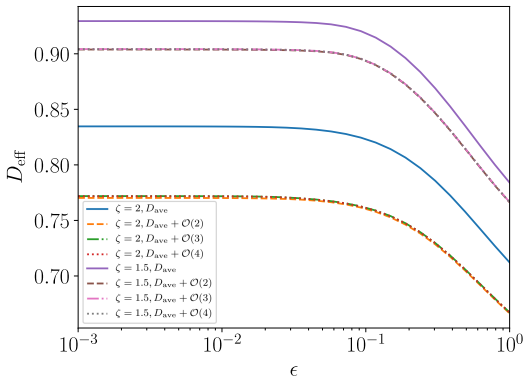

Figure 3.3. The effective diffusion coefficient of two axisymmetric dumbbells with asymmetries $\zeta = 2$ and $\zeta = 1.5$ as a function of relative fluctuations ε, with $v_1 = 0.1$, $v_2 = 0.13$, $v_{12} = 0.15$ and $a_1/a = 0.3$. D_{ave} is the first term of D_{eff}; $D_{\text{ave}} + \mathcal{O}(2)$ is the sum of the first two terms; $D_{\text{ave}} + \mathcal{O}(3)$ includes all but the last correction; and $D_{\text{ave}} + \mathcal{O}(4)$ includes all the terms shown [107].

for $l > a_1 + a_2$ and ∞ otherwise, and the constant constraint parameters satisfy $v_\alpha, v_{12} \ll 1$. The mobility functions are calculated using the method of Jeffrey and Onishi [110], for two unequal rigid spheres in an unbounded fluid, in terms of the ratio of subunits sizes $\zeta = a_2/a_1$ and the non-dimensionalised distance between the subunits.

In Fig. 3.3, we have plotted the effective diffusion coefficient D_{eff} against the relative amplitude of thermal fluctuations of the dumbbell $\varepsilon = \sqrt{k_{\text{B}}T/ka^2}$, for different values of ζ. As expected, the diffusion coefficient of the dumbbell decreases with increasing asymmetry. The figure also shows that D_{eff} increases with the stiffness of the potential, with its maximum value in the limit of a rigid potential. Finally, since the mobility functions scale as powers of $1/l$ a small deformation in the dumbbell will have an amplified contribution to the diffusion coefficient.

3.3.3 Fluctuation-dissipation theorem

To verify the validity of the averaging scheme, we check that the effective diffusion equation for the com motion obtained with the method we have described satisfies the fluctuation dissipation theorem, specifically, the Einstein relation $\mu_{\text{eff}} = D_{\text{eff}}/k_{\text{B}}T$, where μ_{eff} is the effective mobility of the dumbbell. The calculation is performed for a simplified case where the potential has no orientation dependence, and the

effect of anisotropy is neglected. In order to establish the presence of the Einstein relation, the diffusion equation is derived for the suspended dumbbell subjected to a constant external force $\mathbf{f} = \mathrm{f}\,\boldsymbol{e}$, with magnitude f in the direction $\boldsymbol{e}$, through the application of a force of $\mathbf{f}/2$ to each subunit.

Under the influence of the external force, the probability distribution $P_f(\boldsymbol{R}, \boldsymbol{l}; t)$ for $\boldsymbol{R}$ and $\boldsymbol{l}$ satisfies the Smoluchowski equation

$$\partial_t P_f(\boldsymbol{R}, \boldsymbol{l}; t) = \mathcal{L}_{\mathrm{E}} P_f - \frac{1}{4}\nabla_{\boldsymbol{R}} \cdot [\mathbf{M} \cdot \boldsymbol{e} P_f] - \nabla_{\boldsymbol{l}} \cdot [\boldsymbol{\Gamma} \cdot \boldsymbol{e} P_f] \tag{3.60}$$

[80], where $\mathcal{L}_{\mathrm{E}} P_f$ is the equilibrium contribution, which is independent of $\mathbf{f}$. After averaging over the radial coordinate l at fixed orientation, to find the equation satisfied by $\mathcal{P}_f = \int \mathrm{d}l\, l^2 P_f$ and performing the moment expansion of the separation-averaged Smoluchowski equation, with the same closure scheme as was used to derive the diffusion coefficient (3.57), the drift-diffusion equation for the driven system is found to be

$$\partial_t \rho_f = D_{\mathrm{eff}} \nabla^2 \rho_f - \mu_{\mathrm{eff}} \boldsymbol{f} \cdot \nabla \rho_f. \tag{3.61}$$

Indeed, the diffusion and mobility coefficients in this equation are related by the Einstein relation.

3.3.4 Enzyme kinetics

Up to now, we have not considered the effect of kinetics, which describes the process of catalysis of a real enzyme. For this, the three-step Michaelis-Menten kinetics that was described in the introduction is simplified to a discrete two-state model. It is assumed that the enzyme exists in one of two equilibrium states: either it is free, or it is bounded in a complex to a substrate (or product) molecule. The two states are characterised by their interaction potentials, U_{f} and U_{b}, in the free and bound states respectively, which are generally different. The catalytic cycle of an enzyme is then reduced to transitions between these two states, neglecting the non-equilibrium step of substrate being converted into product molecules. This is motivated by the assumption that there is a separation of time scales between the

binding interaction and the chemical step, and the binding interaction is assumed to be faster of the two processes.

To include the effect of kinetics in the result for the long-time effective diffusion coefficient, the equilibrium weight function is redefined for the two-state equilibrium so that the average of a conformation-dependent function becomes

$$\langle\phi\rangle_{\mathrm{MM}} = \langle\phi\rangle_{\mathrm{f}} + f(\mathrm{S},\mathrm{P})[\langle\phi\rangle_{\mathrm{b}} - \langle\phi\rangle_{\mathrm{f}}] \tag{3.62}$$

[80], where $\langle\cdot\rangle_{\mathrm{f}}$ and $\langle\cdot\rangle_{\mathrm{b}}$ are the averages with respect to the free and bound state Boltzmann weights respectively, and $f(S,P)$ is the probability for transitioning between the two states and is therefore a function of the substrate and product concentrations, with limiting values corresponding to different stages in the chemical reaction.

Generically,

$$f(\mathrm{S},\mathrm{P}) = \frac{\mathrm{S}_0}{\mathrm{K}+\mathrm{S}_0} \tag{3.63}$$

[80], where S_0 is the initial substrate concentration and K is the equilibrium constant that depends on the concentration of substrate and product. At early times, when it can be assumed that the substrate concentration has not substantially deviated from its initial value (as not many of the substrate molecules will have been converted into product), $\mathrm{K} = \mathrm{K_S}$, where $\mathrm{K_S}$ is the effective equilibrium constant for substrate binding and is proportional to the ratio of the rates of binding (k_{on}) and unbinding (k_{off}) of substrate molecules. After chemical equilibrium has been reached, $\mathrm{K} = \frac{1}{2}(\mathrm{K_S}+\mathrm{K_P})$, where $\mathrm{K_P}$ is the effective equilibrium constant for product binding, which is proportional to the ratio of the rates of binding and unbinding of product molecules.

3.3.5 The effect of substrate binding on the diffusion coefficient

From the discussion in Section 3.1.3, we expect for the catalytic cycle to be accompanied by conformational changes in the enzyme from its free equilibrium state. The effect of the reduced catalytic cycle due to the presence of substrate

molecules is introduced into the generalised dumbbell model by replacing the averages in eq. (3.57) by (3.62), which leads to a substrate-dependent diffusion coefficient $D(\mathrm{S})$. Neglecting the effect of the rotational constraints for simplicity, the change in diffusion coefficient due to binding interactions is given by

$$\begin{aligned}\Delta D &= D(\mathrm{S}) - D(\mathrm{S}=0) \\ &= \frac{k_\mathrm{B}T}{4}\left\langle m_0\right\rangle_{\mathrm{MM}} - \frac{k_\mathrm{B}T}{6}\frac{\left\langle \gamma_0/l\right\rangle^2_{\mathrm{MM}}}{\left\langle w_0/l^2\right\rangle_{\mathrm{MM}}} - \frac{k_\mathrm{B}T}{4}\left\langle m_0\right\rangle_{\mathrm{f}} - \frac{k_\mathrm{B}T}{6}\frac{\left\langle \gamma_0/l\right\rangle^2_{\mathrm{f}}}{\left\langle w_0/l^2\right\rangle_{\mathrm{f}}}.\end{aligned} \tag{3.64}$$

Assuming that the relative difference in the configurational averages of the mobility functions in the free and bounds states, $[\langle\phi\rangle_\mathrm{b} - \langle\phi\rangle_\mathrm{f}]/\langle\phi\rangle_\mathrm{b}$, is small, the relative change in diffusion coefficient is then

$$\frac{\Delta D}{D_0} = \frac{\langle\mu_\mathrm{b}\rangle - \langle\mu_\mathrm{f}\rangle}{\langle\mu_\mathrm{f}\rangle} \equiv \mathcal{A}\frac{\mathrm{S}_0}{\mathrm{S}_0+\mathrm{K}} \tag{3.65}$$

[26, 80], where $D_0 = D(\mathrm{S}=0)$ and $\mathcal{A}$ is a dimensionless function of the average mobility functions in the two states, which is independent of substrate concentration. Equation (3.65) has two main features; firstly, the dependence on substrate concentration is the same as in the Michealis-Menten equation and secondly, since $\mathcal{A}$ is a ratio of averages of similar functions, it is expected to be of order one. Both features are consistent with the experimental observations for the change in the diffusion coefficient of an enzyme in the presence of its substrate (or inhibitor) [26].

Specific examples of the conformational changes that may occur in an enzyme due to substrate binding have been considered [80], and estimates are provided for the contribution from each to the change in diffusion coefficient given by eq. (3.65). For this, the interaction potential is again assumed to be harmonic and written as

$$U_\mathrm{i} = \frac{1}{2}k_\mathrm{i}(l-x_\mathrm{i})^2\left[1 + v_{1,\mathrm{i}}\,\hat{\boldsymbol{n}}\cdot\hat{\boldsymbol{u}}^1 + v_{2,\mathrm{i}}\,\hat{\boldsymbol{n}}\cdot\hat{\boldsymbol{u}}^2 + v_{12,\mathrm{i}}\,\hat{\boldsymbol{u}}^1\cdot\hat{\boldsymbol{u}}^2\right] \tag{3.66}$$

where the index i = f,b is given to parameters that are conformation dependent. k_i is the stiffness of the potential in state i, x_i is the equilibrium distance between the subunits in either state and $v_{\alpha,\mathrm{i}}$ and $v_{12,\mathrm{i}}$ are the constraints on the rotational degrees of freedom in either state. For the first two examples, the rotational constraints are set to zero to facilitate the analytic calculations. In all cases the potential is

assumed to be sufficiently stiff ($\varepsilon \ll 1$) that the subunits are unlikely to touch so that the lower limit of (3.17) and (3.18) can be extended to $-\infty$ and the averages over the radial coordinate can be approximated.

As discussed in the introduction to this chapter, substrate binding can cause a change in the size of the enzyme on the scale of nm. Correspondingly, in the interaction potentials given by (3.66), $x_\mathrm{f} = a$ and $x_\mathrm{b} = a - \delta l$, where δl is the change in the distance between the subunits upon binding. For a small deformation $\delta l \ll a$ and assuming $k_\mathrm{f} = k_\mathrm{b}$, $\mathcal{A}$ is expanded to first order in δl to give

$$\mathcal{A}_c = \mathcal{G}\frac{\delta l}{a} \tag{3.67}$$

[80], the contribution to $\mathcal{A}$ due to the change in equilibrium size. $\mathcal{G}$ is a new dimensionless number that is the ratio of the mobility functions and their derivatives and is again of order one. From eq. (3.67), the change in diffusion coefficient (3.65), will be of the order of the relative deformation and for a positive δl, an enzyme in the bound state will diffuse faster than when it is free.

Another possibility is that substrate binding changes the stiffness of the interaction between the domains of an enzyme. In this case, the associated potentials have $k_\mathrm{f} \neq k_\mathrm{b}$. Supposing that $x_\mathrm{f} = x_\mathrm{b}$, $\mathcal{A}$ is expanded to first order in the change in stiffness $\delta k = k_\mathrm{b} - k_\mathrm{f}$ to give

$$\mathcal{A}_s = \mathcal{H}\varepsilon^2\frac{\delta k}{k_f} \tag{3.68}$$

[80], where $\mathcal{H}$ is another ratio of the mobility functions and their derivatives. In this case, the change in diffusion coefficient is proportional to the relative change in the stiffness of the interaction between the subunits of the generalised dumbbell. The dumbbell diffuses faster in the bound state if binding increases the stiffness of the interaction between its domains *i.e.*, for $k_\mathrm{b} > k_\mathrm{f}$.

Finally, in the introduction to this chapter, we also discussed the possibility of a flexible enzyme becoming more constrained after substrate binding. The contribution to $\mathcal{A}$ from varying the constraint on rotational fluctuations is given by

$$\mathcal{A}_r = \varepsilon^2 \sum_{\alpha=1,2} v_{\alpha,\mathrm{f}}(v_{\alpha,\mathrm{b}} - v_{\alpha,\mathrm{f}})\mathcal{J}_\alpha \tag{3.69}$$

[80], where $\mathcal{J}_\alpha$ is a dimensionless number which is again composed of the mobility functions and their derivatives and is unique for each subunit.

In the Oseen limit, the mobility functions in (3.57) can be approximated as

$$m_0 \simeq \frac{1}{6\pi\eta}\left(\frac{1}{a_1}+\frac{1}{a_2}\right)+\frac{1}{3\pi\eta l}, \tag{3.70}$$

$$w_0 \simeq \frac{1}{6\pi\eta}\left(\frac{1}{a_1}+\frac{1}{a_2}\right)-\frac{1}{4\pi\eta l}, \tag{3.71}$$

$$\gamma_0 = \frac{1}{6\pi\eta}\left(\frac{1}{a_2}-\frac{1}{a_1}\right). \tag{3.72}$$

In (3.70) we have considered that m_0 includes a contribution from the directional part of the tensor $\mathbf{M}$. Using (3.70)-(3.72), an order of magnitude estimate for the leading order contribution to the relative change in effective diffusion coefficient due to binding interactions is

$$\frac{\Delta D}{D_0} \simeq 2\frac{a_1 a_2}{a_1+a_2}\left(\left\langle\frac{1}{l}\right\rangle_{\mathrm{b}}-\left\langle\frac{1}{l}\right\rangle_{\mathrm{f}}\right). \tag{3.73}$$

This shows that the leading order contribution from the reduced catalytic cycle comes from the change in the average length of the dumbbell upon binding. In the case that the bound state of the dumbbell has a smaller average length, which can happen through $\delta l > 0$ or $\delta k > 0$, binding interactions result in enhanced diffusion. Due to the fluctuation-induced contribution to the effective diffusion coefficient, the next order contribution to (3.73) is due to changes in the fluctuations of the dumbbell upon binding [116]. Therefore, even if the average length of the dumbbell is the same in its free and bound states, the difference in fluctuations in the two states will also result in a change in diffusion coefficient.

3.4 Discussion

Taylor dispersion theory:

The result (3.57) for the long-time diffusion coefficient is not exact, but relies on the averaging procedure described in Section 3.2.3 and on the expansions (3.14) and (3.40)-(3.49) for the interaction between the domains of the model enzyme

and the hydrodynamic functions. An exact expression has been derived by Agudo-Canalejo and Golestanian for the dumbbell with freely rotating subunits [116], using generalised Taylor dispersion theory [93, 117, 118], which turns out to be very similar to eq. (3.57). The difference being that the exact result includes an additional fluctuation-induced term, which comes from the directional parts of the rotation and translation-rotation tensors and has a different structure for the average over the separation coordinate, which is the result of avoiding the averaging procedure. However, our approximate method appears to have a wider range of applicability. For instance, the exact method cannot be used to find the effective transport coefficients for the system in the presence of a substrate concentration gradient, as is done in the Chapter 4.

Hydrodynamic interaction:

In Section 3.3.2 we have given quantitative results for the effective diffusion coefficient of an axisymmetric dumbbell with spherical subunits, for which the hydrodynamic mobility functions can be calculated relatively easily [110]. It remains to provide a quantitative description for a truly asymmetric dumbbell without an axis of symmetry. Some progress has been made on determining the properties of the hydrodynamic interaction between two arbitrary shaped objects. It has been shown that asymmetry leads significant two-body hydrodynamic effects that is not present for spheres [119].

We also note that the complex environment in which enzymes exist would be more realistically described by a viscoelastic theory which could include, for example, the material that makes up the extracellular matrix.

Further questions on enhanced diffusion:

As new experimental results are being reported, it is apparent that substrate-driven enhanced enzyme diffusion is still not fully understood. With regards to experiments, there are questions on the validity of FCS as a method for measuring the diffusivity of enzymes. There have been suggestions that results from FCS experiments could contain the effects of experimental artefacts that could lead to observations which may be falsely interpreted as enhanced diffusion [120–122].

The complication of performing true single-molecule experiments is also being discussed [123].

Due the variety of enzymes and their range of physical and thermodynamic properties, it is likely that enhanced enzyme diffusion is a combination of active mechanisms, such as those described in the introduction, and passive mechanisms like ours. The effects of non-equilibrium activity could be important for fast, exothermic enzymes. Further experiments and theoretical studies (to include simulations) are necessary to establish the importance of each mechanism and any other contributions which have so far been missed. We note that a similar model to ours was recently studied with Brownian dynamics simulations [124].

Oligomeric enzymes:

Most enzymes exist as oligomers or polymers[3] (see Fig.3.4). Some of these oligomeric enzymes can dissociate and re-associate reversibly in response to a stimulus such as enzyme or substrate concentration and temperature, typically with reduced catalytic activity in the dissociated state so that dissociation regulates enzymatic activity. It was recently suggested that enhanced enzyme diffusion in the presence of substrate could be the result of dissociation of enzyme oligomers [120, 125].

In a recent publication, Agudo-Canalejo et al. investigated the diffusion and reaction times of dissociating oligomeric proteins. By comparing the diffusion of dissociating and non-dissociating proteins, they show that dissociation leads to enhanced diffusion, and furthermore can increase catalytic activity in a concentration-dependent way.

For a dimeric protein, which has two monomer subunits, we have shown that the diffusion coefficients of the dimer and monomer are related by

$$D_{\text{dim}} = \frac{1}{2} D_{\text{mon}} - \delta D_{\text{fluc}}, \tag{3.74}$$

where D_{dim} is the diffusion coefficient of the dimer and D_{mon} of the monomer, so that the dimer is expected to diffuse considerably more slowly than the monomer [126]. Hence, the effective diffusion coefficient of a system of proteins is increased if they can

[3] These are structures composed of two or more subunits.

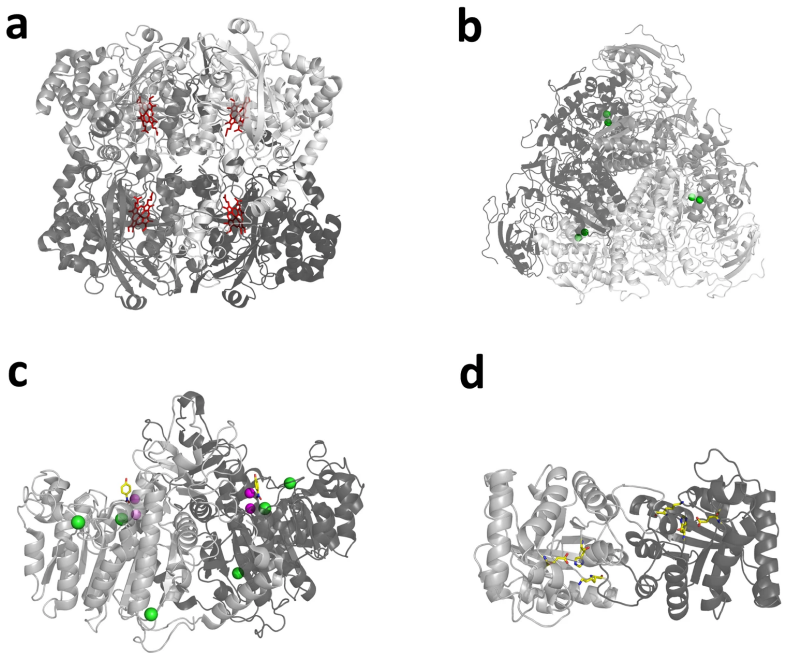

Figure 3.4. The structure of (a) Catalase, (b) Urease, (c) Alkaline phosphatase, and (d) Triose phosphate isomerase. Each region in a different shade of grey is a different monomer. Reprinted by permission from Springer Nature: Nature [31], 2020.

dissociate. However, in the dissociated state, the catalytic activity of the enzymes may be compromised so that enhanced diffusion due to dissociation comes at the cost of a reduction in catalytic activity. A positive interplay between fast diffusion of the monomer, which is prevalent at low protein concentration, and fast re-association into the catalytic dimer at sufficiently high concentration, leads to an increased reactivity of the dissociating enzyme compared to a non-dissociating enzyme.

The reaction time, which is defined as the first passage time for a protein to diffuse to a target, is determined numerically. It is possible that with our probabilistic description we may be able to obtain an analytic result, at least for a simpler system.

CHAPTER 4

Hydrodynamic contribution to chemotaxis

4.1 Introduction

4.1.1 Chemotaxis

It has been known for several decades that bacteria and eukaryotic cells are able to direct their motion in response to local field gradients of, for example, chemicals, temperature, or light intensity [127]. The response could be in the form of an increased translational velocity in a given direction or an angular velocity. This ability has evolved to aid search processes, like finding an optimal region to thrive [128]. In the case of a chemical field, the effect is generically known as *chemotaxis* and causes the *chemotactic* object to move towards or away from the chemical gradient. It has been suggested that chemotaxis is used in living organisms for signalling [129]: In addition to swimming with flagella, chemotaxis of spermatozoa in response to chemical gradients released by the oocyte has been established in many species [130], and theoretical descriptions of the underlying physics have been given [131]. It is generally accepted that chemotactic bacteria perform a preferential random walk with memory of the chemical gradient [128, 132, 133], while cells are able to use their size to determine the direction of a gradient across their body [134].

Recently, chemotaxis has been reported for single enzyme molecules, which do not have the motility and sensory machinery of bacteria and eukaryotic cells. Dey et al. have made a proposal for a micromotor that is fully powered by enzyme catalysis and their ability to chemotax up a chemical gradient [7]. In that scenario the size of the motor could be used to draw a comparison with a chemotactic cell. However, for a single enzyme molecule, the ability to respond to a chemical gradient is a very surprising observation because of its size and its implication on the necessary timescale of such a gradient response. A perceivable response of an enzyme to a local gradient would be the culmination of overcoming thermal fluctuations and viscous effects that are expected to be significant for dynamics at molecular length scales and are amplified in cellular environments.

4.1.2 Experimental observations of enzyme chemotaxis

In the past decade there have been reports of chemotactic behaviour of catalytically active enzymes in gradients of their substrate, where enzymes move preferentially up [7, 22, 23, 27, 29, 30, 32, 78, 135] or down [33] a substrate concentration gradient, with speeds of up to the order of μm/s [29]. This includes many of the enzymes that have also been reported to exhibit enhanced diffusion in a uniform concentration of their substrate. Notably the enzyme urease has been reported to move up [29] and down [33] a substrate concentration gradient in conflicting observations. Experiments have been performed to show that the motion in concentration gradients is due to a directed and preferential drift rather than enhanced diffusion [22, 78]. Experiments have also suggested that chemotaxis may be observed for enzymes that are prevented from catalysing substrate molecules into product [23] and for molecular dyes in the direction of an increasing concentration of a polymer to which they bind reversibly [136].

Very recently, similar experiments with vesicles decorated with catalytically active enzymes have reported chemotaxis and anti-chemotaxis (towards decreasing substrate concentration) depending on the enzyme that is attached to the vesicle– one of the enzymes is reported to lead to both types of chemical response of the

vesicle [137]. The observation of chemotaxis was attributed to enzyme catalysis, while anti-chemotaxis was described as the result of repulsive interactions between the lipids of the vesicle to which enzymes are attached and substrate molecules.

These chemotaxis experiments are commonly performed in microfluidic devices, typically with two inlets, through which solutions with different compositions of enzyme, substrate and buffer are injected. An example of the setup is shown in Fig. 4.1. The intensity profile of the enzymes (which are labelled with fluorescence) is measured across the channels over time to determine their motion. As shown in Fig. 4.1, if a solution containing substrate molecules is injected into one inlet and a solution of enzymes into the other, chemotaxis up the substrate concentration gradient would result in a drift of the enzymes in the direction of the substrate when compared to a situation in which a solution with no substrate is injected into the inlet. It has been suggested that the concentrations [138] and initial concentration profiles [139] that are injected into the microfluidic channels could be significant for the steady-state profile of the enzyme. It has been shown that it is possible to separate catalytically active enzyme molecules from inactive molecules with similar physical properties by exploiting the effect of chemotaxis in a microfluidic network [32].

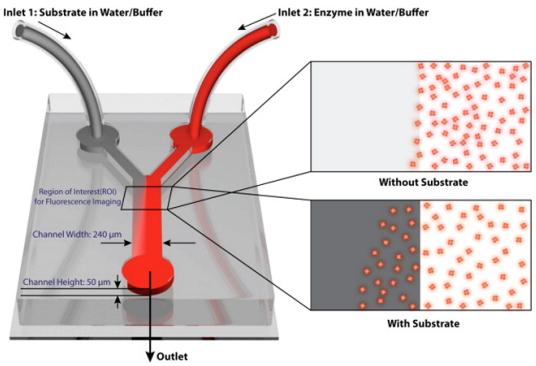

Figure 4.1. A two-inlet microfluidics device, showing chemotaxis of an enzyme towards increasing substrate concentration. This figure has been reproduced from Sengupta et al. [29].

4.1.3 Models of enzyme chemotaxis

As is the case for enhanced diffusion, there is still no consensus on the mechanism (or mechanisms) that is responsible for the observation of enzyme chemotaxis in substrate concentration gradients. Classical descriptions of chemotaxis do not include the effect of the catalytic cycle, and therefore cannot fully describe chemotaxis in catalytically active enzymes. As discussed in the review by Feng and Gilson, the alternative suggestions put forward so far broadly fall into two groups [139].

On one side are the theories that predict the existence of an average force on an enzyme that is directed towards or away from the substrate (or ligand) gradient. The initial proposal for this mechanism was provided by Schurr et al. [140], to explain the chemotaxis of macromolecules which are not enzymes but has since been used to explain the observation of chemotaxis of enzymes [22, 136]. The theory relies on the thermodynamics of binding, specifically, the difference in the free energies of the free and bound state enzyme or macromolecule. Subsequent theories of this type have incorporated substrate-driven enhanced diffusion [78] (on the basis that experimental observations suggest a link between the two), in an attempt to reconcile the high speeds of chemotaxis reported in experiments with the predictions of the original theory of Schurr et al..

The second group consists of mechanisms that are based on a position dependent diffusion coefficient, which is inferred phenomenologically from the dependence of an enzyme's diffusion coefficient on a uniform substrate concentration that has been widely observed in the context of enhanced diffusion. But as discussed by Schnitzer et al. [134], determining the correct form for the dynamical equations of such systems with position dependent diffusion coefficients requires some amount of care.

Recently, Agudo-Canalejo et al. introduced a microscopic model for the chemotaxis of enzymes in which enhanced diffusion, the dependence of the diffusion coefficient on substrate concentration and the possibility of anti-chemotaxis are natural consequences of the model [138]. The main idea is that a careful consideration of enzyme kinetics leads to two types of drift velocity for an enzyme in a solute concentration gradient which are in competition: a phoretic velocity due to surface

interactions between the substrate molecules and the enzyme and a "binding-induced" velocity which arises because of the difference in the diffusion coefficient of the free enzyme and enzyme-substrate complex. We will discuss the model in detail, as we extend it to include the effect of fluctuations to investigate the relationship between an externally imposed chemical gradient and the structure and function of an enzyme.

4.1.4 Diffusiophoresis

Before introducing our model, we briefly discuss the physics of phoretic motion, a force-free and torque-free propulsion mechanism that is driven by interfacial interactions between a microscopic (or nanoscopic) particle in a fluid and local gradients of fields such as an electrostatic potential (electrophoresis), temperature (thermophoresis) and solute concentration (diffusiophoresis) [141]. The field gradient may be externally imposed (as will be the case in our discussion) or it can be generated by the particle itself if it is suitably asymmetric [142, 143], and the resulting propulsion velocity depends on the microscopic details of the system. Phoresis is an intrinsically non-equilibrium mechanism due to the continuous conversion of energy from local interactions.

The propulsion velocity due to diffusiophoresis can be found by solving the Stokes' equation for the parallel component of the flow velocity, due to the solute concentration gradient within the interaction range of the phoretic particle [141]. This is the so called "slip" velocity:

$$\boldsymbol{v}_{\mathrm{s}} = \mu \left(\mathbf{1} - \hat{\boldsymbol{n}}\hat{\boldsymbol{n}}\right) \cdot \nabla \rho_{\mathrm{s}}, \tag{4.1}$$

which holds when the thickness of the interfacial layer is small compared to the radius of the particle [142]. In (4.1), $\hat{\boldsymbol{n}}$ is the unit normal to the surface of the particle, ρ_{s} is the solute concentration field and μ is a mobility for the motion. In a fluid of viscosity η and temperature T the phoretic mobility is given by

$$\mu = \frac{k_{\mathrm{B}}T}{\eta} \int_a^\infty \mathrm{d}z \, z \left[1 - \mathrm{e}^{-\phi(z)/k_{\mathrm{B}}T}\right], \tag{4.2}$$

where a is the radius of the phoretic particle, z is the normal coordinate from its surface and $\phi(z)$ is the interaction between the solute particles and the surface of the phoretic particle. The sign of μ is determined by the sign of the interaction $\phi(z)$.

Using the Lorentz reciprocal theorem [108] to relate the slip velocity (4.1) from the force-free and torque-free motion of the particle to the velocity of the disturbance field due to an object of the same shape with an instantaneous velocity $\mathbf{V}$ due to the action of an external force, the translational phoretic velocity due to the distribution of slip velocities on the surface of a spherical particle is

$$\mathbf{V} = -\frac{1}{4\pi a^2}\int_{\mathcal{S}} \mathrm{d}S\, \boldsymbol{v}_{\mathrm{s}} \tag{4.3}$$

[144]. A similar consideration for the torque-free rotational motion gives the rotational phoretic velocity

$$\boldsymbol{\Omega} = -\frac{3}{8\pi a^3}\int_{\mathcal{S}} \mathrm{d}S\, \hat{\boldsymbol{n}} \times \boldsymbol{v}_{\mathrm{s}} \tag{4.4}$$

[144]. This angular velocity leads to an alignment response for a polarisable particle. We will derive the translational and rotational phoretic velocities explicitly from a microscopic description of our system starting from the Smoluchowski equation.

4.1.5 Overview

In this chapter, we study the response of our model enzyme to an externally imposed substrate concentration gradient. A coupling between hydrodynamics and the concentration gradient arises naturally in our asymmetric dumbbell model. Our model predicts that an enzyme will present complex alignment dynamics in response to the substrate concentration gradient, in addition to a response to a hydrodynamic density gradient– even at the level of a single enzyme molecule.

We start from a microscopic description of the system in Section 4.2 and present the steps for deriving the phoretic mobilities associated with the subunits of the asymmetric dumbbell. In Section 4.3, we derive and discuss the drift-diffusion equation for the dynamics of the system in the hydrodynamic limit. The alignment mechanisms are examined in detail. We also study the effect of the reduced catalytic

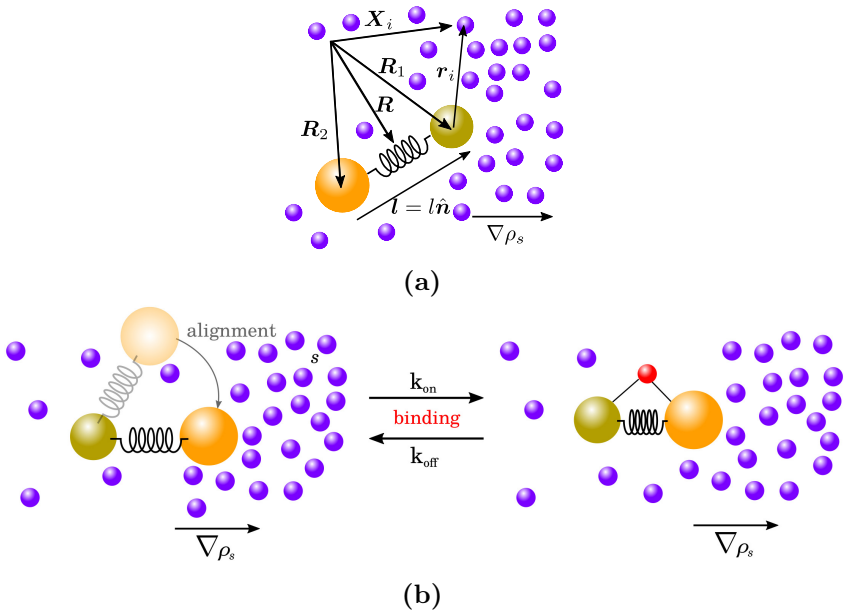

Figure 4.2. (a) Our model enzyme in a concentration gradient $\nabla\rho_s$ of substrate molecules. The free enzyme interacts with substrate molecules in the bulk through pairwise hydrodynamic and surface interactions. (b) Additionally, the free enzyme can bind to a substrate molecule to form a complex with rate k_{on} which unbinds with rate k_{off} [145].

cycle. Finally, we conclude with a discussion of the possible implications of our results and suggestions for improvements to our model.

4.2 Model

To study the response of an enzyme to a substrate concentration gradient we consider our asymmetric dumbbell in a bath of substrate molecules. Again, we assume that all boundaries are far enough from the dumbbell that we can neglect boundary effects. For simplicity, we consider an axisymmetric dumbbell with spherical subunits which may be of different sizes and can have different surface properties. In addition to the binding interactions, which are attractive and short-ranged (typically non-covalent interactions such as hydrogen bonds and hydrophobic interactions), we also consider *non-specific interactions* between the surface of the dumbbell and substrate molecules. These can be different for the two subunits. The non-specific interactions are the non-binding interactions that can be attractive or repulsive between the dumbbell and substrate molecules that are sufficiently

close, and include van der Waals, electrostatic and steric interactions. We also consider hydrodynamic interactions between the subunits of the dumbbell and the substrate molecules in the bulk.

4.2.1 Smoluchowski equation for $N+2$ particles

The system consists of the subunits of the dumbbell that are located at positions $\boldsymbol{R}_1$ and $\boldsymbol{R}_2$ and substrate molecules S at positions $\boldsymbol{X}_i$, with $i = 1, \ldots, N$. The configuration, including the dumbbell and substrate molecules, is characterised by the $(N+2)$-particle distribution $\rho_{N+2}(\boldsymbol{R}_1, \boldsymbol{R}_2, \boldsymbol{X}_1, \ldots, \boldsymbol{X}_N; t)$, whose stochastic dynamics evolves under the Smoluchowski equation

$$\begin{aligned}
\partial_t \rho_{N+2} = &\sum_{i,j=1}^{2} \nabla_{\boldsymbol{R}_i} \cdot \Big(\boldsymbol{\mu}^{ij} \cdot [k_\mathrm{B}T \nabla_{\boldsymbol{R}_j} \rho_{N+2} + (\nabla_{\boldsymbol{R}_j} \phi^{N+2}) \rho_{N+2}] \Big) \\
&+ \sum_{i=1}^{N} \Bigg\{ \sum_{j=1}^{2} \Big[\nabla_{\boldsymbol{R}_j} \cdot \Big(\boldsymbol{\mu}^{js} \cdot [k_\mathrm{B}T \nabla_{\boldsymbol{X}_i} \rho_{N+2} + (\nabla_{\boldsymbol{X}_i} \phi^{N+2}) \rho_{N+2}] \Big) \\
&+ \nabla_{\boldsymbol{X}_i} \cdot \Big(\boldsymbol{\mu}^{sj} \cdot [k_\mathrm{B}T \nabla_{\boldsymbol{R}_j} \rho_{N+2} + (\nabla_{\boldsymbol{R}_j} \phi^{N+2}) \rho_{N+2}] \Big) \Big] \\
&+ \nabla_{\boldsymbol{X}_i} \cdot \Big(\boldsymbol{\mu}^{ss} \cdot [k_\mathrm{B}T \nabla_{\boldsymbol{X}_i} \rho_{N+2} + (\nabla_{\boldsymbol{X}_i} \phi^{N+2}) \rho_{N+2}] \Big) \Bigg\}. \qquad (4.5)
\end{aligned}$$

Where $\boldsymbol{\mu}^{ij} = \mathbf{M}^{ij}_{\mathrm{TT}}$ are the hydrodynamic mobility tensors due to the translational modes of the subunits, $\boldsymbol{\mu}^{js}$ are the hydrodynamic mobility tensors due to the coupling of translational modes of the subunits with substrate molecules and $\boldsymbol{\mu}^{ss}$ is the self-mobility tensor of a substrate molecule in the presence of the other molecules and the dumbbell. Strictly, the hydrodynamic tensors as well as the interaction potential ϕ^{N+2} depend on the position of all $N+2$ particles. We assume that the suspension is dilute to avoid this complication.

In a sufficiently dilute solution, where three-body and higher order interactions are rare, the interaction potential ϕ^{N+2} can be approximated as the sum of pair potentials between the dumbbell subunits and the pair potentials between each subunit and a substrate molecule with

$$\phi^{N+2}(\boldsymbol{R}_1, \boldsymbol{R}_2, \boldsymbol{X}_1, \ldots, \boldsymbol{X}_N) = U(\boldsymbol{R}_1, \boldsymbol{R}_2) + \sum_{j=1}^{2} \sum_{i=1}^{N} \phi^{js}(\boldsymbol{R}_j - \boldsymbol{X}_i), \qquad (4.6)$$

where U is again the pair interaction between the dumbbell subunits and ϕ^{js} is the pair interaction between subunit j and a substrate molecule. Furthermore, if the substrate molecules are small (which is typically the case), we can assume that the subunit self-mobilities μ^{ii} are constant, and for $i \neq j$, the cross-mobilities μ^{ij} contain only the effect of pair interactions between the subunits.

Since we are only interested in the dynamics of the dumbbell, we define the two-particle distribution ρ_{e} for the dumbbell by integrating over the N degrees of freedom of the substrate molecules such that

$$\rho_{\mathrm{e}}(\boldsymbol{R}_1, \boldsymbol{R}_2; t) = \int \mathrm{d}\boldsymbol{X}_1 \ldots \mathrm{d}\boldsymbol{X}_N \, \rho_{N+2}(\boldsymbol{R}_1, \boldsymbol{R}_2, \boldsymbol{X}_1, \ldots, \boldsymbol{X}_N; t). \tag{4.7}$$

Integrating over the substrate degrees of freedom in the Smoluchowksi equation (4.5) for the $N + 2$ particle distribution, we obtain

$$\partial_t \rho_{\mathrm{e}}(\boldsymbol{R}_1, \boldsymbol{R}_2; t) = \sum_{i,j=1}^{2} \Big\{ \nabla_{\boldsymbol{R}_i} \cdot \Big(\boldsymbol{\mu}^{ij} \cdot \Big[k_{\mathrm{B}} T \nabla_{\boldsymbol{R}_j} \rho_{\mathrm{e}} + (\nabla_{\boldsymbol{R}_j} U) \rho_{\mathrm{e}} \Big] \Big) + N \nabla_{\boldsymbol{R}_i} \cdot \int_{\boldsymbol{X}} (\boldsymbol{\mu}^{is} - \boldsymbol{\mu}^{ij}) (\nabla_{\boldsymbol{X}} \phi^{js}) \rho_{\mathrm{es}} \Big\}, \tag{4.8}$$

after using the relation $\nabla_{\boldsymbol{R}_j} \phi^{N+2} = \nabla_{\boldsymbol{R}_j} U - \sum_{i=1}^{N} \nabla_{\boldsymbol{X}_i} \phi^{js}(\boldsymbol{R}_j, \boldsymbol{X}_i)$ and ignoring boundary terms, using the fact that the mobility tensors are divergence-free (so that $\nabla_{\boldsymbol{X}} \boldsymbol{\mu}^{ij} = \nabla_{\boldsymbol{X}} \boldsymbol{\mu}^{js} = 0$[1]). The equation for the two-particle distribution is not closed as it retains information of higher order interactions through the three-particle distribution $\rho_{\mathrm{es}}(\boldsymbol{R}_1, \boldsymbol{R}_2, \boldsymbol{X}; t)$, which is coupled to the four-particle distribution and so on, so that a closure approximation is needed to write a closed equation for evolution of ρ_{e}.

4.2.2 Closure and no-overlap approximation

For a dilute solution with the assumption that substrate molecules are much smaller than the dumbbell so that the substrate concentration field relaxes quickly, a

[1]The divergences vanish if the substrate molecules are assumed to be point-like and if the substrate molecules are not point-like, for the hydrodynamic tensors expanded to order $\mathcal{O}(1/r^6)$ in the distance between the subunits and substrate molecules [109].

natural closure approximation is

$$\rho_{\mathrm{es}}(\boldsymbol{R}_1,\boldsymbol{R}_2,\boldsymbol{X};t)\approx\rho_{\mathrm{e}}(\boldsymbol{R}_1,\boldsymbol{R}_2)\frac{\rho_{\mathrm{s}}(\boldsymbol{X};t)}{N}\mathrm{e}^{-\frac{\phi^{1s}+\phi^{2s}}{k_{\mathrm{B}}T}}. \tag{4.9}$$

Where $\rho_{\mathrm{s}}(\boldsymbol{X};t)$ is an externally controlled substrate concentration field with diffusivity D_{s}, that satisfies the Laplace equation with no normal flux boundary conditions on the surface of the subunits:

$$D_{\mathrm{s}}\nabla^2\rho_{\mathrm{s}}=0 \quad \text{and} \quad -D_{\mathrm{s}}\partial_{\perp}\rho_{\mathrm{s}}=0. \tag{4.10}$$

We have used the fact that the typically smaller substrate molecules diffuse more quickly than an enzyme so that the substrate concentration relaxes quickly, and we can neglect its time derivative. The gradient and normal derivative are with respect to spherical coordinates (r_i,θ_i,φ_i) centred on each subunit i, with unit vectors $(\hat{\boldsymbol{r}}_i,\hat{\boldsymbol{\theta}}_i,\hat{\boldsymbol{\varphi}}_i)$ and a common zenith $\hat{\boldsymbol{z}}$ for the two subunits. The substrate concentration in the vicinity of a subunit of radius a_i, assuming that far from the subunit there is a concentration gradient $\nabla\rho_s^{\infty}=|\nabla\rho_s^{\infty}|\hat{\boldsymbol{z}}$ of substrate molecules pointing in the $\hat{\boldsymbol{z}}$-direction, is thus given by the following solution to (4.10)

$$\rho_s(r_i,\theta_i,\varphi_i)=\rho_s^{\infty}+|\nabla\rho_s^{\infty}|\left(r_i+\frac{1}{2}\frac{a_i^3}{r_i^2}\right)\cos\theta_i. \tag{4.11}$$

The radial coordinate r_i is related to the original coordinates through $\boldsymbol{X}=\boldsymbol{R}_i+r_i\hat{\boldsymbol{r}}_i$.

Using eq. (4.9), the coupling term in the Smoluchowski equation for the dumbbell (4.8) becomes

$$N\int_{\boldsymbol{X}}(\boldsymbol{\mu}^{is}-\boldsymbol{\mu}^{ij})(\nabla_X\phi^{js})\rho_{\mathrm{es}}\approx\rho_{\mathrm{e}}\int_{\boldsymbol{X}}(\boldsymbol{\mu}^{is}-\boldsymbol{\mu}^{ij})(\nabla_X\phi^{js})\rho_{\mathrm{s}}\mathrm{e}^{-\frac{\phi^{1s}+\phi^{2s}}{k_{\mathrm{B}}T}}. \tag{4.12}$$

A second approximation is needed to be able to write the remaining integral over the substrate position into a manifestly phoretic form that it proportional to the gradient of the substrate concentration. In eq. (4.12), there is still a coupling of the interactions ϕ^{1s} and ϕ^{2s} between the two subunits and the substrate molecules through the Boltzmann weight. We assume that the range of these potentials is much shorter than the typical distance between the subunits so that the two

potentials do not overlap and a substrate molecule never "feels" both subunits simultaneously. In this limit, we have

$$\begin{aligned}\rho_{\mathrm{e}}\int_{\boldsymbol{X}}(\boldsymbol{\mu}^{is}-\boldsymbol{\mu}^{ij})(\nabla_X\phi^{js})\rho_{\mathrm{s}}\mathrm{e}^{-\frac{\phi^{1s}+\phi^{2s}}{k_{\mathrm{B}}T}}\approx&\rho_{\mathrm{e}}\int_{\boldsymbol{X}}(\boldsymbol{\mu}^{is}-\boldsymbol{\mu}^{ij})(\nabla_X\phi^{js})\rho_{\mathrm{s}}\mathrm{e}^{-\frac{\phi^{js}}{k_{\mathrm{B}}T}}\\ =&\,k_{\mathrm{B}}T\rho_{\mathrm{e}}\int_{\boldsymbol{X}}(\boldsymbol{\mu}^{is}-\boldsymbol{\mu}^{ij})(\mathrm{e}^{-\frac{\phi^{js}}{k_{\mathrm{B}}T}}-1)\nabla_{\boldsymbol{X}}\rho_{\mathrm{s}},\end{aligned} \tag{4.13}$$

since the gradient will only contribute to the integral in the region near subunit j, where a substrate molecule does not feel the potential from the other subunit. The final step comes from integration by parts, ignoring boundary terms and using the fact that the hydrodynamic tensors are divergence-free.

Finally, the Smoluchowski equation for the distribution of the dumbbell (4.7) can be written as

$$\begin{aligned}\partial_t\rho_{\mathrm{e}}(\boldsymbol{R}_1,\boldsymbol{R}_2;t)=\sum_{i,j=1}^{2}\Bigg\{&\nabla_{\boldsymbol{R}_i}\cdot\left\{\boldsymbol{\mu}^{ij}\cdot\left[k_{\mathrm{B}}T\nabla_{\boldsymbol{R}_j}\rho_{\mathrm{e}}+(\nabla_{\boldsymbol{R}_j}U)\rho_{\mathrm{e}}\right]\right\}\\&+\nabla_{\boldsymbol{R}_i}\cdot\left[k_{\mathrm{B}}T\rho_{\mathrm{e}}\int_{\boldsymbol{X}}(\boldsymbol{\mu}^{is}-\boldsymbol{\mu}^{ij})(\mathrm{e}^{-\frac{\phi^{js}}{k_{\mathrm{B}}T}}-1)\nabla_{\boldsymbol{X}}\rho_{\mathrm{s}}\right]\Bigg\}.\end{aligned} \tag{4.14}$$

The first line of this equation is the contribution from the isolated enzyme that we have studied in detail in Chapter 3, and the second line corresponds to phoretic response to the gradient of substrate molecules. Since we define $\boldsymbol{\mu}^{ii}$ to be the self-mobility of a single subunit i, for $i=j$ it describes diffusiophoresis of a single particle, whereas for $i\neq j$, the term is unique to the geometry of the dumbbell.

4.2.3 Integration of phoretic terms

4.2.3.1 Self-type phoretic terms

We first calculate the integrals for the phoretic response of the individual subunits

$$\int_{\boldsymbol{X}}(\boldsymbol{\mu}^{is}-\boldsymbol{\mu}^{ii})(\mathrm{e}^{-\frac{\phi^{is}}{k_{\mathrm{B}}T}}-1)\nabla_{\boldsymbol{X}}\rho_{\mathrm{s}}. \tag{4.15}$$

Assuming that substrate molecules are point-like, we have the hydrodynamic mobility tensor

$$\boldsymbol{\mu}^{is}=\frac{1}{6\pi\eta a_i}\left[\frac{1}{4}\left(3\frac{a_i}{r_i}+\frac{a_i^3}{r_i^3}\right)\mathbf{1}+\frac{3}{4}\left(\frac{a_i}{r_i}-\frac{a_i^3}{r_i^3}\right)\hat{\boldsymbol{r}}_i\hat{\boldsymbol{r}}_i\right] \tag{4.16}$$

[109] between subunit i and a substrate molecule. Combining this with expression (3.5) for the self-mobility tensor of a subunit, we have

$$\boldsymbol{\mu}^{is} - \boldsymbol{\mu}^{ii} = \frac{1}{6\pi\eta a_i}\left[\left(-1 + \frac{3}{4}\frac{a_i}{r_i} + \frac{1}{4}\frac{a_i^3}{r_i^3}\right)(\mathbf{1} - \hat{\boldsymbol{r}}_i\hat{\boldsymbol{r}}_i) + \left(-1 + \frac{3}{2}\frac{a_i}{r_i} - \frac{1}{2}\frac{a_i^3}{r_i^3}\right)\hat{\boldsymbol{r}}_i\hat{\boldsymbol{r}}_i\right]. \tag{4.17}$$

Using the gradient operator in spherical coordinates

$$\nabla f = \partial_r f\hat{\boldsymbol{r}} + \frac{1}{r}\partial_\theta f\hat{\boldsymbol{\theta}} + \frac{1}{r\sin\theta}\partial_\varphi f\hat{\boldsymbol{\varphi}}, \tag{4.18}$$

the gradient of the substrate field in the coordinates centred at each subunit is

$$\nabla\rho_s = |\nabla\rho_s^\infty|\left[\left(1 - \frac{a_i^3}{r_i^3}\right)\cos\theta_i\hat{\boldsymbol{r}}_i - \left(1 + \frac{1}{2}\frac{a_i^3}{r_i^3}\right)\sin\theta_i\hat{\boldsymbol{\theta}}_{\boldsymbol{i}}\right]. \tag{4.19}$$

To evaluate (4.15), we need

$$\begin{aligned}(\mathbf{1} - \hat{\boldsymbol{r}}_i\hat{\boldsymbol{r}}_i)\nabla\rho_s &= -|\nabla\rho_s^\infty|\left(1 + \frac{1}{2}\frac{a_i^3}{r_i^3}\right)\sin\theta_i\hat{\boldsymbol{\theta}}_{\boldsymbol{i}} \\ (\hat{\boldsymbol{r}}_i\hat{\boldsymbol{r}}_i)\nabla\rho_s &= |\nabla\rho_s^\infty|\left(1 - \frac{a_i^3}{r_i^3}\right)\cos\theta_i\hat{\boldsymbol{r}}_i.\end{aligned} \tag{4.20}$$

Using the definition of the radial unit vectors in Cartesian coordinates:

$$\hat{\boldsymbol{r}} = \sin\theta\cos\varphi\hat{\boldsymbol{x}} + \sin\theta\sin\varphi\hat{\boldsymbol{y}} + \cos\theta\hat{\boldsymbol{z}} \quad \text{and} \quad \hat{\boldsymbol{\theta}} = \cos\theta\cos\varphi\hat{\boldsymbol{x}} + \cos\theta\sin\varphi\hat{\boldsymbol{y}} - \sin\theta\hat{\boldsymbol{z}}, \tag{4.21}$$

we calculate the integrals generated by (4.20) over the solid angle

$$\int \mathrm{d}\Omega\sin\theta\hat{\boldsymbol{\theta}} = -\frac{8\pi}{3}\hat{\boldsymbol{z}} \quad \text{and} \quad \int \mathrm{d}\Omega\cos\theta\hat{\boldsymbol{r}} = \frac{4\pi}{3}\hat{\boldsymbol{z}}. \tag{4.22}$$

Finally, we obtain the following expression for (4.15)

$$\int_{\boldsymbol{X}}(\boldsymbol{\mu}^{is} - \boldsymbol{\mu}^{ii})(\mathrm{e}^{-\frac{\phi^{is}}{k_\mathrm{B}T}} - 1)\nabla_{\boldsymbol{X}}\rho_s = -\frac{A_i}{\eta}\nabla_{\boldsymbol{R}}\rho_s^\infty, \tag{4.23}$$

where

$$A_i \equiv \frac{1}{6a_i}\int_{a_i}^\infty \mathrm{d}r_i\, r_i^2\,(\mathrm{e}^{-\frac{\phi^{is}}{k_\mathrm{B}T}} - 1)\left(4 - 4\frac{a_i}{r_i} + \frac{a_i^4}{r_i^4} - \frac{a_i^6}{r_i^6}\right) \tag{4.24}$$

and the substrate gradient is no longer inside the integral. For very short-ranged interactions, we can use the approximation $r_i = a_i + \delta$ with $\delta \ll a_i$. The terms inside the rightmost parenthesis in the integral (4.24) become $6\delta/a_i$ to the lowest order, giving

$$A_i \approx \int_0^\infty \mathrm{d}\delta\,\delta(\mathrm{e}^{-\frac{\phi^{is}(\delta)}{k_\mathrm{B}T}} - 1) \equiv \lambda_i^2 \tag{4.25}$$

where λ_i is the Derjaguin length, the interaction range of subunit i [141, 146, 147].

4.2.3.2 Cross-type phoretic terms

We also need to evaluate integrals of the type

$$\int_{\boldsymbol{X}} (\boldsymbol{\mu}^{is} - \boldsymbol{\mu}^{12})(\mathrm{e}^{-\frac{\phi^{js}}{k_\mathrm{B}T}} - 1)\nabla_{\boldsymbol{X}}\rho_s \tag{4.26}$$

with $i \neq j$. Firstly, we use the following approximation for the hydrodynamic mobility tensor between the subunits

$$\boldsymbol{\mu}^{12} \simeq \frac{1}{8\pi\eta}\left[\left(\frac{1}{l} + \frac{a_1^2 + a_2^2}{3l^3}\right)\mathbf{1} + \left(\frac{1}{l} - \frac{a_1^2 + a_2^2}{l^3}\right)\hat{\boldsymbol{n}}\hat{\boldsymbol{n}}\right] \tag{4.27}$$

which is equal to $(\boldsymbol{\mu}^{21})^\mathrm{T}$ by the Lorentz reciprocal theorem [108]. We also need expressions for $\boldsymbol{\mu}^{2s}$ near subunit 1, and $\boldsymbol{\mu}^{1s}$ near subunit 2. Using the relation $\boldsymbol{r}_2 = \boldsymbol{r}_1 - \boldsymbol{l}$, and expanding in powers of r_1/l up to order $O(r_1^2/l^2) \sim O(a_1^2/l^2)$, which is of the same order as $\boldsymbol{\mu}^{12}$, we can write $\boldsymbol{\mu}^{2s}$ as

$$\begin{aligned}\boldsymbol{\mu}^{2s} \simeq \frac{1}{8\pi\eta}\Bigg\{ &\left[\frac{1}{l}\left(1 + \alpha_1\frac{r_1}{l} + \frac{1}{2}(3\alpha_1^2 - 1)\frac{r_1^2}{l^2}\right) + \frac{1}{3}\frac{a_2^2}{l^3}\right]\mathbf{1} \\ &+ \left[\frac{1}{l}\left(1 + 3\alpha_1\frac{r_1}{l} + \frac{3}{2}(5\alpha_1^2 - 1)\frac{r_1^2}{l^2}\right) - \frac{a_2^2}{l^3}\right]\hat{\boldsymbol{n}}\hat{\boldsymbol{n}} \\ &- \frac{r_1}{l^2}\left[1 + 3\alpha_1\frac{r_1}{l}\right](\hat{\boldsymbol{r}}_1\hat{\boldsymbol{n}} + \hat{\boldsymbol{n}}\hat{\boldsymbol{r}}_1) + \frac{r_1^2}{l^3}\hat{\boldsymbol{r}}_1\hat{\boldsymbol{r}}_1\Bigg\},\end{aligned} \tag{4.28}$$

with $\alpha_1 \equiv \hat{\boldsymbol{n}} \cdot \hat{\boldsymbol{r}}_i$. A similar expression can be obtained for $\boldsymbol{\mu}^{1s}$ near of subunit 2

$$\begin{aligned}\boldsymbol{\mu}^{1s} \simeq \frac{1}{8\pi\eta}\Bigg\{ &\left[\frac{1}{l}\left(1 - \alpha_2\frac{r_2}{l} + \frac{1}{2}(3\alpha_2^2 - 1)\frac{r_2^2}{l^2}\right) + \frac{1}{3}\frac{a_1^2}{l^3}\right]\mathbf{1} \\ &+ \left[\frac{1}{l}\left(1 - 3\alpha_2\frac{r_2}{l} + \frac{3}{2}(5\alpha_2^2 - 1)\frac{r_2^2}{l^2}\right) - \frac{a_1^2}{l^3}\right]\hat{\boldsymbol{n}}\hat{\boldsymbol{n}} \\ &+ \frac{r_2}{l^2}\left[1 - 3\alpha_2\frac{r_2}{l}\right](\hat{\boldsymbol{r}}_2\hat{\boldsymbol{n}} + \hat{\boldsymbol{n}}\hat{\boldsymbol{r}}_2) + \frac{r_2^2}{l^3}\hat{\boldsymbol{r}}_2\hat{\boldsymbol{r}}_2\Bigg\},\end{aligned} \tag{4.29}$$

with $\alpha_2 \equiv \hat{\boldsymbol{n}} \cdot \hat{\boldsymbol{r}}_2$.

With the same assumptions as in the previous case, the concentration gradient can be extracted from the integral in the same way, giving

$$\int_{\boldsymbol{X}} (\boldsymbol{\mu}^{is} - \boldsymbol{\mu}^{12})(\mathrm{e}^{-\frac{\phi^{js}}{k_\mathrm{B}T}} - 1)\nabla_{\boldsymbol{X}}\rho_s = -\frac{a_j^3}{l^3}\frac{B_j}{\eta}\left(\hat{\boldsymbol{n}}\hat{\boldsymbol{n}} - \frac{\mathbf{1}}{3}\right)\nabla_{\boldsymbol{R}}\rho_s^\infty \tag{4.30}$$

where

$$B_i \equiv \frac{1}{10}\int_{a_i}^\infty \mathrm{d}r_i\, r_i\,(\mathrm{e}^{-\frac{\phi^{is}}{k_\mathrm{B}T}} - 1)\left(1 - 5\frac{r_i}{a_i} + 5\frac{r_i^3}{a_i^3}\right). \tag{4.31}$$

For very short-ranged interactions we find

$$B_i \approx \frac{a_i}{10}\int_0^\infty \mathrm{d}\delta\,(\mathrm{e}^{-\frac{\phi^{is}(\delta)}{k_\mathrm{B}T}}-1) \equiv \frac{a_i}{10}\gamma_i \tag{4.32}$$

where we have defined γ_i, another length scale of the order of the interaction range that is distinct from the Derjaguin length. It is equivalent to Anderson's *adsorption length*, which represents the amount of substrate adsorbed, per area of surface, divided by the bulk concentration at equilibrium [141]. Comparing (4.25) and (4.32) we should expect $B_i \gg A_i$, given that A_i is of the order of the interaction range squared but B_i is of the order of the product of particle size and the interaction range. Typically, the Derjaguin length is of the order of a few angstroms [141], an order of magnitude less than the hydrodynamic radius of an enzyme.

4.2.3.3 Higher order corrections due to the perturbation of the substrate concentration field by the second subunit

In calculating the phoretic terms A_i and B_i, it was assumed that the concentration of substrate molecules around a subunit is unaffected by the presence of the other subunit. Here we show that this is not the case and calculate the lowest order correction to the concentration field and its effect on the phoretic terms.

From eq. (4.19) for the substrate concentration gradient around a single particle of radius a, if we did a naive superposition of the fields around two particles of radii a_1 and a_2, we would write it as

$$\nabla\rho_\mathrm{s}^\mathrm{naive} = \rho_\mathrm{s}^{(0)} + \rho_\mathrm{s}^{(1)} + \rho_\mathrm{s}^{(2)}, \tag{4.33}$$

with

$$\nabla\rho_\mathrm{s}^{(0)} = |\nabla\rho_\mathrm{s}^\infty|\left[\cos\theta_1\hat{\boldsymbol{r}}_1 - \sin\theta_1\hat{\boldsymbol{\theta}}_1\right] = |\nabla\rho_\mathrm{s}^\infty|\left[\cos\theta_2\hat{\boldsymbol{r}}_2 - \sin\theta_2\hat{\boldsymbol{\theta}}_2\right] = |\nabla\rho_\mathrm{s}^\infty|\hat{\boldsymbol{z}}, \tag{4.34}$$

$$\nabla\rho_\mathrm{s}^{(1)} = -|\nabla\rho_\mathrm{s}^\infty|\frac{a_1^3}{r_1^3}\left[\cos\theta_1\hat{\boldsymbol{r}}_1 + \frac{1}{2}\sin\theta_1\hat{\boldsymbol{\theta}}_1\right] = |\nabla\rho_\mathrm{s}^\infty|\frac{a_1^3}{r_1^3}\left[-\hat{\boldsymbol{r}}_1\hat{\boldsymbol{r}}_1 + \frac{1}{2}\hat{\boldsymbol{\theta}}_1\hat{\boldsymbol{\theta}}_1\right]\hat{\boldsymbol{z}}, \tag{4.35}$$

and

$$\nabla\rho_\mathrm{s}^{(2)} = -|\nabla\rho_\mathrm{s}^\infty|\frac{a_2^3}{r_2^3}\left[\cos\theta_2\hat{\boldsymbol{r}}_2 + \frac{1}{2}\sin\theta_2\hat{\boldsymbol{\theta}}_2\right] = |\nabla\rho_\mathrm{s}^\infty|\frac{a_2^3}{r_2^3}\left[-\hat{\boldsymbol{r}}_2\hat{\boldsymbol{r}}_2 + \frac{1}{2}\hat{\boldsymbol{\theta}}_2\hat{\boldsymbol{\theta}}_2\right]\hat{\boldsymbol{z}}. \tag{4.36}$$

The naive superposition is a solution of the Laplace equation which satisfies the boundary condition at infinity but does *not* satisfy the no normal flux boundary condition at the surface of the particles. Indeed, the contribution $\nabla\rho_{\mathrm{s}}^{(2)}$ in the proximity of particle 1 is, to lowest order in $1/l$,

$$\begin{aligned}\nabla\rho_{\mathrm{s}}^{(2)} &= \nabla\rho_{\mathrm{s}}^{(2)}(r_1=0) + O\left(|\nabla\rho_{\mathrm{s}}^{\infty}|\frac{a_2^3 r_1}{l^4}\right)\\ &= |\nabla\rho_{\mathrm{s}}^{\infty}|\frac{3}{2}\frac{a_2^3}{l^3}\left[\frac{\mathbf{1}}{3}-\hat{\boldsymbol{n}}\hat{\boldsymbol{n}}\right]\hat{\boldsymbol{z}} + O\left(|\nabla\rho_{\mathrm{s}}^{\infty}|\frac{a_2^3 r_1}{l^4}\right),\end{aligned} \tag{4.37}$$

where we have used the fact that at the centre of particle 1 we have $r_2 = l$, $\hat{\boldsymbol{r}}_2\hat{\boldsymbol{r}}_2\cdot\hat{\boldsymbol{z}} = \hat{\boldsymbol{n}}\hat{\boldsymbol{n}}\cdot\hat{\boldsymbol{z}}$, and $\hat{\boldsymbol{\theta}}_2\hat{\boldsymbol{\theta}}_2\cdot\hat{\boldsymbol{z}} = (\mathbf{1}-\hat{\boldsymbol{n}}\hat{\boldsymbol{n}})\cdot\hat{\boldsymbol{z}}$. Therefore, to order $1/l^3$, the effect of the presence of particle 2 is that it generates a uniform gradient around particle 1, that violates the no flux boundary condition. To cancel out this gradient while still satisfying the Laplace equation, we need to add a new term of the form

$$\nabla\rho_{\mathrm{s}}^{(1,n)} = |\nabla\rho_{\mathrm{s}}^{\infty}|\frac{3}{2}\frac{a_2^3}{l^3}\frac{a_1^3}{r_1^3}\left[-\hat{\boldsymbol{r}}_1\hat{\boldsymbol{r}}_1+\frac{1}{2}\hat{\boldsymbol{\theta}}_1'\hat{\boldsymbol{\theta}}_1'\right]\left[\frac{\mathbf{1}}{3}-\hat{\boldsymbol{n}}\hat{\boldsymbol{n}}\right]\hat{\boldsymbol{z}}, \tag{4.38}$$

where the unit vector $\hat{\boldsymbol{\theta}}_1'$ corresponds to spherical coordinates centred at particle 1, but with the zenith direction parallel to $[\mathbf{1}/3-\hat{\boldsymbol{n}}\hat{\boldsymbol{n}}]\,\hat{\boldsymbol{z}}$. It is easy to see that (4.38) will cancel out the contribution of (4.37) to the radial gradient at the surface of particle 1 in the exact same way that (4.35) cancels out the contribution of (4.34). The same reasoning can be applied to the gradient generated by particle 1 in the proximity of particle two, resulting in a new term of the form

$$\nabla\rho_{\mathrm{s}}^{(2,n)} = |\nabla\rho_{\mathrm{s}}^{\infty}|\frac{3}{2}\frac{a_1^3}{l^3}\frac{a_2^3}{r_2^3}\left[-\hat{\boldsymbol{r}}_2\hat{\boldsymbol{r}}_2+\frac{1}{2}\hat{\boldsymbol{\theta}}_2'\hat{\boldsymbol{\theta}}_2'\right]\left[\frac{\mathbf{1}}{3}-\hat{\boldsymbol{n}}\hat{\boldsymbol{n}}\right]\hat{\boldsymbol{z}}, \tag{4.39}$$

where the unit vector $\hat{\boldsymbol{\theta}}_2'$ corresponds to spherical coordinates centred at particle 2 with the zenith direction parallel to $[\mathbf{1}/3-\hat{\boldsymbol{n}}\hat{\boldsymbol{n}}]\,\hat{\boldsymbol{z}}$.

Overall, the solute concentration gradient can therefore be written to order a_i^3/l^3 as

$$\nabla\rho_{\mathrm{s}} \approx \rho_{\mathrm{s}}^{(0)} + \rho_{\mathrm{s}}^{(1)} + \rho_{\mathrm{s}}^{(2)} + \rho_{\mathrm{s}}^{(1,n)} + \rho_{\mathrm{s}}^{(2,n)}. \tag{4.40}$$

This expression satisfies the Laplace equation, the boundary condition at infinity and the no normal flux boundary conditions at the surface of the particles up to order a_i^3/l^3.

The a_i^3/l^3 corrections to $\nabla\rho_\mathrm{s}$ just described have an effect on the A-type contributions to the phoretic velocity. The integral (4.23) picks up a correction, becoming

$$\int_{\boldsymbol{X}} \left(\boldsymbol{\mu}^{is} - \boldsymbol{\mu}^{ii}\right) \cdot (\mathrm{e}^{-\frac{\phi^{is}}{k_\mathrm{B}T}} - 1)\nabla_{\boldsymbol{X}}\rho_\mathrm{s} = -\frac{A_i}{\eta}\left[1 + \frac{3}{2}\frac{a_j^3}{l^3}\left(\frac{\mathbf{1}}{3} - \hat{\boldsymbol{n}}\hat{\boldsymbol{n}}\right)\right]\nabla\rho_\mathrm{s}^\infty. \tag{4.41}$$

The B-type contribution (4.30) is however unchanged to order a_i^3/l^3 because the corresponding corrections would be of order a_i^6/l^6.

4.2.4 Separation averaging

Introducing the results (4.23) and (4.30) for the integration of the phoretic terms into (4.14) and changing coordinates to the com and elongation coordinates of the dumbbell, $\boldsymbol{R} = (\boldsymbol{R}_1 + \boldsymbol{R}_2)/2$ and $\boldsymbol{l} = \boldsymbol{R}_2 - \boldsymbol{R}_1$, with $\boldsymbol{l} = l\hat{\boldsymbol{n}}$, the Smoluchowski equation can be rewritten as

$$\begin{aligned}\partial_t\rho_\mathrm{e}(\boldsymbol{R},\boldsymbol{l};t) =& \frac{1}{2}\nabla_{\boldsymbol{R}}\cdot\left\{\frac{1}{2}\mathbf{M}\cdot k_\mathrm{B}T\nabla_{\boldsymbol{R}}\rho_\mathrm{e} + \boldsymbol{\Gamma}\cdot[k_\mathrm{B}T\nabla_{\boldsymbol{l}}\rho_\mathrm{e} + (\nabla_{\boldsymbol{l}}U)\rho_\mathrm{e}]\right\}\\ &+ \nabla_{\boldsymbol{l}}\cdot\left\{\mathbf{W}\cdot[k_\mathrm{B}T\nabla_{\boldsymbol{l}}\rho_\mathrm{e} + (\nabla_{\boldsymbol{l}}U)\rho_\mathrm{e}] + \frac{1}{2}\boldsymbol{\Gamma}\cdot k_\mathrm{B}T\nabla_{\boldsymbol{R}}\rho_\mathrm{e}\right\}\\ &- \nabla_{\boldsymbol{R}}\cdot\left(\rho_\mathrm{e}\frac{\boldsymbol{\sigma}_1 + \boldsymbol{\sigma}_2}{2}\cdot\nabla_{\boldsymbol{R}}\rho_\mathrm{s}^\infty\right) - \nabla_{\boldsymbol{l}}\cdot[\rho_\mathrm{e}(\boldsymbol{\sigma}_2 - \boldsymbol{\sigma}_1)\cdot\nabla_{\boldsymbol{R}}\rho_\mathrm{s}^\infty],\end{aligned} \tag{4.42}$$

where the translation, rotation and coupling tensors are defined as before

$$\mathbf{M} = \boldsymbol{\mu}^{11} + \boldsymbol{\mu}^{22} + 2\boldsymbol{\mu}^{12}, \tag{4.43}$$

$$\mathbf{W} = \boldsymbol{\mu}^{11} + \boldsymbol{\mu}^{22} - 2\boldsymbol{\mu}^{12} \tag{4.44}$$

$$\boldsymbol{\Gamma} = \boldsymbol{\mu}^{22} - \boldsymbol{\mu}^{11}. \tag{4.45}$$

We have also defined

$$\boldsymbol{\sigma}_1 \equiv \frac{k_\mathrm{B}T}{\eta}\left[A_1\mathbf{1} + \frac{a_2^3}{l^3}\left(B_2 - \frac{3}{2}A_1\right)\left(\hat{\boldsymbol{n}}\hat{\boldsymbol{n}} - \frac{\mathbf{1}}{3}\right)\right] \tag{4.46}$$

and

$$\boldsymbol{\sigma}_2 \equiv \frac{k_\mathrm{B}T}{\eta}\left[A_2\mathbf{1} + \frac{a_1^3}{l^3}\left(B_1 - \frac{3}{2}A_2\right)\left(\hat{\boldsymbol{n}}\hat{\boldsymbol{n}} - \frac{\mathbf{1}}{3}\right)\right], \tag{4.47}$$

which are the phoretic mobility tensors of subunits 1 and 2, respectively. In each of them, the first term corresponds to the mobility of the isolated subunit, whereas the second term is a correction due to the presence of the other subunit (decaying as $1/l^3$ and positive since $B_i \gg A_i$).

We rewrite eq. (4.42) as the following to show explicitly which terms contribute to the Smoluchowski equation for the separation-averaged distribution

$$\begin{aligned}
&\partial_t \rho_{\mathrm{e}}(\boldsymbol{R},\hat{\boldsymbol{n}},l;t) = \frac{1}{4}\nabla_{\boldsymbol{R}}\cdot(k_{\mathrm{B}}T\mathbf{M}\cdot\nabla_{\boldsymbol{R}}\rho_{\mathrm{e}}) \\
&+\boldsymbol{\mathcal{R}}\cdot\left(k_{\mathrm{B}}T\frac{W_I}{l^2}\boldsymbol{\mathcal{R}}\rho_{\mathrm{e}}\right)+\frac{1}{2}\boldsymbol{\mathcal{R}}\cdot\left(k_{\mathrm{B}}T\frac{\Gamma_I}{l}\hat{\boldsymbol{n}}\times\nabla_{\boldsymbol{R}}\rho_{\mathrm{e}}\right) \\
&-\frac{1}{2}\nabla_{\boldsymbol{R}}\cdot\left(k_{\mathrm{B}}T\frac{\Gamma_I}{l}\hat{\boldsymbol{n}}\times\boldsymbol{\mathcal{R}}\rho_{\mathrm{e}}\right)+\frac{1}{2}\nabla_{\boldsymbol{R}}\cdot\left[(\Gamma_I+\Gamma_D)\left(k_{\mathrm{B}}T\frac{\partial\rho_{\mathrm{e}}}{\partial l}+U'\rho_{\mathrm{e}}\right)\hat{\boldsymbol{n}}\right] \\
&+\frac{1}{2}\frac{1}{l^2}\frac{\partial}{\partial l}\left[l^2k_{\mathrm{B}}T(\Gamma_I+\Gamma_D)\hat{\boldsymbol{n}}\cdot\nabla_{\boldsymbol{R}}\rho_{\mathrm{e}}\right]+\frac{1}{l^2}\frac{\partial}{\partial l}\left[l^2(W_I+W_D)\left(k_{\mathrm{B}}T\frac{\partial\rho_{\mathrm{e}}}{\partial l}+U'\rho_{\mathrm{e}}\right)\right] \\
&-\nabla_{\boldsymbol{R}}\cdot\left(\rho_{\mathrm{e}}\frac{\boldsymbol{\sigma}_1+\boldsymbol{\sigma}_2}{2}\cdot\nabla_{\boldsymbol{R}}\rho_{\mathrm{s}}^{\infty}\right)-\boldsymbol{\mathcal{R}}\cdot\left[\hat{\boldsymbol{n}}\times\rho_{\mathrm{e}}\frac{\boldsymbol{\sigma}_2-\boldsymbol{\sigma}_1}{l}\cdot\nabla_{\boldsymbol{R}}\rho_s^{\infty}\right] \\
&-\frac{1}{l^2}\frac{\partial}{\partial l}\left\{l^2\rho_{\mathrm{e}}\left[(\boldsymbol{\sigma}_2-\boldsymbol{\sigma}_1)\cdot\nabla_{\boldsymbol{R}}\rho_s^{\infty}\right]\cdot\hat{\boldsymbol{n}}\right\},
\end{aligned} \tag{4.48}$$

using the following decomposition of the hydrodynamic mobility tensors into their isotropic and directional parts

$$\mathbf{M}=M_I\mathbf{1}+M_D\hat{\boldsymbol{n}}\hat{\boldsymbol{n}};\quad \mathbf{W}=W_I\mathbf{1}+W_D\hat{\boldsymbol{n}}\hat{\boldsymbol{n}};\quad \boldsymbol{\Gamma}=\Gamma_I\mathbf{1}+\Gamma_D\hat{\boldsymbol{n}}\hat{\boldsymbol{n}}. \tag{4.49}$$

Using the same averaging scheme as in Chapter 3, where now the separation-averaged enzyme distribution is written as

$$\tilde{\rho}_{\mathrm{e}}=\int_{a_1+a_2}^{\infty}\mathrm{d}l\,l^2\rho_{\mathrm{e}} \tag{4.50}$$

and the average of a function that depends on the subunit separation is

$$\langle f\rangle=\frac{1}{\tilde{\rho}_{\mathrm{e}}}\int_{a_1+a_2}^{\infty}\mathrm{d}l\,l^2\,f(l)\,\rho_{\mathrm{e}}. \tag{4.51}$$

Finally, the average of eq. (4.48) over l, while treating the dumbbell orientation as constant is

$$\begin{aligned}
&\partial_t\tilde{\rho}_{\mathrm{e}}(\boldsymbol{R},\hat{\boldsymbol{n}};t)=\frac{1}{4}\nabla_{\boldsymbol{R}}\cdot(k_{\mathrm{B}}T\langle\mathbf{M}\rangle\cdot\nabla_{\boldsymbol{R}}\tilde{\rho}_{\mathrm{e}})+\boldsymbol{\mathcal{R}}\cdot\left(k_{\mathrm{B}}T\left\langle\frac{W_I}{l^2}\right\rangle\boldsymbol{\mathcal{R}}\tilde{\rho}_{\mathrm{e}}\right) \\
&+\frac{1}{2}\boldsymbol{\mathcal{R}}\cdot\left(k_{\mathrm{B}}T\left\langle\frac{\Gamma_I}{l}\right\rangle(\hat{\boldsymbol{n}}\times\nabla_{\boldsymbol{R}}\tilde{\rho}_{\mathrm{e}})\right)-\frac{1}{2}\nabla_{\boldsymbol{R}}\cdot\left(k_{\mathrm{B}}T\left\langle\frac{\Gamma_I}{l}\right\rangle(\hat{\boldsymbol{n}}\times\boldsymbol{\mathcal{R}}\tilde{\rho}_{\mathrm{e}})\right) \\
&-\nabla_{\boldsymbol{R}}\cdot\left(\tilde{\rho}_{\mathrm{e}}\frac{\langle\boldsymbol{\sigma}_1+\boldsymbol{\sigma}_2\rangle}{2}\cdot\nabla_{\boldsymbol{R}}\rho_{\mathrm{s}}^{\infty}\right)-\boldsymbol{\mathcal{R}}\cdot\left[\tilde{\rho}_{\mathrm{e}}\left\langle\frac{\boldsymbol{\sigma}_2-\boldsymbol{\sigma}_1}{l}\right\rangle\cdot\hat{\boldsymbol{n}}\times\nabla_{\boldsymbol{R}}\rho_s^{\infty}\right]
\end{aligned} \tag{4.52}$$

4.3 Results

4.3.1 Drift-diffusion equation

Equation (4.52) for the separation-averaged distribution of the dumbbell $\tilde{\rho}_{\mathrm{e}}$ can be written as a drift-diffusion equation as

$$\begin{aligned}\partial_t\tilde{\rho}_{\mathrm{e}}(\boldsymbol{R},\hat{\boldsymbol{n}};t) =&\nabla_{\boldsymbol{R}}\cdot[\boldsymbol{D}_t\cdot\nabla_{\boldsymbol{R}}\tilde{\rho}_{\mathrm{e}}-(\langle\boldsymbol{\Sigma}^{\mathrm{v}}\rangle\cdot\nabla_{\boldsymbol{R}}\rho_{\mathrm{s}})\tilde{\rho}_{\mathrm{e}}]\\ &+\boldsymbol{\mathcal{R}}\cdot[D_r\boldsymbol{\mathcal{R}}\tilde{\rho}_{\mathrm{e}}-\langle\Sigma^{\omega}_I\rangle(\hat{\boldsymbol{n}}\times\nabla_{\boldsymbol{R}}\rho_{\mathrm{s}})\tilde{\rho}_{\mathrm{e}}]\\ &+\boldsymbol{\mathcal{R}}\cdot[\boldsymbol{D}_c\cdot\nabla_{\boldsymbol{R}}\tilde{\rho}_{\mathrm{e}}]+\nabla_{\boldsymbol{R}}\cdot[(\boldsymbol{D}_c)^{\mathrm{T}}\cdot\boldsymbol{\mathcal{R}}\tilde{\rho}_{\mathrm{e}}].\end{aligned}\tag{4.53}$$

The superscript of the substrate field has been dropped as we would anyway like to describe dynamics at length scales much larger than those associated with the dumbbell. We have defined the average translational diffusion tensor

$$\boldsymbol{D}_t\equiv\frac{1}{4}k_{\mathrm{B}}T\langle\mathbf{M}\rangle,\tag{4.54}$$

the average rotational diffusion coefficient

$$D_r\equiv k_{\mathrm{B}}T\left\langle\frac{W_I}{l^2}\right\rangle,\tag{4.55}$$

the average translation-rotation coupling tensor

$$[\boldsymbol{D}_c]_{ij}\equiv\frac{k_{\mathrm{B}}T}{2}\left\langle\frac{\Gamma_I}{l}\right\rangle\epsilon_{ikj}\hat{n}_k,\tag{4.56}$$

with transpose $(\boldsymbol{D}_c)^{\mathrm{T}}$, satisfying $(\boldsymbol{D}_c)^{\mathrm{T}}=-\boldsymbol{D}_c$, the translational phoretic mobility tensor

$$\boldsymbol{\Sigma}^{\mathrm{v}}\equiv\frac{1}{2}\boldsymbol{\sigma}_1+\boldsymbol{\sigma}_2\equiv\Sigma^{\mathrm{v}}_I\mathbf{1}+\Sigma^{\mathrm{v}}_D\hat{\boldsymbol{n}}\hat{\boldsymbol{n}}.\tag{4.57}$$

and the rotational phoretic mobility tensor, that controls the response of the orientation vector of the dumbbell to the local substrate

$$\boldsymbol{\Sigma}^{\omega}\equiv\frac{\boldsymbol{\sigma}_2-\boldsymbol{\sigma}_1}{l}\equiv\Sigma^{\omega}_I\mathbf{1}+\Sigma^{\omega}_D\hat{\boldsymbol{n}}\hat{\boldsymbol{n}}.\tag{4.58}$$

We will now discuss the terms in eq. (4.53). We note that there are three independent mechanisms for the response of the dumbbell to the gradient in the

substrate field as shown by Saha et al. for catalytic colloids in a chemical field [63]. Firstly, the dumbbell has a translational phoretic velocity

$$\boldsymbol{v} = -\langle \Sigma_I^{\mathrm{v}} \rangle \nabla_{\boldsymbol{R}} \rho_{\mathrm{s}} - \langle \Sigma_D^{\mathrm{v}} \rangle \hat{\boldsymbol{n}}\hat{\boldsymbol{n}} \cdot \nabla_{\boldsymbol{R}} \rho_{\mathrm{s}}, \tag{4.59}$$

with a phoretic contribution controlled by Σ_I that is along the substrate gradient and a second contribution controlled by Σ_D that couples the director of the dumbbell $\hat{\boldsymbol{n}}$ to the substrate gradient so that the net motion is biased towards (or away from) the substrate gradient. The dumbbell also has an angular phoretic velocity due to the substrate gradient

$$\boldsymbol{\omega} = -\langle \Sigma_I^{\omega} \rangle \hat{\boldsymbol{n}} \times \nabla_{\boldsymbol{R}} \rho_{\mathrm{s}}, \tag{4.60}$$

that is controlled by Σ_I^{ω}, which rotates the dumbbell in a direction that is perpendicular to its instantaneous orientation and the substrate concentration gradient. The sense of rotation determined by the sign of Σ_I^{ω}.

Although these terms are generic and not specific to the asymmetric dumbbell geometry, there are some interesting features that are due to the specific geometry: $\Sigma_I^{\omega} = 0$ if the subunits have the same phoretic mobility, and Σ_I^{v} and Σ_D^{v} are larger than they would be were the subunits not hydrodynamically coupled. We also note that the angular velocity falls off more rapidly with the separation of the subunits than the translational velocity, since it becomes more difficult to rotate a longer dumbbell in response to the substrate gradient than to translate it. The final line of eq. (4.53) are the contributions due to the asymmetric dumbbell geometry and couple the asymmetry of the dumbbell to its macroscopic dynamics through the hydrodynamic interactions between the subunits.

4.3.2 Moment expansion: Single molecule alignment

Exactly as in Chapters 2 and 3, eq. (4.53) is expanded in the moments of $\tilde{\rho}_{\mathrm{e}}$, retaining the zeroth and first order moments

$$c(\boldsymbol{R};t) = \int \mathrm{d}\hat{\boldsymbol{n}}\, \tilde{\rho}_{\mathrm{e}} \quad \text{and} \quad \boldsymbol{p}(\boldsymbol{R};t) = \int \mathrm{d}\hat{\boldsymbol{n}}\, \hat{\boldsymbol{n}} \tilde{\rho}_{\mathrm{e}}, \tag{4.61}$$

which again are the relevant fields in the macroscopic limit. From (4.53), we find

$$\begin{aligned}\partial_t c(\boldsymbol{R};t) &= \frac{k_\mathrm{B}T}{4}\left(\langle M_I\rangle + \frac{1}{3}\langle M_D\rangle\right)\nabla^2_{\boldsymbol{R}} c + \frac{k_\mathrm{B}T}{4}\langle M_D\rangle\nabla_{\boldsymbol{R}}\cdot(\nabla_{\boldsymbol{R}}\cdot\boldsymbol{Q}) \\ &+ k_\mathrm{B}T\left\langle\frac{\Gamma_I}{l}\right\rangle\nabla_{\boldsymbol{R}}\cdot\boldsymbol{p} - \frac{k_\mathrm{B}T}{2\eta}\nabla_{\boldsymbol{R}}\cdot\left[(A_1+A_2)(\nabla_{\boldsymbol{R}}\rho_\mathrm{s})c\right] \\ &- \frac{k_\mathrm{B}T}{2\eta}\nabla_{\boldsymbol{R}}\cdot\left[\left\langle\frac{1}{l^3}\right\rangle\left(a_1^3B_1 + a_2^3B_2 - \frac{3}{2}\left(a_2^3A_1 + a_1^3A_2\right)\right)(\nabla_{\boldsymbol{R}}\rho_\mathrm{s})\cdot\boldsymbol{Q}\right]\end{aligned} \tag{4.62}$$

and

$$\begin{aligned}\partial_t\boldsymbol{p}(\boldsymbol{R};t) &= \frac{k_\mathrm{B}T}{4}\left(\langle M_I\rangle + \frac{1}{5}\langle M_D\rangle\right)\nabla^2_{\boldsymbol{R}}\boldsymbol{p} + \frac{k_\mathrm{B}T}{10}\langle M_D\rangle\nabla_{\boldsymbol{R}}(\nabla_{\boldsymbol{R}}\cdot\boldsymbol{p}) \\ &+ \frac{k_\mathrm{B}T}{4}\langle M_D\rangle\nabla_{\boldsymbol{R}}\cdot\left(\nabla_{\boldsymbol{R}}\cdot\boldsymbol{Q}^{(3)}\right) + 2k_\mathrm{B}T\left\langle\frac{\Gamma_I}{l}\right\rangle\nabla_{\boldsymbol{R}}\cdot\boldsymbol{Q} - \frac{k_\mathrm{B}T}{3}\left\langle\frac{\Gamma_I}{l}\right\rangle\nabla_{\boldsymbol{R}}c \\ &- 2k_\mathrm{B}T\left\langle\frac{W_I}{l^2}\right\rangle\boldsymbol{p} - \frac{k_\mathrm{B}T}{2\eta}\nabla_{\boldsymbol{R}}\cdot\left[(\nabla_{\boldsymbol{R}}\rho_\mathrm{s})\boldsymbol{p}\right](A_1+A_2) \\ &- \frac{k_\mathrm{B}T}{2\eta}\left\langle\frac{1}{l^3}\right\rangle\left(a_1^3B_1 + a_2^3B_2 - \frac{3}{2}\left(a_2^3A_1 + a_1^3A_2\right)\right)\partial_{R_j} \\ &\times\left[(\partial_{R_k}\rho_\mathrm{s})\left(Q^{(3)}_{ijk} + \frac{1}{5}\left(\delta_{ij}p_k + \delta_{ik}p_j - \frac{2}{3}\delta_{jk}p_i\right)\right)\boldsymbol{e}_i\right] - \langle\Sigma^\omega_I\rangle(\nabla_{\boldsymbol{R}}\rho_\mathrm{s})\cdot\left(\boldsymbol{Q} - \frac{2}{3}c\mathbf{1}\right).\end{aligned} \tag{4.63}$$

As in the previous cases, eqs. (4.62) and (4.63) are coupled to higher order moments of $\tilde{\rho}_\mathrm{e}$. The hierarchy is closed in the same way, with a gradient expansion and by setting $\boldsymbol{Q}(\boldsymbol{R};t) = \int \mathrm{d}\hat{\boldsymbol{n}}\left(\hat{\boldsymbol{n}}\hat{\boldsymbol{n}} - \frac{1}{3}\right)\tilde{\rho}_\mathrm{e}$ and higher order moments to zero. With these approximations and considering times beyond the rotational diffusion time, we find the following expression for the first order moment

$$\boldsymbol{p} = \frac{1}{3D^r}\left[-D_c\nabla_{\boldsymbol{R}}c + \langle\Sigma^\omega_I\rangle(\nabla_{\boldsymbol{R}}\rho_\mathrm{s})c\right]. \tag{4.64}$$

Equation (4.64) describes polarisation of the dumbbell beyond its rotational diffusion time. The first term corresponds to a purely hydrodynamic mechanism that is controlled by the translation-rotation coupling scalar D_c. It tends to align the model enzyme with a gradient in *enzyme* concentration $\nabla_{\boldsymbol{R}}c$, so that the smaller subunit is in the lower concentration region, and the larger subunit in the higher concentration region (this is because D_c is positive or negative when subunit 2 is smaller or larger than subunit 1, respectively). The second term corresponds to a phoretic mechanism which aligns the enzyme with the gradient in the *substrate* concentration field $\nabla_{\boldsymbol{R}}\rho_\mathrm{s}$,

with positive and negative values of Σ_I^ω resulting in subunit 2 being in the region of higher or lower substrate concentration, respectively.

We note that to lowest order, the sign of Σ_I^ω is controlled by the sign of $(A_2 - A_1)$, which leads to the intuitive result that subunit 2 is in the region of higher substrate concentration when $A_2 > A_1$ (i.e., when subunit 2 undergoes a stronger phoretic attraction towards the substrate than subunit 1), and vice versa when $A_1 > A_2$. In the special case in which the two subunits interact identically with the substrate ($A_1 = A_2 = A$ and $B_1 = B_2 = B$), the sign of Σ_I^ω is controlled by the sign of the higher order corrections $(a_2^3 - a_1^3)(B - \frac{3}{2}A)$. Because in general we expect B to be much larger so that $B - \frac{3}{2}A \approx B$, the enzyme will align so that the largest subunit is in the region of higher or lower substrate concentration if the interactions are attractive ($B > 0$) or repulsive ($B < 0$), respectively.

4.3.3 Effective mobility

Using eq. (4.64) in (4.62), we find the following drift-diffusion equation within the closure scheme described

$$\partial_t c(\boldsymbol{R}; t) = \nabla_{\boldsymbol{R}} \cdot \left[D_{\text{eff}} \nabla_{\boldsymbol{R}} c - \Sigma_{\text{eff}} (\nabla_{\boldsymbol{R}} \rho_{\text{s}}) c \right], \tag{4.65}$$

with long-time effective diffusion coefficient as in Chapter 3 (for an axisymmetric dumbbell) and phoretic mobility

$$\Sigma_{\text{eff}} = \langle \Sigma_I^{\text{v}} \rangle + \frac{1}{3} \langle \Sigma_D^{\text{v}} \rangle - \frac{2}{3} \frac{\langle \Gamma_I / l \rangle}{\langle W_I / l^2 \rangle} \langle \Sigma_I^\omega \rangle, \tag{4.66}$$

The effective phoretic mobility has a similar form to the effective diffusion coefficient, with positive contributions from the average translational modes and a contribution due to internal fluctuations. The correction will typically have (to the lowest the order $\langle 1/l \rangle$) the same sign as $A_L - A_S$, where the subscripts L and S indicate the larger and smaller subunit, respectively.

Defining an average mobility as

$$\bar{\Sigma} = \frac{k_{\text{B}} T}{\eta} \frac{A_1 + A_2}{2}, \tag{4.67}$$

the sum of the phoretic mobilities of two non-interacting subunits, the difference between the effective mobility (4.66) (of two interacting subunits) and the average mobility is given by

$$\frac{\Sigma_{\text{eff}}-\bar{\Sigma}}{\bar{\Sigma}} = -\frac{4}{3}\frac{\langle \Gamma_I/l\rangle}{\langle W_I/l^2\rangle\,(1+\tilde{A})}\left\{(\tilde{A}-1)\left\langle\frac{1}{l}\right\rangle+\frac{a_1^3}{3}\left\langle\frac{1}{l^4}\right\rangle\left[\alpha\left(\zeta^3\tilde{A}-1\right)+\frac{3}{2}\left(\tilde{A}-\zeta^3\right)\right]\right\}, \tag{4.68}$$

with relative phoretic mobility $\tilde{A}=A_2/A_1$, relative size of the subunits $\zeta=a_2/a_1$, and where we have taken for simplicity $B_i=\alpha A_i$, with the same proportionality constant for both subunits. From eqs. (4.25) and (4.32), α is of the order of the particle size a_i divided by the interaction length λ_i, about an order of magnitude for nm-size enzymes and angstrom Derjaguin length, and thus we take $\alpha\approx 10$.

In Fig. 4.3 we have plotted the corrections (4.68) to the average mobility as a function of the relative fluctuations of the dumbbell, for some selected values of $\tilde{A}$ and ζ. For $\zeta=1$ (i.e., subunits of equal size), there is no change in mobility for interacting subunits in any case. For $\tilde{A}=0$ (see Fig. 4.3(a)), when the interaction of subunit 2 with the substrate is negligible, the effective mobility is reduced if subunit 2 is larger than subunit 1 ($\zeta>1$), and enhanced if subunit 2 is smaller ($\zeta<1$). For $\tilde{A}=1$ (Fig. 4.3(b)), when the interactions of the two subunits with the substrate are equal, the corrections are smaller (the correction of order $\langle 1/l\rangle$ vanishes and only the correction of order $\langle 1/l^4\rangle$ survives) but they always enhance the effective mobility of the dumbbell, independently of whether subunit 2 is larger or smaller than subunit 1. For $\tilde{A}=2$ and $\tilde{A}=-2$ (Figs. 4.3(c) and 4.3(d)), when the interactions of the subunit 2 with the substrate dominate over the interactions of subunit 1 with the substrate (no matter the sign, i.e., $|\tilde{A}|>1$), the effective mobility is reduced if subunit 2 is smaller than subunit 1 ($\zeta<1$) and enhanced if subunit 2 is larger ($\zeta>1$). Generally, the absolute change in mobility is a decreasing function of the relative fluctuations of the dumbbell. We note that, in the previous sentences, "reduced" and "enhanced" refer to the *magnitude* of the

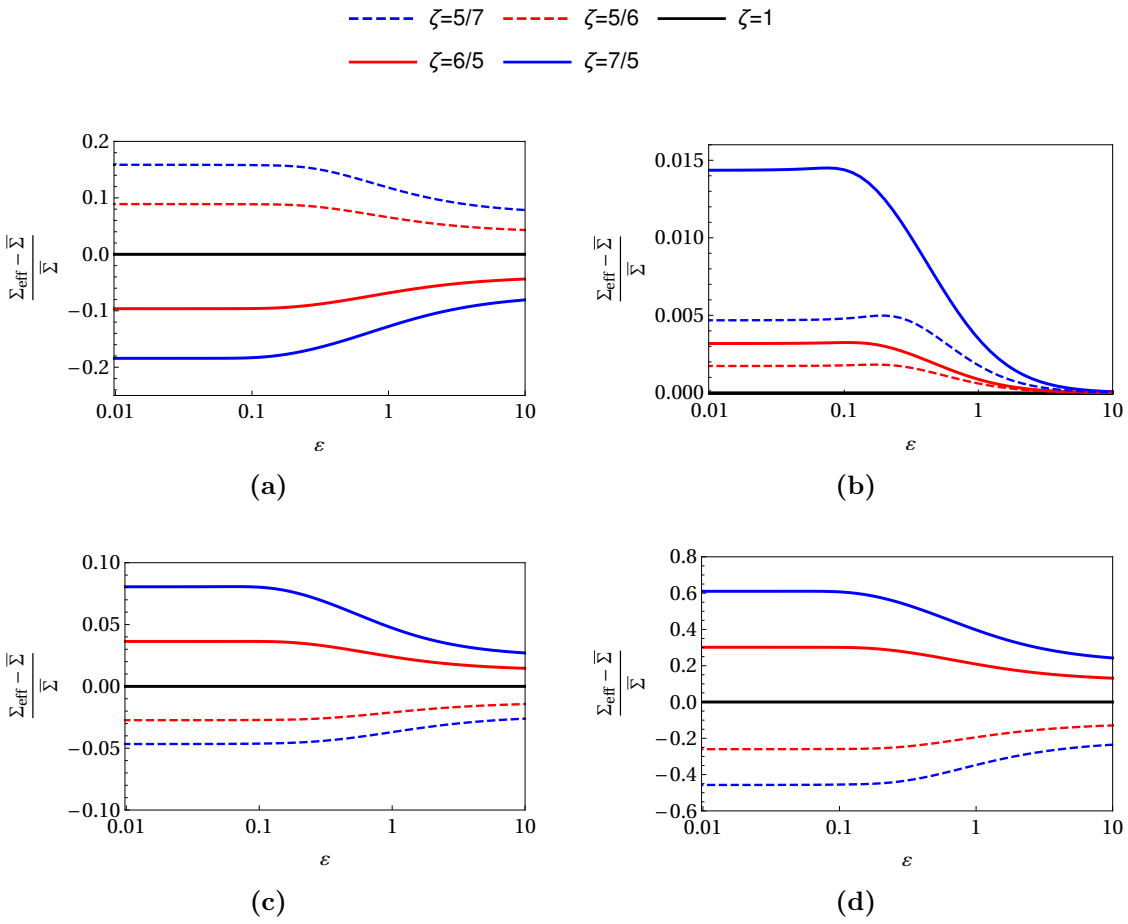

Figure 4.3. $(\Sigma_{\text{eff}} - \bar{\Sigma})/\bar{\Sigma}$ from eq. (4.68) for subunits interacting via a harmonic potential with stiffness k as a function of the fluctuation parameter $\varepsilon = \sqrt{k_{\text{B}}T/ka^2}$, where a is the typical size of the dumbbell. The lines represent different values of the ratio between the subunit sizes ζ, and the ratio $a_1/a = 0.3$ is constant in all plots. The Oseen mobility functions have been used for all plots. In (a) $\tilde{A} = 0$, (b) $\tilde{A} = 1$, (c) $\tilde{A} = 2$, and (d) $\tilde{A} = -2$ [145].

mobility independently of its sign, i.e., reduction and enhancement of a negative average mobility imply making its value less and more negative, respectively.

If the two subunits have balancing mobilities ($A_2 = -A_1$, where we choose $A_1 > 0$ without loss of generality), the average mobility is zero ($\bar{\Sigma} = 0$) and the relative correction given by eq. (4.68) is ill-defined. We can instead define another dimensionless quantity

$$\frac{\Sigma_{\text{eff}}}{\Sigma_1} = \frac{2}{3}\frac{\langle \Gamma_I/l \rangle}{\langle W_I/l^2 \rangle}\left[2\left\langle \frac{1}{l} \right\rangle + \frac{a_1^3}{3}\left\langle \frac{1}{l^4} \right\rangle \left(\alpha + \frac{3}{2}\right)\left(1 + \zeta^3\right)\right], \tag{4.69}$$

where $\Sigma_i = k_{\text{B}}TA_i/\eta$ is the mobility of subunit i in isolation (which is opposite to the mobility of subunit 2, i.e., $\Sigma_1 = -\Sigma_2$). In Fig. 4.4 we have plotted (4.69) as

a function of the relative fluctuations of the dumbbell. The sign is controlled by $\langle \Gamma_I / l \rangle$, which is positive if subunit 1 is larger than subunit 2, and negative if subunit 2 is larger than subunit 1. The sign of the effective mobility is thus governed by that of the mobility of the largest subunit. Moreover, if the subunits are of equal size the effective mobility vanishes, as expected from symmetry.

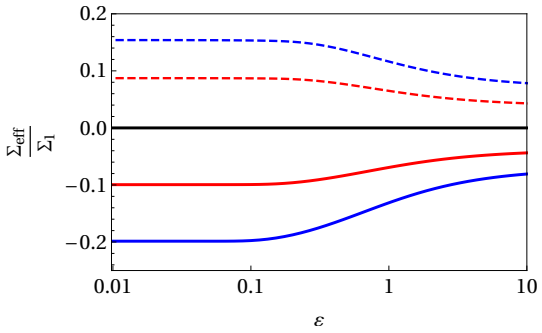

Figure 4.4. $\Sigma_{\text{eff}}/\Sigma_1$ from eq. (4.69) for subunits with balancing mobilities $A_2 = -A_1$ and $A_1 > 0$, interacting via a harmonic potential as a function of the dimensionless fluctuation parameter $\varepsilon = \sqrt{k_{\text{B}}T/ka^2}$. The effective mobility vanishes for subunits of equal size, and its sign is determined by the sign of the mobility of the larger subunit [145].

4.3.4 Enzyme kinetics

In this section we will derive the effective drift-diffusion equation for the dumbbell which also interacts with substrate molecules through binding interactions in the reduced catalytic cycle. Both the effective diffusion coefficient and phoretic mobility depend on the interaction potential $U(l)$ between the subunits of the dumbbell. The phoretic mobility in addition depends on the interaction ϕ^{is} between the subunits and substrate molecules nearby. As we have discussed in Chapter 3, we expect that $U(l)$ will be modified by binding interactions, and now also ϕ^{is}. Therefore, the phoretic mobility in addition to the diffusion coefficient will also be modified. We denote the effective diffusion coefficient and phoretic mobility in the free state by D_f and Σ_f, respectively, and in the bound state by D_b and Σ_b.

Agudo-Canalejo et al. have shown that substrate binding results in an additional contribution to the drift velocity of an enzyme in a substrate concentration gradient, due to the difference in diffusion coefficient between the free and bound states of

the enzyme [138]. The same study also showed that the phoretic drift velocity, just like the diffusion coefficient [26, 80], has a Michaelis-Menten-like dependence on substrate concentration. However, they did not consider the effect of internal fluctuations, as an enzyme was modelled as a single particle. The derivation of the effective diffusion coefficient presented in this section closely follows their derivation for a single particle.

Assuming that the rotational diffusion time of an enzyme is faster than the mean binding time (this could be an attribute of a specific enzyme, or because the solution is sufficiently dilute that there is a long time between encounters of an enzyme with a substrate molecule), at a time of the order of the mean binding time, the enzyme can either be free or bound to a substrate. If $\mathrm{S}_{\mathrm{on}}(\boldsymbol{R}, \boldsymbol{X})$ is the probability that a dumbbell at position $\boldsymbol{R}$ binds to a substrate molecule at position $\boldsymbol{X}$, to form a complex at $\boldsymbol{R}$, and $\mathrm{S}_{\mathrm{off}}(\boldsymbol{R}, \boldsymbol{X})$ is the probability that the complex at $\boldsymbol{R}$ decomposes into a free dumbbell at position $\boldsymbol{R}$ and a substrate molecule at $\boldsymbol{X}$, the densities of the two states obey the following equations:

$$\begin{aligned}\partial_t c_{\mathrm{f}}(\boldsymbol{R};t) =& \nabla_{\boldsymbol{R}} \cdot [D_{\mathrm{f}} \nabla_{\boldsymbol{R}} c_{\mathrm{f}} - \Sigma_{\mathrm{f}}(\nabla_{\boldsymbol{R}} \rho_{\mathrm{s}}) c_{\mathrm{f}}] - c_{\mathrm{f}} \int_{\boldsymbol{X}} \mathrm{S}_{\mathrm{on}}(\boldsymbol{R}, \boldsymbol{X}) \rho_{\mathrm{s}}(\boldsymbol{X}) \mathrm{e}^{-\frac{\phi_{\mathrm{f}}^{1s} + \phi_{\mathrm{f}}^{2s}}{k_{\mathrm{B}} T}} \\ &+ c_{\mathrm{b}} \int_{\boldsymbol{X}} \mathrm{S}_{\mathrm{off}}(\boldsymbol{R}, \boldsymbol{X}) \end{aligned} \tag{4.70}$$

and

$$\begin{aligned}\partial_t c_{\mathrm{b}}(\boldsymbol{R};t) =& \nabla_{\boldsymbol{R}} \cdot [D_{\mathrm{b}} \nabla_{\boldsymbol{R}} c_{\mathrm{b}} - \Sigma_{\mathrm{b}}(\nabla_{\boldsymbol{R}} \rho_{\mathrm{s}}) c_{\mathrm{b}}] + c_{\mathrm{f}} \int_{\boldsymbol{X}} \mathrm{S}_{\mathrm{on}}(\boldsymbol{R}, \boldsymbol{X}) \rho_{\mathrm{s}}(\boldsymbol{X}) \mathrm{e}^{-\frac{\phi_{\mathrm{b}}^{1s} + \phi_{\mathrm{b}}^{2s}}{k_{\mathrm{B}} T}} \\ &- c_{\mathrm{b}} \int_{\boldsymbol{X}} \mathrm{S}_{\mathrm{off}}(\boldsymbol{R}, \boldsymbol{X}) \end{aligned} \tag{4.71}$$

where

$$c_{\mathrm{f}}(\boldsymbol{R};t) = \int \mathrm{d}\hat{\boldsymbol{n}}\, \tilde{\rho}_{\mathrm{f}} \quad \text{and} \quad c_{\mathrm{b}}(\boldsymbol{R};t) = \int \mathrm{d}\hat{\boldsymbol{n}}\, \tilde{\rho}_{\mathrm{b}} \tag{4.72}$$

are the free and bound state densities, and the $\tilde{\rho}_{\mathrm{i}}$ with $\mathrm{i} = \mathrm{f}, \mathrm{b}$ are the elongation-averaged dumbbell distributions in the two states with interaction potentials $U_{\mathrm{f}}(l)$ and $U_{\mathrm{b}}(l)$, respectively. The non-contact interactions between the dumbbell subunits and substrate molecules are denoted by ϕ_{f}^{is} and ϕ_{b}^{is} in the free and bound states.

The integrals over the substrate position $\boldsymbol{X}$ in eqs. (4.70) and (4.71) can be performed by invoking the approximation of very short-ranged interactions to choose

$$\mathrm{S}_{\mathrm{on}}(\boldsymbol{R},\boldsymbol{X}) = k_{\mathrm{on}}\delta(\boldsymbol{R}-\boldsymbol{X}) \quad \text{and} \quad \mathrm{S}_{\mathrm{off}}(\boldsymbol{R},\boldsymbol{X}) = k_{\mathrm{off}}\delta(\boldsymbol{R}-\boldsymbol{X}). \tag{4.73}$$

After redefining k_{on} to include the constant $\exp\left[-(\phi_{\mathrm{f}}^{1s}(0)+\phi_{\mathrm{f}}^{2s}(0))/k_{\mathrm{B}}T\right]$, (4.70) and (4.71) become

$$\partial_t c_{\mathrm{f}}(\boldsymbol{R};t) = \nabla_{\boldsymbol{R}}\cdot\left[D_{\mathrm{f}}\nabla_{\boldsymbol{R}}c_{\mathrm{f}} - \Sigma_{\mathrm{f}}(\nabla_{\boldsymbol{R}}\rho_{\mathrm{s}})c_{\mathrm{f}}\right] - k_{\mathrm{on}}\rho_{\mathrm{s}}(\boldsymbol{R})c_{\mathrm{f}} + k_{\mathrm{off}}c_{\mathrm{b}} \tag{4.74}$$

and

$$\partial_t c_{\mathrm{b}}(\boldsymbol{R};t) = \nabla_{\boldsymbol{R}}\cdot\left[D_{\mathrm{b}}\nabla_{\boldsymbol{R}}c_{\mathrm{b}} - \Sigma_{\mathrm{b}}(\nabla_{\boldsymbol{R}}\rho_{\mathrm{s}})c_{\mathrm{b}}\right] + k_{\mathrm{on}}\rho_{\mathrm{s}}(\boldsymbol{R})c_{\mathrm{f}} - k_{\mathrm{off}}c_{\mathrm{b}}. \tag{4.75}$$

The experimentally relevant quantity is the total enzyme concentration

$$c_{\mathrm{tot}}(\boldsymbol{R};t) = c_{\mathrm{f}}(\boldsymbol{R};t) + c_{\mathrm{b}}(\boldsymbol{R};t), \tag{4.76}$$

since in the experimental set-up the free enzyme is indistinguishable from the complex. Assuming that the drift-diffusion dynamics of the dumbbell is much slower than the binding-unbinding time, the stationary limit of eqs. (4.74) and (4.75) gives

$$k_{\mathrm{on}}c_{\mathrm{f}}(\boldsymbol{R};t)\rho_{\mathrm{s}}(\boldsymbol{R}) \approx k_{\mathrm{off}}c_{\mathrm{b}}(\boldsymbol{R};t). \tag{4.77}$$

Combining the stationary condition (4.77) with eq. (4.76), we find

$$c_{\mathrm{f}} = \frac{K}{K+\rho_{\mathrm{s}}}c_{\mathrm{tot}} \quad \text{and} \quad c_{\mathrm{b}} = \frac{\rho_{\mathrm{s}}}{K+\rho_{\mathrm{s}}}c_{\mathrm{tot}}. \tag{4.78}$$

Finally, the sum of (4.74) and (4.75) using (4.78) gives the drift-diffusion equation for the total enzyme concentration

$$\partial_t c_{\mathrm{tot}}(\boldsymbol{R};t) = \nabla_{\boldsymbol{R}}\cdot\left\{D(\boldsymbol{R})\nabla_{\boldsymbol{R}}c_{\mathrm{tot}} - \left[\boldsymbol{v}_{\mathrm{ph}}(\boldsymbol{R}) + \boldsymbol{v}_{\mathrm{bi}}(\boldsymbol{R})\right]c_{\mathrm{tot}}\right\}, \tag{4.79}$$

which has the same form as the diffusion equation derived by Agudo-Canalejo [138]. The diffusion coefficient and phoretic velocity are averaged over the two states with a Michaelis-Menten weight, with

$$D(\boldsymbol{R}) = D_{\mathrm{f}} + (D_{\mathrm{b}} - D_{\mathrm{f}})\frac{\rho_{\mathrm{s}}(\boldsymbol{R})}{K+\rho_{\mathrm{s}}(\boldsymbol{R})}, \tag{4.80}$$

$$\boldsymbol{v}_{\mathrm{ph}}(\boldsymbol{R}) = \left[\Sigma_{\mathrm{f}} + (\Sigma_{\mathrm{b}} - \Sigma_{\mathrm{f}})\,\frac{\rho_{\mathrm{s}}(\boldsymbol{R})}{K + \rho_{\mathrm{s}}(\boldsymbol{R})}\right]\nabla_{\boldsymbol{R}}\rho_{\mathrm{s}}, \tag{4.81}$$

and a binding-induced contribution to the drift velocity that is due to the difference in diffusion coefficient of the enzyme in the free and bound states

$$\boldsymbol{v}_{\mathrm{bi}}(\boldsymbol{R}) = -(D_{\mathrm{b}} - D_{\mathrm{f}})\nabla_{\boldsymbol{R}}\left(\frac{\rho_{\mathrm{s}}(\boldsymbol{R})}{K + \rho_{\mathrm{s}}(\boldsymbol{R})}\right). \tag{4.82}$$

For attractive interactions ϕ^{is} between the enzyme and substrate molecules, both the diffusion coefficient and the phoretic velocity are increasing functions of substrate concentration, which tend to their values in the bound state at substrate saturation. The direction of the binding induced velocity depends on whether binding enhances the translational diffusion of the enzyme or diminishes it; if diffusion is enhanced by binding (so that $D_{\mathrm{b}} > D_{\mathrm{f}}$), the velocity is directed towards decreasing substrate concentration, and if diffusion is diminished upon binding (so that $D_{\mathrm{b}} < D_{\mathrm{f}}$), the velocity is directed towards increasing substrate concentration [138].

As we have discussed in detail, it is expected that binding leads to enhanced diffusion, so that the enzyme points away from increasing substrate concentration. In these circumstances, the phoretic and binding induced velocities are in opposite directions, which leads to competition between the two mechanisms. The consequences are described in detail by Agudo-Canalejo et al. [138], with the interesting conclusion that the competition between the two velocities, which is linked to enhanced enzyme diffusion and the sign of the interactions between an enzyme and substrate molecules can lead to different steady-state distributions for the enzyme. Another interesting observation from eqs. (4.81) and (4.82) is that the phoretic velocity is favoured at high substrate concentration, whereas at low concentrations, the binding-induced velocity is dominant.

The diffusion coefficient and drift velocities in (4.80)-(4.82) include corrections due to the internal fluctuations of the dumbbell. In (4.80) and (4.82), $D_{\mathrm{f,b}}$ are given by (3.57), with the relevant interaction potential, and in the expression for the phoretic velocity $\Sigma_{\mathrm{f,b}}$ are given by (4.66).

Noting that the binding-induced velocity can be rewritten as

$$\boldsymbol{v}_{\mathrm{bi}}(\boldsymbol{R}) = -\nabla_{\boldsymbol{R}}D(\boldsymbol{R}), \tag{4.83}$$

in the absence of phoresis (if an enzyme only interacts with substrate molecules through binding so that $\boldsymbol{v}_{\mathrm{ph}} = 0$), eq. (4.79) may be rewritten as

$$\partial_t c_{\mathrm{tot}}(\boldsymbol{R}; t) = \nabla^2_{\boldsymbol{R}} \left[D(\boldsymbol{R}) c_{\mathrm{tot}} \right] . \tag{4.84}$$

The stationary limit of eq. (4.84), gives $c_{\mathrm{tot}}(\boldsymbol{R}) \propto 1/D(\boldsymbol{R})$ which corresponds to a tendency to accumulate in regions where the diffusion coefficient is lowest [138].

4.4 Discussion

Timescale ordering:

The form of eq. (4.79) also depends on details of the enzymes' kinetics in the following way. We have focused on the case of rotational diffusion being faster than the mean binding time, which allowed us to follow the steps leading to eq. (4.79) in the order that has been presented. If instead one assumes that the binding rate is much faster than rotational diffusion, this final section, where we have considered the effect of binding, should be performed before the moment expansion. This reordering would alter the expressions (4.80)-(4.82). Furthermore, $\boldsymbol{v}_{\mathrm{bi}}$ could no longer be written exactly as the derivative of the diffusion coefficient. Generically, any quantity that depends on the coupling between the local (fast) and global (slow) dynamics will be determined by this timescale separation.

Collective effects:

We have not considered many-enzyme interactions here, nor in Chapter 3 because of the dilute conditions in which the experiments mentioned were conducted. However, phoretic and hydrodynamic interactions are long-ranged so the effect of the two alignment mechanisms are likely to be significant for a system of many interacting enzymes at higher concentrations [143], for example in metabolic pathways, where clusters of enzymes interacting by swapping reactants have been observed [24]. The prediction of clustered phases by Saha et al. for a collection of phoretic colloids [63] and bound states for an interacting pair [148] in the absence of attractive interactions and of Mikhailov et al. on collective hydrodynamics of active proteins [35], suggest that the subtle balance of translational and rotational coupling mediated by both

hydrodynamic and chemical fields that we have uncovered here for a single enzyme will lead to interesting collective behaviour. Beyond the closure approximation that was used to derive (4.64), we expect a non-linear coupling of the two alignment mechanisms, which could also result in interesting collective behaviour.

Boundary effects:

Enzymes will typically be in confinement and may experience interaction with the confining boundaries, which could be the cell membrane for example. It would therefore be interesting to consider the effect of a nearby wall on the alignment dynamics of our model enzyme. We could consider the hydrodynamic interactions between the dumbbell and the wall by constructing an image dumbbell on the other side of the wall.

Fluid flow:

Another important point to note is that we have not considered the effect of fluid flow that is present in the microfluidic devices of the enzyme chemotaxis experiments. In the presence of flow, both enzyme and substrate molecules are constantly being advected by the flow. We have assumed that enough time has passed for the fluid flow and concentration profiles of the enzyme and substrate to have stabilised.

CHAPTER 5

Hydrodynamic correlations of a pair of enzymes

At sufficiently high concentration, it is possible that hydrodynamic interactions between enzymes indeed become important for the dynamics of individuals as suggested by Riedel et al. [31]. To investigate this, we consider the simplest case of a pair of interacting enzymes using our dumbbell model. We derive the dynamical equations for a pair of identical dumbbells that are coupled by solvent-mediated hydrodynamic interactions in two cases: firstly, when the dumbbells are freely suspended and secondly, we consider a situation where the dumbbells are tethered by a constraint force on one of their subunits. Our focus is on the effect of hydrodynamic correlations between the dumbbells on the internal dynamics of each dumbbell.

5.1 Model

Assuming no-slip boundary conditions on the surface of the subunits of the two dumbbells, and that the velocity of the fluid vanishes at infinity, the velocity of each subunit is equal to the velocity of the fluid at the position of the subunit. Therefore, their velocities can be determined by solving Stokes' equation at the position of each subunit. We have already discussed the linearity of this solution, which comes from the linearity of Stokes' equation. Considering the dynamics of one of the dumbbells α

in the presence of the other, the velocity of its i-th subunit at position $\boldsymbol{R}_i^\alpha$ is given by

$$\dot{\boldsymbol{R}}_i^\alpha = \sum_{\beta=1,2} \sum_{j=1,2} \boldsymbol{G}(\boldsymbol{R}_i^\alpha, \boldsymbol{R}_j^\beta) \cdot \frac{\boldsymbol{f}_j^\beta}{8\pi\eta} \tag{5.1}$$

where superscripts label the dumbbells and subscripts label subunits. The tensor $\boldsymbol{G}(\boldsymbol{R}_i^\alpha, \boldsymbol{R}_j^\beta)$ is the Green's function of Stokes' equation that depends on the viscosity of the fluid and the geometry of the system, specifically, on local boundary conditions, and has $\boldsymbol{G}(\boldsymbol{R}_i^\alpha, \boldsymbol{R}_i^\alpha) \approx G(a_i)\mathbf{1}$, which is the approximation that the subunits are sufficiently far from any boundaries so that their friction coefficients can be assumed to be constant. As before, a_i is the radius of the i-th subunit. There is an internal force (from a potential like eq. (3.15)) $\boldsymbol{f}_j^\beta$ on the subunit at position $\boldsymbol{R}_j^\beta$, but we do not consider the effect of random forces.

5.2 Results

5.2.1 Free enzymes

For freely-suspended enzymes, eq. (5.1) can be recast into the following equations for the average and relative coordinates

$$\begin{aligned}\dot{\boldsymbol{R}}^\alpha = \sum_{\beta=1,2} \Big[&\boldsymbol{G}(\boldsymbol{R}^\alpha - \boldsymbol{l}^\alpha, \boldsymbol{R}^\beta - \boldsymbol{l}^\beta) + \boldsymbol{G}(\boldsymbol{R}^\alpha + \boldsymbol{l}^\alpha, \boldsymbol{R}^\beta - \boldsymbol{l}^\beta) \\ &- \boldsymbol{G}(\boldsymbol{R}^\alpha - \boldsymbol{l}^\alpha, \boldsymbol{R}^\beta + \boldsymbol{l}^\beta) - \boldsymbol{G}(\boldsymbol{R}^\alpha + \boldsymbol{l}^\alpha, \boldsymbol{R}^\beta + \boldsymbol{l}^\beta) \Big] \cdot \frac{\boldsymbol{f}^\beta}{16\pi\eta}, \end{aligned} \tag{5.2}$$

$$\begin{aligned}\dot{\boldsymbol{l}}^\alpha = \sum_{\beta=1,2} \Big[&\boldsymbol{G}(\boldsymbol{R}^\alpha + \boldsymbol{l}^\alpha, \boldsymbol{R}^\beta - \boldsymbol{l}^\beta) - \boldsymbol{G}(\boldsymbol{R}^\alpha - \boldsymbol{l}^\alpha, \boldsymbol{R}^\beta - \boldsymbol{l}^\beta) \\ &- \boldsymbol{G}(\boldsymbol{R}^\alpha + \boldsymbol{l}^\alpha, \boldsymbol{R}^\beta + \boldsymbol{l}^\beta) + \boldsymbol{G}(\boldsymbol{R}^\alpha - \boldsymbol{l}^\alpha, \boldsymbol{R}^\beta + \boldsymbol{l}^\beta) \Big] \cdot \frac{\boldsymbol{f}^\beta}{16\pi\eta}. \end{aligned} \tag{5.3}$$

In eqs. (5.2) and (5.3) we have imposed a force-free condition

$$\boldsymbol{f}_1^\alpha = -\boldsymbol{f}_2^\alpha = \boldsymbol{f}^\alpha, \tag{5.4}$$

for each dumbbell in the absence of external forces. For spherical subunits, the Green's functions for the hydrodynamic flows can be approximated by the following

$$\boldsymbol{G}(\boldsymbol{R}^\alpha - \boldsymbol{l}^\alpha) = \frac{4}{3a_1}\mathbf{1}; \quad \boldsymbol{G}(\boldsymbol{R}^\alpha + \boldsymbol{l}^\alpha) = \frac{4}{3a_2}\mathbf{1}; \quad \boldsymbol{G}(\boldsymbol{R}^\alpha - \boldsymbol{l}^\alpha, \boldsymbol{R}^\alpha + \boldsymbol{l}^\alpha) = \frac{1}{l^\alpha}\left(\mathbf{1} + \hat{\boldsymbol{n}}^\alpha \hat{\boldsymbol{n}}^\alpha\right), \tag{5.5}$$

which are the leading order contributions for an individual enzyme. The remaining tensors, which determine the interaction between the two enzymes, are Taylor expanded about their average positions, giving

$$\begin{aligned}
\boldsymbol{G}(\boldsymbol{R}^\alpha \pm \boldsymbol{l}^\alpha, \boldsymbol{R}^\beta \pm \boldsymbol{l}^\beta) =& \boldsymbol{G}(\boldsymbol{R}^\alpha, \boldsymbol{R}^\beta) \pm \boldsymbol{l}^\alpha \cdot \nabla_\alpha \boldsymbol{G}(\boldsymbol{R}^\alpha, \boldsymbol{R}^\beta) \pm \boldsymbol{l}^\beta \cdot \nabla_\beta \boldsymbol{G}(\boldsymbol{R}^\alpha, \boldsymbol{R}^\beta) \\
&+ \frac{1}{2}\left(\boldsymbol{l}^\alpha \cdot \nabla_\alpha\right)^2 \boldsymbol{G}(\boldsymbol{R}^\alpha, \boldsymbol{R}^\beta) + \frac{1}{2}\left(\boldsymbol{l}^\beta \cdot \nabla_\beta\right)^2 \boldsymbol{G}(\boldsymbol{R}^\alpha, \boldsymbol{R}^\beta) \\
&+ \left(\boldsymbol{l}^\alpha \cdot \nabla_\alpha\right)\left(\boldsymbol{l}^\beta \cdot \nabla_\beta\right) \boldsymbol{G}(\boldsymbol{R}^\alpha, \boldsymbol{R}^\beta) \ldots \\
\boldsymbol{G}(\boldsymbol{R}^\alpha \pm \boldsymbol{l}^\alpha, \boldsymbol{R}^\beta \mp \boldsymbol{l}^\beta) =& \boldsymbol{G}(\boldsymbol{R}^\alpha, \boldsymbol{R}^\beta) \pm \boldsymbol{l}^\alpha \cdot \nabla_\alpha \boldsymbol{G}(\boldsymbol{R}^\alpha, \boldsymbol{R}^\beta) \mp \boldsymbol{l}^\beta \cdot \nabla_\beta \boldsymbol{G}(\boldsymbol{R}^\alpha, \boldsymbol{R}^\beta) \\
&+ \frac{1}{2}\left(\boldsymbol{l}^\alpha \cdot \nabla_\alpha\right)^2 \boldsymbol{G}(\boldsymbol{R}^\alpha, \boldsymbol{R}^\beta) + \frac{1}{2}\left(\boldsymbol{l}^\beta \cdot \nabla_\beta\right)^2 \boldsymbol{G}(\boldsymbol{R}^\alpha, \boldsymbol{R}^\beta) \\
&- \left(\boldsymbol{l}^\alpha \cdot \nabla_\alpha\right)\left(\boldsymbol{l}^\beta \cdot \nabla_\beta\right) \boldsymbol{G}(\boldsymbol{R}^\alpha, \boldsymbol{R}^\beta) \ldots,
\end{aligned} \tag{5.6}$$

where ∇_α is the gradient with respect to the average position of enzyme α. Using these approximations, and assuming that the internal dumbbell force is torque-free so that $\boldsymbol{f}^\alpha = -f^\alpha \hat{\boldsymbol{n}}^\alpha$, the leading order contributions from the Green's functions give, for eqs. (5.2) and (5.3)

$$\dot{R}_i^\alpha = \frac{1}{12\pi\eta}\left(\frac{1}{a_2} - \frac{1}{a_1}\right) f^\alpha n_i^\alpha + \frac{1}{8\pi\eta} \sum_{\beta \neq \alpha} \partial_k^\beta G_{ij}(\boldsymbol{R}^\alpha, \boldsymbol{R}^\beta) l^\beta f^\beta n_k^\beta n_j^\beta \tag{5.7}$$

and

$$\dot{l}_i^\alpha = \frac{1}{8\pi\eta}\left[\frac{2}{3}\left(\frac{1}{a_1} + \frac{1}{a_2}\right) - \frac{1}{l^\alpha}\right] f^\alpha n_i^\alpha + \frac{1}{4\pi\eta} \sum_{\beta \neq \alpha} \partial_k^\alpha \partial_m^\beta G_{ij}(\boldsymbol{R}^\alpha, \boldsymbol{R}^\beta) l^\alpha l^\beta f^\beta n_k^\alpha n_m^\beta n_j^\beta. \tag{5.8}$$

Noting that

$$\dot{l}_i^\alpha = l^\alpha \dot{n}_i^\alpha + \dot{l}^\alpha n_i^\alpha, \tag{5.9}$$

equation (5.8) has two parts. For the elongation of a dumbbell, we find

$$\dot{l}^\alpha = \mu f^\alpha + h f^\beta, \tag{5.10}$$

with mobility constant

$$\mu \equiv \frac{1}{8\pi\eta}\left[\frac{2}{3}\left(\frac{1}{a_1} + \frac{1}{a_2}\right) - \frac{1}{l_0}\right], \tag{5.11}$$

and hydrodynamic coupling

$$h \equiv \frac{l_0^2}{4\pi\eta} \sum_{\beta\neq\alpha} \partial_k \partial_m G_{ij}(\boldsymbol{R}^\alpha - \boldsymbol{R}^\beta) f^\beta n_k^\alpha n_m^\beta n_j^\beta n_i^\alpha, \tag{5.12}$$

for small elongations around the equilibrium length l_0 of the dumbbells, and having defined the separation of the dumbbells $\boldsymbol{R} = \boldsymbol{R}^1 - \boldsymbol{R}^2$, so that the derivatives in (5.12) are with respect to $\boldsymbol{R}$. For the orientation dynamics, we find

$$\dot{n}_i^\alpha = \frac{1}{4\pi\eta} \sum_{\beta\neq\alpha} \partial_l \partial_k G_{mj}(\boldsymbol{R}^\alpha - \boldsymbol{R}^\beta) l^\beta n_l^\alpha n_j^\beta n_k^\beta (\delta_{im} - n_m^\alpha n_i^\alpha) f^\beta. \tag{5.13}$$

Equations (5.7) and (5.10)-(5.13) are the dynamical equations with the leading order contributions from the Green's functions. Since we are interested in the effect of hydrodynamic coupling on internal dynamics, we will focus on eq. (5.10)-(5.12). For now, the nonlinear equation (5.13) for the orientations of the dumbbells are replaced by simpler conditions.

5.2.1.1 Orientation–averaged coupling

When freely suspended in the bulk, we consider the orientation of each dumbbell to be uniformly distributed on a sphere so that the orientation average of a function $f(\hat{\boldsymbol{n}}^1, \hat{\boldsymbol{n}}^2)$ is given by

$$\tilde{f} \equiv \frac{1}{(4\pi)^2} \int f(\hat{\boldsymbol{n}}^1(\theta_1, \varphi_1), \hat{\boldsymbol{n}}^2(\theta_2, \varphi_2)) \sin(\theta_1) \sin(\theta_2) \mathrm{d}\theta_1 \mathrm{d}\varphi_1 \mathrm{d}\theta_2 \mathrm{d}\varphi_2. \tag{5.14}$$

Therefore, the orientation–averaged hydrodynamic coupling

$$\tilde{h} = \frac{l_0^2}{36\pi\eta} \sum_{\beta\neq\alpha} \partial_i \partial_j G_{ij}(\boldsymbol{R}^\alpha - \boldsymbol{R}^\beta) f^\beta, \tag{5.15}$$

is identically zero due to the incompressibility of the fluid, and a surface-induced alignment is needed to break the spherical symmetry which will result in a non-vanishing coupling.

5.2.2 Tethered enzymes

We now consider a situation where the two dumbbells are tethered to a surface by an external constraint force $\boldsymbol{F}^\alpha$ that fixes the position of the largest subunit (chosen to be subunit 2) and satisfies the force balance $\boldsymbol{f}_2^\alpha = \boldsymbol{F}^\alpha - \boldsymbol{f}_1^\alpha$. From equation (5.1), we solve for the constraint forces from the system of equations that comes from implementing the constraint that the velocity of subunit 2 of each dumbbell, $\dot{\boldsymbol{R}}_2^\alpha$, vanishes. For the constrained system, we describe the dynamics in terms of the relative coordinate and the position of second subunit which is fixed, rather than the average coordinate.

In the limit that the dumbbells are well separated (when $d > l_0$, where d is the distance between the dumbbells), the equation of motion for the relative coordinate is

$$\begin{aligned}
\dot{l}_i^\alpha &= -\frac{(\boldsymbol{R}^\alpha - \boldsymbol{l}^\alpha)_i}{2} \\
&= \left[G(a_1)\delta_{ik} - G(a_2)^{-1}G_{ij}(\boldsymbol{R}^\alpha - \boldsymbol{l}^\alpha, \boldsymbol{R}^\alpha + \boldsymbol{l}^\alpha)G_{jk}(\boldsymbol{R}^\alpha + \boldsymbol{l}^\alpha, \boldsymbol{R}^\alpha - \boldsymbol{l}^\alpha)\right]\frac{f_k^\alpha}{16\pi\eta} \\
&+ \left[1 - \boldsymbol{l}^\alpha\cdot\nabla_\alpha - \boldsymbol{l}^\beta\cdot\nabla_\beta + \frac{1}{2}(\boldsymbol{l}^\alpha\cdot\nabla_\alpha)^2 + \frac{1}{2}(\boldsymbol{l}^\beta\cdot\nabla_\beta)^2 + (\boldsymbol{l}^\alpha\cdot\nabla_\alpha)(\boldsymbol{l}^\beta\cdot\nabla_\beta)\right] \\
&\times G_{ij}(\boldsymbol{R}^\alpha + \boldsymbol{l}^\alpha, \boldsymbol{R}_\beta + \boldsymbol{l}^\beta)\frac{f_j^\beta}{16\pi\eta},
\end{aligned} \tag{5.16}$$

where we have used $G_{ij}(\boldsymbol{R}^\alpha \pm \boldsymbol{l}^\alpha) = G(a_k)\delta_{ij}$ with $k = 1(2)$ for the minus(plus) sign, and the subscript for the subunit has been dropped from the forces with the understanding that the remaining forces are the forces on subunit 1. As before, (5.16) is decomposed into the equations for the sizes and orientations of the dumbbells as

$$\begin{aligned}
\dot{l}^\alpha &= \left\{G(a_1) - G(a_2)^{-1}\left[G_I(l^\alpha) + G_D(l^\alpha)\right]^2\right\}\frac{f^\alpha}{16\pi\eta} \\
&+ \left[1 - \boldsymbol{l}^\alpha\cdot\nabla_\alpha - \boldsymbol{l}^\beta\cdot\nabla_\beta + \frac{1}{2}(\boldsymbol{l}^\alpha\cdot\nabla_\alpha)^2 + \frac{1}{2}(\boldsymbol{l}^\beta\cdot\nabla_\beta)^2 + (\boldsymbol{l}^\alpha\cdot\nabla_\alpha)(\boldsymbol{l}^\beta\cdot\nabla_\beta)\right] \\
&\times G_{ij}(\boldsymbol{R}^\alpha + \boldsymbol{l}^\alpha, \boldsymbol{R}^\beta + \boldsymbol{l}^\beta)\frac{f^\beta}{16\pi\eta}\hat{n}_j^\beta\hat{n}_i^\alpha
\end{aligned} \tag{5.17}$$

$$\begin{aligned}
\dot{n}_i^\alpha =& \frac{1}{l^\alpha}\left[1 - \boldsymbol{l}^\alpha\cdot\nabla_\alpha - \boldsymbol{l}^\beta\cdot\nabla_\beta + \frac{1}{2}(\boldsymbol{l}^\alpha\cdot\nabla_\alpha)^2 + \frac{1}{2}(\boldsymbol{l}^\beta\cdot\nabla_\beta)^2 + (\boldsymbol{l}^\alpha\cdot\nabla_\alpha)(\boldsymbol{l}^\beta\cdot\nabla_\beta)\right] \\
&\times G_{mj}(\boldsymbol{R}^\alpha + \boldsymbol{l}^\alpha, \boldsymbol{R}^\beta + \boldsymbol{l}^\beta)n_j^\beta(\delta_{im} - n_m^\alpha n_i^\alpha)\frac{f^\beta}{16\pi\eta},
\end{aligned} \tag{5.18}$$

where we have also used the approximation $\mathbf{G}(\boldsymbol{R}^\alpha - \boldsymbol{l}^\alpha, \boldsymbol{R}^\alpha + \boldsymbol{l}^\alpha) = G_I(l^\alpha)\mathbf{1} + G_D(l^\alpha)\hat{\boldsymbol{n}}^\alpha\hat{\boldsymbol{n}}^\alpha$, with $G_I(l^\alpha)$ and $G_D(l^\alpha)$ that are different to (5.5) due to the proximity of the dumbbells to a wall. From eq. (5.17) a tethered dumbbell has mobility

$$\mu^\alpha = G(a_1) - G(a_2)^{-1}\left[G_I(l^\alpha) + G_D(l^\alpha)\right]^2, \tag{5.19}$$

and the leading contribution to hydrodynamic coupling is

$$h = \frac{1}{16\pi\eta}\hat{\boldsymbol{n}}^\alpha \cdot \boldsymbol{G}(\boldsymbol{R}^\alpha + \boldsymbol{l}^\alpha, \boldsymbol{R}^\beta + \boldsymbol{l}^\beta) \cdot \hat{\boldsymbol{n}}^\beta. \tag{5.20}$$

In eq. (5.20), $\boldsymbol{G}(\boldsymbol{R}^\alpha + \boldsymbol{l}^\alpha, \boldsymbol{R}^\beta + \boldsymbol{l}^\beta)$ is the Green's function of the Stokes equation with the appropriate boundary conditions at the surface to which the enzymes are tethered. To simplify notation, from here on, we will write $\boldsymbol{R}^\alpha + \boldsymbol{l}^\alpha = \boldsymbol{R}^\alpha$ for the position of the second subunit. Defining $\overline{\boldsymbol{R}} = \boldsymbol{R}^1 - \overline{\boldsymbol{R}}^2$, where $\overline{\boldsymbol{R}}^2 = (x_2, y_2, -z_2)$ is the position of the image of the second subunit of the second dumbbell with respect to the surface, for a no-slip wall,

$$\begin{aligned} G_{ij}(\boldsymbol{R}) =& \frac{1}{8\pi\eta}\Bigg\{\frac{\delta_{ij}}{|\,\boldsymbol{R}\,|} + \frac{R_i R_j}{|\,\boldsymbol{R}\,|^3} - \frac{\delta_{ij}}{|\,\overline{\boldsymbol{R}}\,|} - \frac{\overline{R}_i\overline{R}_j}{|\,\overline{\boldsymbol{R}}\,|^3} \\ &+ 2z_2(\delta_{jp}\delta_{pk} - \delta_{j3}\delta_{3k})\frac{\partial}{\partial\overline{R}_k}\left[\frac{z_2\overline{R}_i}{|\,\overline{\boldsymbol{R}}\,|^3} - \left(\frac{\delta_{i3}}{|\,\overline{\boldsymbol{R}}\,|} + \frac{\overline{R}_i\overline{R}_3}{|\,\overline{\boldsymbol{R}}\,|^3}\right)\right]\Bigg\}, \end{aligned} \tag{5.21}$$

where i, j and $k = 1, 2, 3$ indices and $p = 1, 2$ are the Cartesian indices, is the Blake tensor [149]. We assume that the surface is in the xy-plane, with the x-axis parallel to the line separating the dumbbells, and the z-axis is perpendicular to the surface and parallel to the dumbbells. The tensor is simplified by taking the positions $\boldsymbol{R}^1 = (0, 0, h_z)$ and $\boldsymbol{R}^2 = (d, 0, h_z)$. In addition to the change in sign due to the relative orientation of the enzymes, the sign of the coupling can also be controlled by varying the ratio of the tethering height h_z and the separation d. Writing the coupling constant h as a function of the ratio $H = h_z/d$, we find that it is negative up to a value H^*, and above this, the coupling between the dumbbells is positive. This means that for a positive force f^β, for $H < H^*$ the coupling acts to a reduce the length of the coupled enzyme, and for $H > H^*$, the coupling leads to an increase in length.

It is interesting to consider the tethering surface as the interface between two immiscible liquids, which is perhaps more biologically relevant. In this case, the Green's function is the Aderogba-Blake tensor [150]

$$G_{ij}(\boldsymbol{R}) = \frac{\delta_{ij}}{|\,\boldsymbol{R}\,|} + \frac{R_i R_j}{|\,\boldsymbol{R}\,|^3} + \left(\frac{1-\hat{\eta}}{1+\hat{\eta}}\delta_{jp}\delta_{pk} - \delta_{j3}\delta_{3k}\right)\left(\frac{\delta_{ik}}{|\,\overline{\boldsymbol{R}}\,|} + \frac{\overline{R}_i\overline{R}_k}{|\,\overline{\boldsymbol{R}}\,|^3}\right) + \frac{2\hat{\eta}}{1+\hat{\eta}} z_2(\delta_{jp}\delta_{pk} - \delta_{j3}\delta_{3k})\frac{\partial}{\partial \overline{R}_k}\left[\frac{z_2\overline{R}_i}{|\,\overline{\boldsymbol{R}}\,|^3} - \left(\frac{\delta_{i3}}{|\,\overline{\boldsymbol{R}}\,|} + \frac{\overline{R}_i\overline{R}_3}{|\,\overline{\boldsymbol{R}}\,|^3}\right)\right], \quad (5.22)$$

where $\hat{\eta} = \eta_2/\eta_1$ is the ratio of the viscosities of the two liquids, and η_1 (η in eq. (5.20)) is the viscosity of the region containing the dumbbells. The limiting cases of $\hat{\eta} \to \infty$ and $\hat{\eta} \to 0$ give the tensors for a rigid no-slip wall and free surface, respectively. We find that H^* decreases with $\hat{\eta}$. We also find that the coupling between the dumbbells increases as $\hat{\eta}$ decreases. Note that the case $\hat{\eta} \to 1$ does not reproduce the infinite fluid tensor because there is a distribution of normal stress over the surface so that the normal velocity is zero.

CHAPTER 6

Summary and outlook

6.1 Summary

We have shown that intrinsically asymmetric objects such as enzymes, display rich and interesting dynamics at nanoscopically small scales. For catalytically active enzymes we have developed a theoretical framework for studying the correlations between their dynamical properties and function of performing catalytic turnover.

We have studied the diffusive motion of a flexible generalised dumbbell as a minimal model of an enzyme, focusing on the effect of internal asymmetry and the coupling between internal and external degrees of freedom. In our simple model, local thermal fluctuations of the dumbbell lead to hydrodynamic coupling of its components. We have shown that the long-time diffusion coefficient of the dumbbell has a negative fluctuation-induced correction in the presence of solvent-mediated hydrodynamic interactions compared to a rigid symmetric structure. The correction is coupled to asymmetry and vanishes for a symmetric dumbbell. Motivated by the rotational motion of the domains of real enzyme molecules, we considered the effect of rotational constraints which limit the rotations of the subunits. As expected, the inclusion of constraints on the rotational motion reduces the negative fluctuation-induced correction to the effective diffusion coefficient. Due to the simplicity of the model, these results are generic and extendable to more complex modular structures.

In ref. [80], the generalised dumbbell model is used to study the effect of the catalytic cycle on the diffusive dynamics of a catalytically active enzyme. By considering a reduced cycle, which is equivalent to studying the dynamics at timescales much smaller than the rate of product formation for reactions were the binding interaction is faster than the time for converting a substrate molecule into product, it is shown that enhanced diffusion of an enzyme molecule in the presence of its substrate can be explained in a purely equilibrium picture for enzymes that diffuse faster when bounded to a ligand. The equilibrium model for enhanced diffusion relies on the conformational changes of the enzyme that accompany the catalytic cycle, rather than any non-equilibrium aspect of the cycle, making the results consistent with the observation of enhanced diffusion of enzymes in the presence of other ligands (such as inhibitors) which bind irreversibly to the active site but are not catalysed [26]. The contribution to enhanced diffusion coming from the model is a contribution to the random motion that is present for all substrate concentrations and it is therefore not limited by the thermodynamic constraints on the transduction of the free energy of reaction into mechanical work [151].

As an application of our asymmetric dumbbell model, we studied the response of an enzyme molecule to a concentration gradient of its substrate. By considering the separate interactions between the domains of the dumbbell with substrate molecules we have predicted the exciting possibility of aligning a single enzyme molecule with a concentration gradient of its substrate (or indeed another chemical other than its substrate with which it interacts) and furthermore, a gradient in enzyme concentration. The dumbbell is polarised by its subunits having different interactions with substrate molecules, and by the hydrodynamic coupling between its translational and rotational modes due to asymmetry.

The interactions of the enzyme with the substrate concentration gradient produces a drift velocity and a tendency to align parallel or anti-parallel to the gradient, depending on the sign of the interactions between the enzyme and substrate molecules. The angular velocity of the dumbbell is determined by the subunit that interacts most strongly with the substrate. Specifically, the enzyme will

typically orient so that the subunit that is most attracted to the substrate (or least repelled from the substrate, if both are repelled) is in the region of higher substrate concentration. If both subunits have equal interactions with the substrate, the enzyme will reorient so that the larger subunit is in the region of higher or lower substrate concentration if the interactions are attractive or repulsive, respectively. The second alignment mechanism, due to gradients in the concentration field of the *enzyme*, that is controlled by the strength of the coupling between the translational and rotational motion of the enzyme, leads to reorientation so that the larger subunit is in the region of higher enzyme concentration.

We have also shown that the result from Chapter 3 that the diffusion coefficient of a modular macromolecule is overestimated if it is considered as a rigid, symmetric object also applies to the drift velocity in the presence of a substrate concentration gradient. The drift velocity in a substrate gradient is modified for a flexible macromolecule in the same way as the diffusion coefficient. Though the form of the fluctuation-induced corrections we present is specific to the ordering of the time-scales of the system, specifically the reorientation time of the dumbbell and the time for binding interactions with substrate molecules, the ordering we considered of the rotational diffusion being faster than the mean binding time is the most relevant given that it corresponds to the ordering that is typically observed in enzymes.

Finally, in Chapter 5 we provided some preliminary results on the effect of hydrodynamic coupling between a pair of our model enzymes on the internal dynamics of one of them. When the dumbbells are constrained to a surface and their orientations are fixed, we find that the sign of the coupling depends on the distance between the dumbbells. Furthermore, the strength of the coupling changes with the ratio of the viscosities of the suspending and surface regions.

As experimental progress on enzyme dynamics continues, we look forward to our prediction of single molecule alignment being realised. Furthermore, our simple model could inspire the design an alignable nano-scale object.

6.2 Outlook

Although the field is fast garnering interest, still, the interesting results so far have been on single molecules. As our experimental colleagues are pushing the frontiers of single-molecule techniques in order to understand the long-contested observations of enhanced enzyme diffusion and chemotaxis of single enzymes, there is an opportunity for theoretical research to set the agenda for investigating collective behaviour in enzymatic systems. Perhaps the most interesting question that is accessible with our simple model is concerning the collective dynamics of enzymes that is induced by the typical interactions that one would expect in their cellular environment. We have already made some progress in this direction.

A specific goal, which would be the culmination of theoretical and experimental studies, would be to provide a microscopic theory for the assembly of enzyme structures, such as those in metabolic pathways, that is capable of reproducing the compositional accuracy of real enzyme assemblies in noisy cellular environments. There has been some effort to understand the conditions under which protein assemblies form [24, 152], but to our knowledge, these studies have so far not included the contributions from the rich dynamics already present at the level of an individual enzyme.

At the single-molecule level, an understanding of the mechanisms that are responsible for enhanced enzyme diffusion and chemotaxis could lead to the discovery of useful design features for nanoengineering.

APPENDIX A

Higher order moments

To check the consistency of the moment expansion in Chapter 3, we consider the translational motion of an axisymmetric dumbbell, for which the hydrodynamic tensors can be decomposed into isotropic and directional parts as $\boldsymbol{A} = A_I(l)\mathbf{1} + A_D(l)\hat{\boldsymbol{n}}\hat{\boldsymbol{n}}$. For this example, the separation-averaged Smoluchowski equation is

$$\begin{aligned}\mathcal{L}_{\mathrm{T}}\mathcal{P}(\boldsymbol{R},\hat{\boldsymbol{n}};t) =& \frac{k_{\mathrm{B}}T}{4}\nabla_{\boldsymbol{R}}\cdot[\langle\mathbf{M}\rangle\cdot\nabla_{\boldsymbol{R}}\mathcal{P}] - k_{\mathrm{B}}T\left\langle\frac{\Gamma_{\mathrm{I}}}{l}\right\rangle\nabla_{\boldsymbol{R}}\cdot[(\hat{\boldsymbol{n}}\times\boldsymbol{\mathcal{R}}\mathcal{P})+\hat{\boldsymbol{n}}\mathcal{P}] \\ &+ k_{\mathrm{B}}T\left\langle\frac{\mathrm{W}_{\mathrm{I}}}{l^2}\right\rangle\boldsymbol{\mathcal{R}}^2\mathcal{P}. \end{aligned} \tag{A.1}$$

The first four moments of this equation are:

$$\begin{aligned}\partial_t\rho(\boldsymbol{R};t) =& \frac{k_{\mathrm{B}}T}{4}\left(\langle\mathrm{M}_{\mathrm{I}}\rangle+\frac{1}{3}\langle\mathrm{M}_{\mathrm{D}}\rangle\right)\nabla^2_{\boldsymbol{R}}\rho + \frac{k_{\mathrm{B}}T}{4}\langle\mathrm{M}_{\mathrm{D}}\rangle\,\partial_{R_i}\partial_{R_j}Q_{ij} \\ &+ k_{\mathrm{B}}T\left\langle\frac{\Gamma_{\mathrm{I}}}{l}\right\rangle\nabla_{\boldsymbol{R}}\cdot\boldsymbol{p}, \end{aligned} \tag{A.2}$$

$$\begin{aligned}\partial_t p_i(\boldsymbol{R};t) =& \frac{k_{\mathrm{B}}T}{4}\left(\langle\mathrm{M}_{\mathrm{I}}\rangle+\frac{1}{5}\langle\mathrm{M}_{\mathrm{D}}\rangle\right)\nabla^2_{\boldsymbol{R}}p_i \\ &+ \frac{k_{\mathrm{B}}T}{4}\langle\mathrm{M}_{\mathrm{D}}\rangle\left[\frac{2}{5}\partial_{R_i}(\nabla_{\boldsymbol{R}}\cdot\boldsymbol{p})+\partial_{R_j}\partial_{R_k}Q^{(3)}_{ijk}\right] \\ &- \frac{k_{\mathrm{B}}T}{3}\left\langle\frac{\Gamma_{\mathrm{I}}}{l}\right\rangle\partial_{R_i}\rho + 2k_{\mathrm{B}}T\left\langle\frac{\Gamma_{\mathrm{I}}}{l}\right\rangle\partial_{R_j}Q_{ij} - 2k_{\mathrm{B}}T\left\langle\frac{\mathrm{W}_{\mathrm{I}}}{l^2}\right\rangle p_i, \end{aligned} \tag{A.3}$$

$$\partial_t Q_{ij}(\boldsymbol{R};t) = \frac{k_\mathrm{B}T}{4}\left\langle \mathrm{M_I}\right\rangle \nabla^2_{\boldsymbol{R}} Q_{ij} - 6k_\mathrm{B}T\left\langle \frac{\mathrm{W_I}}{l^2}\right\rangle Q_{ij}$$
$$+ \frac{k_\mathrm{B}T}{4}\left\langle \mathrm{M_D}\right\rangle \left[\partial_{R_k}\partial_{R_l} Q^{(4)}_{ijkl} - \frac{1}{3}\partial_{R_k}\partial_{R_l} Q_{kl}\delta_{ij} - \frac{2}{15}\left(\frac{1}{3}\nabla^2_{\boldsymbol{R}} c\delta_{ij} - \partial_{R_i}\partial_{R_j} c\right)\right]$$
$$+ k_\mathrm{B}T\left\langle \frac{\Gamma_\mathrm{I}}{l}\right\rangle \left[3\partial_{R_k} Q^{(3)}_{ijk} + \frac{4}{15}\nabla_{\boldsymbol{R}}\cdot\boldsymbol{p}\delta_{ij} - \frac{2}{5}\left(\partial_{R_i} p_j + \partial_{R_j} p_i\right)\right], \tag{A.4}$$

and

$$\partial_t Q^{(3)}_{ijk}(\boldsymbol{R};t) = \frac{k_\mathrm{B}T}{4}\left\langle \mathrm{M_I}\right\rangle \nabla^2_{\boldsymbol{R}} Q^{(3)}_{ijk} - 12k_\mathrm{B}T\left\langle \frac{\mathrm{W_I}}{l^2}\right\rangle Q^{(3)}_{ijk} + 4k_\mathrm{B}T\left\langle \frac{\Gamma_\mathrm{I}}{l}\right\rangle \partial_{R_l} Q^{(4)}_{ijkl}$$
$$+ \frac{k_\mathrm{B}T}{4}\left\langle \mathrm{M_D}\right\rangle \left\{\partial_{R_l}\partial_{R_m} Q^{(5)}_{ijklm} - \frac{1}{5}\partial_{R_l}\partial_{R_m}\left(Q^{(3)}_{lmi}\delta_{jk} + Q^{(3)}_{lmj}\delta_{ik} + Q^{(3)}_{lmk}\delta_{ij}\right)\right.$$
$$- \frac{2}{175}\left[\nabla^2_{\boldsymbol{R}} p_i + 2\partial_{R_i}(\nabla_{\boldsymbol{R}}\cdot\boldsymbol{p})\right]\delta_{jk} - \frac{2}{175}\left[\nabla^2_{\boldsymbol{R}} p_j + 2\partial_{R_j}(\nabla_{\boldsymbol{R}}\cdot\boldsymbol{p})\right]\delta_{ik}$$
$$\left. - \frac{2}{175}\left[\nabla^2_{\boldsymbol{R}} p_k + 2\partial_{R_k}(\nabla_{\boldsymbol{R}}\cdot\boldsymbol{p})\right]\delta_{ij} + \frac{2}{35}\left(\partial_{R_i}\partial_{R_j} p_k + \partial_{R_i}\partial_{R_k} p_j + \partial_{R_j}\partial_{R_k} p_i\right)\right\}$$
$$- k_\mathrm{B}T\left\langle \frac{\Gamma_\mathrm{I}}{l}\right\rangle \left(\partial_{R_i} Q^{(2)}_{jk} + \partial_{R_j} Q^{(2)}_{ik} + \partial_{R_k} Q^{(2)}_{ij}\right)$$
$$- \frac{2}{5}\left\langle \frac{\Gamma_\mathrm{I}}{l}\right\rangle \partial_{R_l}\left(Q^{(2)}_{il}\delta_{jk} + Q^{(2)}_{jl}\delta_{ik} + Q^{(2)}_{kl}\delta_{ij}\right). \tag{A.5}$$

It is straightforward to see that none of the terms in the stationary values of Q and $Q^{(3)}$ survive the closure scheme. Note also that the coupling between moments is not tridiagonal.

APPENDIX B

Definition of $\mathcal{K}_\alpha$, $\mathcal{L}_{\alpha\beta}$, $\mathcal{M}_{\alpha\beta}$ and $\mathcal{N}_{\alpha\beta}$

$$\mathcal{K}_\alpha = \frac{1}{9}\left[\frac{\langle\gamma_0\varphi/x\rangle^2}{\langle\gamma_0/x\rangle^2}\frac{\langle w_0/x^2\rangle}{\left\langle\psi_0^{(\alpha)}\right\rangle} + \frac{\langle\gamma_0\varphi/x\rangle}{\langle\gamma_0/x\rangle}\frac{\left\langle\psi_0^{(\alpha)}\varphi\right\rangle}{\left\langle\psi_0^{(\alpha)}\right\rangle} - \frac{\langle\gamma_0\varphi/x\rangle}{\langle\gamma_0/x\rangle}\frac{\langle w_0\varphi/x^2\rangle}{\left\langle\psi_0^{(\alpha)}\right\rangle} - \frac{\langle w_0\varphi/x^2\rangle}{\langle w_0/x^2\rangle}\frac{\left\langle\psi_0^{(\alpha)}\varphi\right\rangle}{\left\langle\psi_0^{(\alpha)}\right\rangle}\right] \tag{B.1}$$

In the Oseen limit, $\mathcal{K}_\alpha$ can be calculated with the mobility functions in the main text in addition to

$$\psi_0^{(\alpha)} \simeq \frac{1}{8\pi\eta a_\alpha^3}; \tag{B.2}$$

$$\psi_0^{(12)} \simeq \frac{1}{16\pi\eta x^3}. \tag{B.3}$$

The remaining coefficients are defined as

$$\mathcal{L}_{\alpha\beta} = \frac{1}{27}\left[2\frac{\langle\gamma_{12}\varphi/x\rangle}{\langle\gamma_0/x\rangle}\frac{\langle\gamma_0\varphi/x\rangle}{\langle\gamma_0/x\rangle}\frac{\langle w_0/x^2\rangle}{\left\langle\psi_0^{(\beta)}\right\rangle} - \frac{\langle\gamma_{12}\varphi/x\rangle}{\langle\gamma_0/x\rangle}\frac{\langle w_0\varphi/x^2\rangle}{\left\langle\psi_0^{(\beta)}\right\rangle} - \frac{\langle w_0\varphi/x^2\rangle}{\langle w_0/x^2\rangle}\frac{\left\langle\psi_{12}^{(12)}\varphi\right\rangle}{\left\langle\psi_0^{(\beta)}\right\rangle} + \frac{\langle\gamma_0\varphi/x\rangle}{\langle\gamma_0/x\rangle}\frac{\left\langle\psi_{12}^{(12)}\varphi\right\rangle}{\left\langle\psi_0^{(\beta)}\right\rangle} - \frac{\langle w_{12}\varphi/x^2\rangle}{\left\langle\psi_0^{(\beta)}\right\rangle}\frac{\langle\gamma_0\varphi/x\rangle}{\langle\gamma_0/x\rangle} + \frac{\langle\gamma_{12}\varphi/x\rangle}{\langle\gamma_0/x\rangle}\frac{\left\langle\psi_0^{(\beta)}\varphi\right\rangle}{\left\langle\psi_0^{(\beta)}\right\rangle} - \frac{\langle w_{12}\varphi/x^2\rangle}{\langle w_0/x^2\rangle}\frac{\left\langle\psi_0^{(\beta)}\varphi\right\rangle}{\left\langle\psi_0^{(\beta)}\right\rangle}\right] - \frac{1}{27}\mathcal{K}_\beta\frac{\left\langle\psi_{12}^{(12)}\varphi\right\rangle}{\left\langle\psi_0^{(\alpha)}\right\rangle}, \tag{B.4}$$

$$\mathcal{M}_{\alpha\beta} = \frac{1}{27}\left[\frac{\langle\gamma_0\varphi/x\rangle}{\langle\gamma_0/x\rangle} - \frac{\langle w_0\varphi/x^2\rangle}{\langle w_0/x^2\rangle}\right]\frac{\left\langle\left(\psi_\beta^{(\alpha)} - \psi_\beta^{(12)}\right)\varphi\right\rangle}{\left\langle\psi_0^{(\alpha)}\right\rangle}, \tag{B.5}$$

and

$$\mathcal{N}_{\alpha\beta} = -\frac{1}{27}\mathcal{K}_\beta \frac{\left\langle \left(\psi_0^{(\alpha)} - \psi_0^{(12)}\right)\varphi \right\rangle}{\left\langle \psi_0^{(\alpha)} \right\rangle}. \tag{B.6}$$

References

[1] M. C. Marchetti et al. “Hydrodynamics of soft active matter”. In: *Rev. Mod. Phys.* 85.3 (2013), pp. 1143–1189.

[2] K. Yehl et al. “High-speed DNA-based rolling motors powered by RNase H”. In: *Nat. Nanotechnol.* 11.2 (2016), pp. 184–190.

[3] L. K. E. A. Abdelmohsen et al. “Dynamic Loading and Unloading of Proteins in Polymeric Stomatocytes: Formation of an Enzyme-Loaded Supramolecular Nanomotor”. In: *ACS Nano* 10.2 (2016), pp. 2652–2660.

[4] X. Ma et al. “Motion Control of Urea-Powered Biocompatible Hollow Microcapsules”. In: *ACS Nano* 10.3 (2016), pp. 3597–3605.

[5] S. Sanchez et al. “Dynamics of Biocatalytic Microengines Mediated by Variable Friction Control”. In: *J. Am. Chem. Soc.* 132.38 (2010), pp. 13144–13145.

[6] S. Sengupta et al. “Self-powered enzyme micropumps”. In: *Nat. Chem.* 6.5 (2014), pp. 415–422.

[7] K. K. Dey et al. “Micromotors Powered by Enzyme Catalysis”. In: *Nano Lett.* 15.12 (2015), pp. 8311–8315.

[8] Xing Ma et al. “Enzyme Catalysis To Power Micro/Nanomachines”. In: *ACS Nano* 10.10 (2016), pp. 9111–9122.

[9] C. J. Brokaw. “Mechanical components of motor enzyme function”. In: *Biophys. J.* 73.2 (1997), pp. 938–951.

[10] D. S. Tsao and M. R. Diehl. “Myosins move ahead of the pack”. In: *Nat. Nanotechnol.* 9.1 (2014), pp. 9–10.

[11] A. Goel and V. Vogel. “Harnessing biological motors to engineer systems for nanoscale transport and assembly”. In: *Nat. Nanotechnol.* 3.8 (2008), pp. 465–475.

[12] J. M. Berg, J. L. Tymoczko, and L. Stryer. *Biochemistry.* 5th ed. New York: W H Freeman, 2002.

[13] H. Suzuki. “Chapter 7: Active Site Structure”. In: *How Enzymes Work: From Structure to Function.* 1st ed. Jenny Stanford Publishing, 2015, pp. 117–140.

[14] G. Krauss. "The Regulations of Enzyme Activity". In: *Biochemistry of Signal Transduction and Regulation*. 3rd ed. Wiley VCH, 2003, pp. 89–114.

[15] R. Golestanian. *Nonequilibrium Statistical Physics*. Lecture notes. 2018.

[16] Willian P. Jencks. *Catalysis in Chemistry and Enzymology*. Mineola, N. Y.: Dover, 1988.

[17] Michael M. Cox and David L. Nelson. "Chapter 6.2: How enzymes work". In: *Lehninger Principles of Biochemistry*. 6th ed. New York: W. H. Freeman, 2013, p. 195.

[18] Stephen J. Benkovic and S. Hammes-Schiffer. "A Perspective on Enzyme Catalysis". In: *Science* 301.5637 (2003), pp. 1196–1202.

[19] A. Warshel et al. "Electrostatic Basis for Enzyme Catalysis". In: *Chem. Rev.* 106.8 (2006), pp. 3210–3235.

[20] T. Shafee. "Evolvability of a viral protease: experimental evolution of catalysis, robustness and specificity". thesis. University of Cambridge, 2013.

[21] David G. Nicholls and Stuart J. Ferguson. *Bioenergetics*. 3rd ed. London: Academic Press, 2003.

[22] X. Zhao et al. "Substrate-driven chemotactic assembly in an enzyme cascade". In: *Nat. Chem.* 10.3 (2018), pp. 311–317.

[23] F. Wu, L. N. Pelster, and S. D. Minteer. "Krebs cycle metabolon formation: metabolite concentration gradient enhanced compartmentation of sequential enzymes". In: *ChemComm* 51.7 (2014), pp. 1244–1247.

[24] L. J. Sweetlove and A. R. Fernie. "The role of dynamic enzyme assemblies and substrate channelling in metabolic regulation". In: *Nat. Commun.* 9.1 (2018), p. 2136.

[25] J. Agudo-Canalejo and R. Golestanian. "Active Phase Separation in Mixtures of Chemically Interacting Particles". In: *Physical Review Letters* 1 (2019), p. 018101.

[26] P. Illien et al. "Exothermicity Is Not a Necessary Condition for Enhanced Diffusion of Enzymes". In: *Nano Lett.* 17.7 (2017), pp. 4415–4420.

[27] H. Yu et al. "Molecular Propulsion: Chemical Sensing and Chemotaxis of DNA Driven by RNA Polymerase". In: *J. Am. Chem. Soc.* 131.16 (2009), pp. 5722–5723.

[28] H. S. Muddana et al. "Substrate Catalysis Enhances Single-Enzyme Diffusion". In: *J. Am. Chem. Soc.* 132.7 (2010), pp. 2110–2111.

[29] S. Sengupta et al. "Enzyme Molecules as Nanomotors". In: *J. Am. Chem. Soc.* 135.4 (2013), pp. 1406–1414.

[30] S. Sengupta et al. "DNA Polymerase as a Molecular Motor and Pump". In: *ACS Nano* 8.3 (2014), pp. 2410–2418.

[31] C. Riedel et al. "The heat released during catalytic turnover enhances the diffusion of an enzyme". In: *Nature* 517.7533 (2015), pp. 227–230.

[32] K. K. Dey et al. "Chemotactic Separation of Enzymes". In: *ACS Nano* 8.12 (2014), pp. 11941–11949.

[33] A.-Y. Jee et al. "Enzyme leaps fuel antichemotaxis". In: *Proc. Natl. Acad. Sci.* 115.1 (2017), p. 201717844.

[34] J. Agudo-Canalejo et al. “Enhanced Diffusion and Chemotaxis at the Nanoscale”. In: *Acc. Chem. Res.* 51.10 (2018), pp. 2365–2372.

[35] A. S. Mikhailov and R. Kapral. “Hydrodynamic collective effects of active protein machines in solution and lipid bilayers”. In: *Proc. Natl. Acad. Sci.* 112.28 (2015), E3639–E3644.

[36] X. Bai and P. G. Wolynes. “On the hydrodynamics of swimming enzymes”. In: *J. Chem. Phys.* 143.16 (2015), p. 165101.

[37] R. Golestanian. “Enhanced Diffusion of Enzymes that Catalyze Exothermic Reactions”. In: *Phys. Rev. Lett.* 115.10 (2015), p. 108102.

[38] W. Hwang and C. Hyeon. “Energetic Costs, Precision, and Transport Efficiency of Molecular Motors”. In: *J. Phys. Chem. Lett.* 9.3 (2018), pp. 513–520.

[39] P. C. Martin, O. Parodi, and P. S. Pershan. “Unified Hydrodynamic Theory for Crystals, Liquid Crystals, and Normal Fluids”. In: *Phys. Rev. A* 6.6 (1972), pp. 2401–2420.

[40] T. Vicsek et al. “Novel Type of Phase Transition in a System of Self-Driven Particles”. In: *Phys. Rev. Lett.* 75.6 (1995), pp. 1226–1229.

[41] J. Toner and Y. Tu. “Long-Range Order in a Two-Dimensional Dynamical XY Model: How Birds Fly Together”. In: *Phys. Rev. Lett.* 75.23 (1995), pp. 4326–4329.

[42] A. Czirók, H. E. Stanley, and T. Vicsek. “Spontaneously ordered motion of self-propelled particles”. In: *J. Phys. A* 30.5 (1997), pp. 1375–1385.

[43] J. Toner and Y. Tu. “Flocks, herds, and schools: A quantitative theory of flocking”. In: *Phys. Rev. E* 58.4 (1998), pp. 4828–4858.

[44] N. D. Mermin and H. Wagner. “Absence of Ferromagnetism or Antiferromagnetism in One- or Two-Dimensional Isotropic Heisenberg Models”. In: *Phys. Rev. Lett.* 17.22 (1966), pp. 1133–1136.

[45] E. Tjhung, D. Marenduzzo, and M. E. Cates. “Spontaneous symmetry breaking in active droplets provides a generic route to motility”. In: *Proc. Natl. Acad. Sci.* 109.31 (2012), pp. 12381–12386.

[46] R. Aditi Simha and S. Ramaswamy. “Hydrodynamic Fluctuations and Instabilities in Ordered Suspensions of Self-Propelled Particles”. In: *Phys. Rev. Lett.* 89.5 (2002), p. 058101.

[47] L. Onsager. “Reciprocal Relations in Irreversible Processes. I.” In: *Phys. Rev.* 37.4 (1931), pp. 405–426.

[48] K. Kruse et al. “Asters, Vortices, and Rotating Spirals in Active Gels of Polar Filaments”. In: *Phys. Rev. Lett.* 92.7 (2004), p. 078101.

[49] K. Kruse et al. “Generic theory of active polar gels: a paradigm for cytoskeletal dynamics”. In: *Eur. Phys. J. E* 16.1 (2005), pp. 5–16.

[50] Y. Hatwalne et al. “Rheology of Active-Particle Suspensions”. In: *Phys. Rev. Lett.* 92.11 (2004), p. 118101.

[51] A. Baskaran and M. C. Marchetti. “Hydrodynamics of self-propelled hard rods”. In: *Phys. Rev. E* 77.1 (2008), p. 011920.

[52] A. Baskaran and M. C. Marchetti. "Enhanced Diffusion and Ordering of Self-Propelled Rods". In: *Phys. Rev. Lett.* 101.26 (2008), p. 268101.

[53] E. Bertin, M. Droz, and G. Grégoire. "Boltzmann and hydrodynamic description for self-propelled particles". In: *Phys. Rev. E* 74.2 (2006), p. 022101.

[54] E. Bertin, M. Droz, and G. Grégoire. "Hydrodynamic equations for self-propelled particles: microscopic derivation and stability analysis". In: *J. Phys. A* 42.44 (2009), p. 445001.

[55] A. Peshkov et al. "Nonlinear Field Equations for Aligning Self-Propelled Rods". In: *Phys. Rev. Lett.* 109.26 (2012), p. 268701.

[56] E. Bertin et al. "Comparison between Smoluchowski and Boltzmann approaches for self-propelled rods". In: *Phys. Rev. E* 92.4 (2015), p. 042141.

[57] A. Ahmadi, T. B. Liverpool, and M. C. Marchetti. "Nematic and polar order in active filament solutions". In: *Phys. Rev. E* 72.6 (2005), p. 060901.

[58] A. Ahmadi, M. C. Marchetti, and T. B. Liverpool. "Hydrodynamics of isotropic and liquid crystalline active polymer solutions". In: *Phys. Rev. E* 74.6 (2006), p. 061913.

[59] M. E. Cates and J. Tailleur. "When are active Brownian particles and run-and-tumble particles equivalent? Consequences for motility-induced phase separation". In: *EPL* 101.2 (2013), p. 20010.

[60] A. P. Solon, M. E. Cates, and J. Tailleur. "Active brownian particles and run-and-tumble particles: A comparative study". In: *Eur. Phys. J.- Spec. Top.* 224.7 (2015), pp. 1231–1262.

[61] D. S. Dean. "Langevin equation for the density of a system of interacting Langevin processes". In: *J. Phys. A* 29.24 (1996), pp. L613–L617.

[62] F. D. C. Farrell et al. "Pattern Formation in Self-Propelled Particles with Density-Dependent Motility". In: *Phys. Rev. Lett.* 108.24 (2012), p. 248101.

[63] S. Saha, R. Golestanian, and S. Ramaswamy. "Clusters, asters, and collective oscillations in chemotactic colloids". In: *Phys. Rev. E* 89.6 (2014).

[64] J. Tailleur and M. E. Cates. "Statistical Mechanics of Interacting Run-and-Tumble Bacteria". In: *Phys. Rev. Lett.* 100.21 (2008), p. 218103.

[65] D. Saintillan and M. J. Shelley. "Instabilities, pattern formation, and mixing in active suspensions". In: *Phys. Fluids* 20.12 (2008), p. 123304.

[66] M. R. Nejad and A. Najafi. "Chemotaxis mediated interactions can stabilize the hydrodynamic instabilities in active suspensions". In: *Soft Matter* 15.15 (2019), pp. 3248–3255.

[67] D. J. Jackson. "Classical Electrodynamics - Section 4". In: *Classical Electrodynamics*. 3rd ed. Wiley, 1999, pp. 145–169.

[68] S. Kim and S. J. Karrila. *Microhydrodynamics: Principles and Selected Applications*. Dover Publications Inc., 2005.

[69] H. Risken. "The Fokker-Planck Equation". In: *The Fokker-Planck Equation*. 2nd ed. Springer Series in Synergetics 18. Germany: Springer-Verlag Berlin Heidelberg, 1996, pp. 179–194.

[70] A. Guth. *Lecture Notes 9 Traceless Symmetric Tensor Approach To Legendre Polynomials and Spherical Harmonics*. Lecture notes. 2012.

[71] W.-N. Zou and Q.-S. Zheng. "Maxwell's multipole representation of traceless symmetric tensors and its application to functions of high-order tensors". In: *P. Roy. Soc. A* 459.2031 (2003), pp. 527–538.

[72] M. Doi and S. F. Edwards. *The theory of polymer dynamics*. International series of monographs on physics (Oxford, England) ; 73. Oxford: Clarendon Press, 1986.

[73] T. Shimada, M. Doi, and K. Okano. "Concentration fluctuation of stiff polymers. III. Spinodal decomposition". In: *J. Chem. Phys.* 88.11 (1988), pp. 7181–7186.

[74] M. E. Cates and J. Tailleur. "Motility-Induced Phase Separation". In: *Annu. Rev. Condens. Matter Phys.* 6.1 (2015), pp. 219–244.

[75] E. L. Elson and D. Magde. "Fluorescence correlation spectroscopy. I. Conceptual basis and theory". In: *Biopolymers* 13.1 (1974), pp. 1–27.

[76] X. Ma et al. "Enzyme-Powered Hollow Mesoporous Janus Nanomotors". In: *Nano Lett.* 15.10 (2015), pp. 7043–7050.

[77] A.-Y. Jee et al. "Catalytic enzymes are active matter". In: *Proc. Natl. Acad. Sci.* 115.46 (2018), E10812–E10821.

[78] F. Mohajerani et al. "A Theory of Enzyme Chemotaxis: From Experiments to Modeling". In: *Biochemistry* 57.43 (2018), pp. 6256–6263.

[79] Y. Zhang and H. Hess. "Enhanced Diffusion of Catalytically Active Enzymes". In: *ACS Cent. Sci.* 5.6 (2019), pp. 939–948.

[80] P. Illien, T. Adeleke-Larodo, and R. Golestanian. "Diffusion of an enzyme: The role of fluctuation-induced hydrodynamic coupling". In: *EPL* 119.4 (2017), p. 40002.

[81] H. Frauenfelder, S. G. Sligar, and P. G. Wolynes. "The energy landscapes and motions of proteins". In: *Science* 254.5038 (1991), pp. 1598–1603.

[82] Z. Bu and D. J. E. Callaway. "Chapter 5 - Proteins MOVE! Protein dynamics and long-range allostery in cell signaling". In: *Advances in Protein Chemistry and Structural Biology*. Ed. by R. Donev. Vol. 83. Protein Structure and Diseases. Academic Press, 2011, pp. 163–221.

[83] A. Mohan et al. "Analysis of Molecular Recognition Features (MoRFs)". In: *J. Mol. Bio.* 362.5 (2006), pp. 1043–1059.

[84] F. Rago et al. "Enzyme Substrate Specificity Conferred by Distinct Conformational Pathways". In: *J. Am. Chem. Soc.* 137.43 (2015), pp. 13876–13886.

[85] B. P. Roberts et al. "Wide-Open Flaps Are Key to Urease Activity". In: *J. Am. Chem. Soc.* 134.24 (2012), pp. 9934–9937.

[86] K. Gunasekaran, B. Ma, and R. Nussinov. "Is allostery an intrinsic property of all dynamic proteins?" In: *Proteins: Structure, Function, and Bioinformatics* 57.3 (2004), pp. 433–443.

[87] S. C. L. Kamerlin and A. Warshel. "At the dawn of the 21st century: Is dynamics the missing link for understanding enzyme catalysis?" In: *Proteins* 78.6 (2010), pp. 1339–1375.

[88] A. K. Dunker et al. “Intrinsically disordered protein”. In: *Journal of Molecular Graphics and Modelling* 19.1 (2001), pp. 26–59.

[89] Z. Bu, J. Cook, and D. J. E Callaway. “Dynamic regimes and correlated structural dynamics in native and denatured alpha-lactalbumin11Edited by M. F. Moody”. In: *J. Mol. Bio.* 312.4 (2001), pp. 865–873.

[90] J. Monod, J. Wyman, and J.-P. Changeux. “On the nature of allosteric transitions: A plausible model”. In: *J. Mol. Bio.* 12.1 (1965), pp. 88–118.

[91] D. E. Koshland, G. Némethy, and D. Filmer. “Comparison of Experimental Binding Data and Theoretical Models in Proteins Containing Subunits*”. In: *Biochemistry* 5.1 (1966), pp. 365–385.

[92] R. J. Hawkins and T. C. B. McLeish. “Coupling of Global and Local Vibrational Modes in Dynamic Allostery of Proteins”. In: *Biophys. J.* 91.6 (2006), pp. 2055–2062.

[93] H. Brenner, A. Nadim, and S. Haber. “Long-time molecular diffusion, sedimentation and Taylor dispersion of a fluctuating cluster of interacting Brownian particles”. In: *J. Fluid Mech.* 183 (1987), pp. 511–542.

[94] P. E. Rouse. “A Theory of the Linear Viscoelastic Properties of Dilute Solutions of Coiling Polymers”. In: *J. Chem. Phys.* 21.7 (1953), pp. 1272–1280.

[95] B. H. Zimm. “Dynamics of Polymer Molecules in Dilute Solution: Viscoelasticity, Flow Birefringence and Dielectric Loss”. In: *J. Chem. Phys.* 24.2 (1956), pp. 269–278.

[96] J. G. Kirkwood and J. Riseman. “The Intrinsic Viscosities and Diffusion Constants of Flexible Macromolecules in Solution”. In: *J. Chem. Phys.* 16.6 (1948), pp. 565–573.

[97] R. Zwanzig, J. Kiefer, and G. H. Weiss. “On the Validity of the Kirkwood-Riseman Theory”. In: *Proc. Natl. Acad. of Sci.* 60.2 (1968), pp. 381–386.

[98] J. Rotne and S. Prager. “Variational Treatment of Hydrodynamic Interaction in Polymers”. In: *J. Chem. Phys.* 50.11 (1969), pp. 4831–4837.

[99] H. C. Öttinger. “Translational diffusivity from the Zimm model”. In: *J. Chem. Phys.* 87.5 (1987), pp. 3156–3165.

[100] H. C. Öttinger. “Gaussian approximation for Hookean dumbbells with hydrodynamic interaction: Translational diffusivity”. In: *Colloid Polym. Sci.* 267.1 (1989), pp. 1–8.

[101] H. C. Öttinger. “Gaussian approximation for Rouse chains with hydrodynamic interaction”. In: *J. of Chem. Phys.* 90.1 (1989), pp. 463–473.

[102] G. Wilemski and M. Fixman. “Diffusion-controlled intrachain reactions of polymers. I Theory”. In: *J. Chem. Phys.* 60.3 (1974), pp. 866–877.

[103] N. Levernier et al. “Non-Markovian closure kinetics of flexible polymers with hydrodynamic interactions”. In: *J. Chem. Phys.* 143.20 (2015), p. 204108.

[104] J. G. de la Torre et al. “Approximate methods for calculating hydrodynamic properties of macromolecules in dilute solution. Theory and application to rigid structures”. In: *Macromolecules* 16.7 (1983), pp. 1121–1127.

[105] J. G. de La Torre and V. A. Bloomfield. "Hydrodynamic properties of macromolecular complexes. I. Translation". In: *Biopolymers* 16.8 (1977), pp. 1747–1763.

[106] J. G. Kirkwood. "The general theory of irreversible processes in solutions of macromolecules". In: *J. Polym. Sci.* 12.1 (1954), pp. 1–14.

[107] T. Adeleke-Larodo, P. Illien, and R. Golestanian. "Fluctuation-induced hydrodynamic coupling in an asymmetric, anisotropic dumbbell". In: *Eur. Phys. J. E* 42.3 (2019), p. 39.

[108] J. Happel and B. Howard. *Low Reynolds number hydrodynamics*. Mechanics of Fluids and Transport Processes. Netherlands: Springer Netherlands, 1983.

[109] B. U. Felderhof. "Hydrodynamic interaction between two spheres". In: *Physica A* 89.2 (1977), pp. 373–384.

[110] D. J. Jeffrey and Y. Onishi. "Calculation of the resistance and mobility functions for two unequal rigid spheres in low-Reynolds-number flow". In: *J. Fluid Mech.* 139 (1984), pp. 261–290.

[111] J. G. de La Torre and V. A. Bloomfield. "Hydrodynamics of macromolecular complexes. II. Rotation". In: *Biopolymers* 16.8 (1977), pp. 1765–1778.

[112] Meh. Kardar and R. Golestanian. "The "friction" of vacuum, and other fluctuation-induced forces". In: *Rev. Mod. Phys.* 71.4 (1999), pp. 1233–1245.

[113] F. London. "The general theory of molecular forces". In: *J. Chem. Soc. Faraday Trans.* 33.0 (1937), 8b–26.

[114] J. Zinn-Justin. *Quantum Field Theory and Critical Phenomena*. Oxford University Press, 2002.

[115] P. C. Martin, E. D. Siggia, and H. A. Rose. "Statistical Dynamics of Classical Systems". In: *Phys. Rev.A* 8.1 (1973), pp. 423–437.

[116] J. Agudo-Canalejo and R. Golestanian. "Diffusion and steady state distributions of flexible chemotactic enzymes". In: *arXiv:1910.04526* (2019).

[117] H. Brenner. "A General Theory of Taylor Dispersion Phenomena IV. Direct Coupling Effects". In: *Chemical Engineering Communications* 18.5-6 (1982), pp. 355–379.

[118] H. Brenner and D. A. Edwards. *Macrotransport processes*. Butterworth-Heinemann series in chemical engineering. Boston ; London: Butterworth-Heinemann, 1993.

[119] T. Goldfriend, H. Diamant, and T. A. Witten. "Hydrodynamic interactions between two forced objects of arbitrary shape. I. Effect on alignment". In: *Phys. Fluids* 27.12 (2015), p. 123303.

[120] J.-P. Günther, M. Börsch, and P. Fischer. "Diffusion Measurements of Swimming Enzymes with Fluorescence Correlation Spectroscopy". In: *Acc. Chem. Res.* 51.9 (2018), pp. 1911–1920.

[121] J.-P. Günther, G. Majer, and P. Fischer. "Absolute diffusion measurements of active enzyme solutions by NMR". In: *J. Chem. Phys.* 150.12 (2019), p. 124201.

[122] Y. Zhang et al. "Aldolase Does Not Show Enhanced Diffusion in Dynamic Light". In: *Nano Lett.* (2018).

[123] M. Xu et al. “Direct Single Molecule Imaging of Enhanced Enzyme Diffusion”. In: *Phys. Rev. Lett.* 123.12 (2019), p. 128101.

[124] S. Kondrat and M. N. Popescu. “Brownian dynamics assessment of enhanced diffusion exhibited by ‘fluctuating-dumbbell enzymes’”. In: *Phys. Chem. Chem. Phys.* 21.35 (2019), pp. 18811–18815.

[125] A.-Y. Jee et al. “Enhanced Diffusion and Oligomeric Enzyme Dissociation”. In: *J. Am. Chem. Soc.* 141.51 (2019), pp. 20062–20068.

[126] J. Agudo-Canalejo, P. Illien, and R. Golestanian. “Cooperatively enhanced reactivity and “stabilitaxis” of dissociating oligomeric proteins”. In: *Proc. Natl. Acad. Sci.* 117.22 (2020), pp. 11894–11900.

[127] J. Arlt et al. “Painting with light-powered bacteria”. In: *Nat. Commun.* 9.1 (2018), p. 768.

[128] H. C. Berg. *E. coli in Motion*. Biological and Medical Physics, Biomedical Engineering. New York: Springer-Verlag, 2004.

[129] E. F. Keller and L. A. Segel. “Model for chemotaxis”. In: *J. Theor. Biol.* 30.2 (1971), pp. 225–234.

[130] M. Eisenbach. “Sperm chemotaxis”. In: *Rev. Reprod.* 4.1 (1999), pp. 56–66.

[131] B. M. Friedrich and F. Jülicher. “Chemotaxis of sperm cells”. In: *Proc. Natl. Acad. Sci.* 104.33 (2007), pp. 13256–13261.

[132] H. C. Berg and D. A. Brown. “Chemotaxis in Escherichia coli analysed by Three-dimensional Tracking”. In: *Nature* 239.5374 (1972), pp. 500–504.

[133] J. E. Segall, S. M. Block, and H. C. Berg. “Temporal comparisons in bacterial chemotaxis.” In: *Proc. Natl. Acad. Sci.* 83.23 (1986), pp. 8987–8991.

[134] M. J. Schnitzer, S. M. Block, and H. C. Berg. “Strategies for chemotaxis”. In: *Biol. Chemotactic Response* 46 (1990), pp. 15–34.

[135] A. Joseph et al. “Chemotactic synthetic vesicles: Design and applications in blood-brain barrier crossing”. In: *Sci. Adv.* 3.8 (2017), e1700362.

[136] R. Guha et al. “Chemotaxis of Molecular Dyes in Polymer Gradients in Solution”. In: *J. Am. Chem. Soc.* 139.44 (2017), pp. 15588–15591.

[137] A. Somasundar et al. “Positive and negative chemotaxis of enzyme-coated liposome motors”. In: *Nat. Nanotechnol.* 14.12 (2019), pp. 1129–1134.

[138] J. Agudo-Canalejo, P. Illien, and R. Golestanian. “Phoresis and Enhanced Diffusion Compete in Enzyme Chemotaxis”. In: *Nano Lett.* 18.4 (2018), pp. 2711–2717.

[139] M. Feng and M. K. Gilson. “Enhanced Diffusion and Chemotaxis of Enzymes”. In: *Annu. Rev. Biophys.* 49.1 (2020), pp. 87–105.

[140] J. M. Schurr et al. “A Theory of Macromolecular Chemotaxis”. In: *J. Phys. Chem. B* 117.25 (2013), pp. 7626–7652.

[141] J. L. Anderson. “Colloid Transport by Interfacial Forces”. In: *Annu. Rev. Fluid Mech.* 21.1 (1989), pp. 61–99.

[142] R. Golestanian, T. B. Liverpool, and A. Ajdari. “Designing phoretic micro- and nano-swimmers”. In: *New J. Phys.* 9.5 (2007), pp. 126–126.

[143] P. Illien, R. Golestanian, and A. Sen. "'Fuelled' motion: phoretic motility and collective behaviour of active colloids". In: *Chem. Soc. Revs.* 46.18 (2017), pp. 5508–5518.

[144] H. A. Stone and A. D. T. Samuel. "Propulsion of Microorganisms by Surface Distortions". In: *Phys. Rev. Lett.* 77.19 (1996), pp. 4102–4104.

[145] T. Adeleke-Larodo, J. Agudo-Canalejo, and R. Golestanian. "Chemical and hydrodynamic alignment of an enzyme". In: *J. Chem. Phy.* 150.11 (2019), p. 115102.

[146] B. V. Derjaguin, N. V. Churaev, and V. M. Muller. "Surface Forces in Transport Phenomena". In: *Kolloidn. Zh* 9.335 (1947).

[147] S. Ebbens et al. "Size dependence of the propulsion velocity for catalytic Janus-sphere swimmers". In: *Phys. Rev. E* 85.2 (2012), p. 020401.

[148] S. Saha, S. Ramaswamy, and R. Golestanian. "Pairing, waltzing and scattering of chemotactic active colloids". In: *New J. Phys.* 21.6 (2019), p. 063006.

[149] J. R. Blake. "A note on the image system for a stokeslet in a no-slip boundary". In: *Math. Proc. Cambridge Philos. Soc.* 70.2 (1971), pp. 303–310.

[150] K. Aderogba and J. R. Blake. "Action of a force near the planar surface between two semi-infinite immiscible liquids at very low Reynolds numbers". In: *Bull. Austral. Math. Soc.* 18.3 (1978), pp. 345–356.

[151] M. Feng and M. K. Gilson. "A Thermodynamic Limit on the Role of Self-Propulsion in Enhanced Enzyme Diffusion". In: *Biophys. J.* 116.10 (2019), pp. 1898–1906.

[152] P. Sartori and S. Leibler. "Lessons from equilibrium statistical physics regarding the assembly of protein complexes". In: *Proc. Natl Acad. Sci.* 117.1 (2020), pp. 114–120.